Investigating endosomal pathway regulation of Liver Kinase B1 in *Drosophila Melanogaster*

Farha Omer

This thesis is submitted in partial fulfillment of the requirements for the degree of Master of Science

Department of Biological Sciences

University of Bergen

Norway

December 2022

Acknowledgment

The present work was conducted from January 2022 to November 2022 in the Fly Lab in Department of Biological Sciences, through the department of Molecular Biology, University of Bergen.

Firstly, and most importantly I would like to thank my supervisor Fergal Michael O'Farrell for his utmost support and patience. I am deeply grateful for this opportunity in the Fly Lab and for Fergal to have made it so easy for me to settle in into a new research environment. It has been challenging, daunting and exciting at the same time and I would like to express how grateful I am for Fergal being there as a mentor despite being busy. I also appreciate his understanding, profound encouragement and all the knowledge he has shared with me throughout the process. Thanks to Aurelia E. Lewis, my co-supervisor for her wise conversations and advise on my thesis to keep me motivated. A special thanks to Sandra Ninzima, for being a savior and to have problem-solved with me whenever I was stuck or needed something. Altogether, thank you to the Fly Group for keeping all our weekly meetings so knowledgeable and fun.

I would like to thank Aina Borve for her patience and technical support throughout the time I needed help with the confocal. I would also like to mention Fatemeh Mazloumi Gavgani for the same who helped me problem-solve mistakes with microscopy at a crucial time. Thanks to Thibault Michel Joseph Tubiana for his efficient virtual correspondence and willingness to advise when I reached out. I would like to mention Lakshmi Narasimha Murthy Chavali for being a friendly face in the department with all the good talks, thesis-related and otherwise. I would also like to mention my batchmate, workspace partner and good friend Ifeoluwa Abigail Oyediran for all the great talks and company.

Last but definitely not the least, I dedicate this thesis to my loving parents Omer Haq and Ghazia Omer, my siblings, my grandmother, and my friends.

Bergen, November 2022

Farha Omer

Table of Contents

Acknowledgment 2

Abbreviations 7

Abstract 10

1. Introduction 11

1.1 *Drosophila melanogaster* as a model organism 11

Figure 1: *Drosophila* autosomal and sex chromosomes. 11

1.2 Life cycle of *Drosophila melanogaster* 12

Figure 2: The *Drosophila* lifecycle. 13

1.3 The Fly Wing 13

Figure 3: The *Drosophila* wing disc patterns. 14

1.4 Investigating gene expression using genetic tools in *Drosophila melanogaster* 14

1.5 GAL4/ UAS expression system 15

Figure 4: Using the GAL4-UAS lines with fluorescent markers. 16

1.6 RNA induced gene silencing 16

1.7 Liver Kinase B1 (LKB1) 17

1.7.1 LKB1 structure and localization 17

Figure 5: Overview and comparison of hLKB1 and dLKB1. 18

1.7.2 LKB1 in *Drosophila* 19

1.7.3 LKB1 as a tumour suppressor 20

1.7.4 Potential oncogenic role of LKB1 20

1.8 Biochemical functions of LKB1 21

1.8.1 LKB1 involvement in polarity control 21

1.8.2 AMPK as a target of LKB1 22

Figure 6: AMPK acts as a heterotrimeric energy sensor. 22

Figure 7: Schematic representation of farnesylation of LKB1 and its interaction with activated AMPK after myristolation. 23

1.8.3 LKB1 and its interaction partners 24

Figure 8: LKB1/AMPK interaction partners..... 24
1.9 Mutated LKB1 and Peutz-Jeghers syndrome (PJS)..... 25
Figure 9: Hyperpigmentation of a patient with Peutz Jeghers Syndrome..... 25
Table 1: Incidence of cancer in Peutz-Jeghers Syndrome by cancer site (105)..... 26
1.10 Endosomal and lysosomal regulation of LKB1..... 27
1.11 LKB1 as an indirect regulator of autophagy..... 28
Figure 10: Regulation of autophagy by insulin signaling and starvation..... 29
2. Aims and Objectives..... 30
3. Materials and Methods..... 31
3.1 Working with flies..... 31
3.1.1 Fly Food..... 31
3.1.2 Anaesthesia for flies..... 31
3.1.3 Virgin collection..... 31
Figure 11: *Drosophila* virgin fly..... 31
3.1.4 Identification of markers for distinguishing genotypes..... 32
Table 2: *Drosophila* fly genetic markers and phenotype..... 32
Table 3: Selection of markers from a genetic cross..... 33
3.2 Larvae Dissection and collection of wing imaginal discs..... 33
3.2.1 Fixation and antibody staining of wing discs..... 33
3.3 Fly stocks..... 34
Table 4: Fly lines and sources..... 34
3.3.1 Wild type LKB1 stock..... 35
3.3.2 Balancer stock..... 36
3.3.3 Stocks used for RNAi experiments..... 36
Table 5: RNAi fly lines used for knockdown of controls..... 36
3.3.4 RNAi line used for starvation experiments..... 36
3.4 Collection of recombinants..... 36

3.5 Confocal and Wide-field Microscopy 37
3.6 Reagents 37
Table 6: Antibodies and mountants used 37
Table 7: Other buffers and reagents 38
3.7 Statistical Analysis 38
3.7.1 Calculation of Slope Average 39
Figure 12: Calculation of slope average in Microsoft excel. 40
3.7.2 Calculation of Total Intensity 40
Figure 13: Calculating Total Intensity as area under the plot. 41
4. Results 42
4.1 Genetic recombination can be induced in *Drosophila Melanogaster* 42
Figure 14: Genetic recombinants can be obtained in *Drosophila* through planned crossing schemes and selection criteria. 43
Figure 15: Relative comparison of protein localization in fly line 150 and 250. 45
4.2 Expression of GFP-tagged wild-type LKB1 from its endogenous promoter is found on the cell membrane 46
Figure 16: Endogenous GFP-LKB1 localizes to the plasma membrane in *Drosophila* wing discs. .. 47
4.3 Mutation in LKB1 CAAX box region and LB domain disrupts its cellular localization 47
Figure 17: Mutation in CAAX box and LB domain disrupts membrane localization of LKB1. 49
Figure 18: Structure prediction of LKB1-WT and LKB1 ΔLBCA using software prediction modelling. 50
4.4 Recombinant fly lines can be used for screening of cellular trafficking regulators 51
4.4.1 Knockdown of LKB1 decreases its localization in the lateral membrane 51
Figure 19: LKB1 localization and levels observed in wild-type 150 and 250 fly lines. 52
Figure 20: Knockdown of LKB1 in 150 and 250 reduces localization of LKB1 in the lateral membrane of *rotund* expression region. 54
Figure 21: Knockdown of LKB1 does not affect apical membrane localization but reduces the lateral membrane and cytoplasmic levels. 56

4.4.2 Knockdown of Wdfy2 increases membrane and endosomal localization of LKB1 56
Figure 22: Knockdown of Wdfy2 in fly line 150, increases membrane localization of LKB1. 57
Figure 23: LKB1 co-localizes with WDFY2 on endosomes. 58
4.4.3 Knockdown of vps34 increases membrane localization of LKB1 59
Figure 24: Membrane localization of LKB1 increases in 150 fly line on vps34 knockdown. 60
Figure 25: Membrane localization of LKB1 increases in LKB1-WT stock on vps34 knockdown. ... 61
4.5 Induction of starvation decreases localization of LKB1 61
Figure 26: LKB1 membrane localization is decreased in starvation induced autophagy. 62
5. Discussion 63
5.1 Methodological considerations and limitations 63
5.2 General Discussion 66
6. Conclusion 70
References 72
Appendix 78

Abbreviations

AKT/PKB	Protein kinase B
AMP	Adenosine monophosphate
AMPK	AMP-activated protein kinase
Ap	*Apterous*
AP	Anterior-Posterior
ATG	Autophagy-related
ATLL	Adult T-cell leukemia/lymphoma
ATM	Ataxia telangiectasia mutated
ATP	Adenosine triphosphate
BDGP	Berkeley *Drosophila* Genome Project
Brg1	Brahma-related gene 1
C. elegans	Caenorhabditis elegans
CAMKKβ	Calcium/calmodulin-dependent protein kinase kinase beta
cAMP	Cyclic AMP
CBS	Cystathionine β-synthase
CIII-PI3K	Class III phosphatidylinositol-3-OH kinase
dLKB1	*Drosophila* LKB1
Dll	Distal-less
DNA	Deoxyribonucleic acid
Dpp	Decapentaplegic
dsRNA	Double-stranded RNA
DV	Dorsal-Ventral
EMS	Ethyl Methane Sulphonate
En	*Engrailed*
GFP	Green Fluorescent Protein
GI	Gastrointestinal tract
hLKB1	Human LKB1
HSP	Heat shock protein
LAMP1	Lysosomal-associated membrane protein 1

LKB1	Liver Kinase B1
MAPK	Mitogen-activated protein kinase
MARK	Microtubule Affinity-regulating Kinase
MO25	Mouse Protein-25
MRLC	Myosin Regulatory Light Chain
mRNA	Messenger RNA
MST4	Mammalian STE20-like protein kinase 4
mTOR	Mammalian target of rapamycin
NADPH	Nicotinamide adenine dinucleotide phosphate
NLS	Nuclear Localization Signal
NMT1	N-myristoyltransferase 1
p53	Tumor protein p53
PAR-1	Protease-activated receptors 1
PD	Proximal-Distal
PGC	Primordial Germ Cell
PI3K	Phosphoinositide 3-kinases
PJS	Peutz Jeghers Syndrome
PKA	Protein kinase A
PKC	Protein kinase C
Rab	Ras-associated binding
RAS	Rat sarcoma virus
RFP	Red Fluorescent Protein
RISC	RNA-induced silencing complex
Rn	Rotund
RNA	Ribonucleic acid
RNAi	RNA interference
RSK	Ribosomal S6 Kinase
Skp2	S-phase kinase-associated protein 2
STK11	Serine/threonine kinase 11
STRAD	STE20-related adapter protein
TF	Transcription factor

TJ	Tight Junctions
TSC	Tuberous sclerosis complex
UAS	Upstream activation Sequence
ULK1	Unc-51 like autophagy activating kinase
Vps15	Vacuolar Protein Sorting 15
Vps34	Vacuolar Protein Sorting 34
WDFY2	WD repeat and FYVE domain-containing protein 2
Wg	Wingless

Abstract

Within a cell, efficient intracellular trafficking is essential for various functions, including cellular polarity, cell signalling, and maintenance of homeostasis by regulation of cellular energy. Liver kinase B1 (LKB1), also known as Stk11 is a gene that acts as an indirect regulator of these biochemical processes by interacting with key endosomal trafficking regulators, such as CIII-PI3K and Rab GTPases which are implicated in various diseases, including cancer. LKB1 is found to be mutated in an autosomal recessive disorder known as Peutz Jeghers Syndrome (PJS), a disease associated with increased risk of development of cancer. The gene was first identified as a tumor suppressor due to its role in controlling bioenergetics, cell growth and several biochemical functions, but it was later suggested that it could also promote tumor progression by promoting cell survival, calling it a contextual oncogene. In cells in culture, LKB1 is transported from the nucleus to the cytosol where it is active in a heterotrimeric complex with MO25 and STRADα. The interaction of LKB1 with its downstream target called AMP-activated protein kinase (AMPK), also regulated by the endo-lysosomal pathway, is crucial in the context of promoting cell survival under conditions of energy stress. Preliminary studies suggest that LKB1 localizes on the (lateral) plasma membrane, in vivo and in polarised cells from where it may be endocytosed, however, the pathway and destination of the protein is not known, in terms of whether it is sorted, recycled, or degraded in the lysosome.

For the purpose of our study, we used Drosophila genetics, structural prediction modelling, high-resolution imaging techniques and statistical analysis to show that LKB1 activity levels and localization are essential for epithelial integrity. We constructed recombinant fly lines with GAL4 driver and UAS-tagged gene expression within a domain of the developing wing epithelial tissue to show that localization and activity of endogenously expressed GFP-tagged LKB1 is affected as a result of knockdown of important trafficking regulators, such as vps34, the catalytic domain of CIII-PI3K, generating PI3P, and WDFY2 a PI3P binding protein. In order to accomplish this different LKB1 versions and quantification methods were evaluated with an aim to establish a method to measure and distinguish between the levels of LKB1 in cytoplasm and in close proximity to the plasma membrane. In addition, we blocked insulin signalling in order to investigate the interplay between starvation induced autophagy and LKB1 regulation.

.

1. Introduction

1.1 *Drosophila melanogaster* as a model organism

Drosophila melanogaster, which belongs to the family Drosophilidae and the order Diptera has proved to be a very useful model organism for investigating several cellular processes and development of tissues and organs. The model system is easy to manipulate genetically due to its short life cycle, lesser ethical concerns, lower cost of maintenance and biological similarity to mammals – especially humans. Many of the important developmental processes are conserved between flies and higher eukaryotes. For instance, flies have 60% homologues in humans. In addition, about 75% human diseases have homologs in flies (1, 2). Their small size is convenient to handle and maintain in a limited space and budget. In addition, flies rapidly reproduce which allows progeny to be readily available.

The *Drosophila* has been used as a useful model organism with tools having evolved through a century, now refined enough to deal with lesser genetic redundancy, having lesser genes than humans thus, making it convenient as a model for studies in developmental biology, genetics and epigenetics (3). No meiotic recombination takes place in *Drosophila* males, which is a useful aspect to explore when working with genetic crosses as it makes it easier to track the chromosomes through different generations. The genome of *Drosophila* comprises of four chromosomes, two of which are larger metacentric chromosomes, one is a small telocentric chromosome and the sex chromosomes, in which the X is a large telocentric chromosome (shown in Figure 1). When writing down genotypes the chromosomes are separated by a semicolon (for example, X; 2nd chromosome; 3rd chromosome). The polytene chromosomes are formed through repetitive rounds of cell division through endoreplication (4). The structure of the chromosomes can be determined by using the appropriate staining and visualizing under the microscope making it easier to position and map out genes. However, polytene staining is a lesser popular approach as compared to genome sequencing nowadays to extract information about chromosome structure. In addition, online databases are available such as FlyBase which consist of genetic and molecular data for *Drosophila* and have made navigation easier (5).

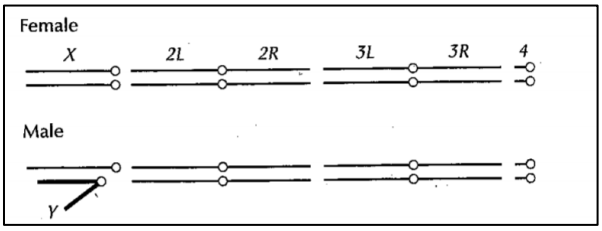

Figure 1: *Drosophila* autosomal and sex chromosomes. The *Drosophila* genome consists of four set of chromosomes. The 2nd and 3rd have a left and right arm which are comparable in size. The 4th chromosome has a left

arm about 1/5th the size of the 2nd and 3rd chromosome and a very small right arm. The X chromosome has a major left arm while the Y chromosomes importance is only defined by a few genes which are mostly needed for appropriate motility of the sperm. Figure retrieved from (6).

The exoskeleton of the fly can be manipulated in many ways (e.g., anesthetizing adult flies in carbon dioxide, making larvae immobile using ice for dissection) and visualized for certain markers and mutations causing characteristic or altered phenotypes respectively, in the compound eye, wings, body color, body structure, bristles and more. The external phenotypes of the fly can prove to be useful to understand specific gene functions.

1.2 Life cycle of *Drosophila melanogaster*

The fly has a short life cycle, making it easier to raise in large numbers for genetic, epigenetic, and developmental studies. In the laboratory *Drosophila* stocks are maintained at 18˚C, for slower generation or 25˚C for the fastest generation of approximately 10 days from the egg to the adult (6). The female lays up to 100 embryos per day after fertilization. Once fertilization has taken place, it typically takes about 10 days for the adult to emerge (eclosion) from the pupa – dependant on the nutritional conditions and the temperature. *Drosophila* undergoes metamorphosis through a cycle of four stages: egg, larval, pupal, and adult stage. The embryo develops after which the hatching and larval stage approaches. The larval stage itself is divided into three further stages called instars distinguished by moulting. Moulting defines the nutritional and size gain of the organism through ingesting the food by feeding on the surface of the medium. In about 2 days after the emergence of the third instar larva, it moves to a dry spot, perhaps on the clean wall of the tube and stops moving. At this stage the larval cuticle hardens and surrounds the organism to give rise to the pupal case and eventual full metamorphosis within a 5-day period. During earlier pupal stages larval tissues are destroyed through apoptosis and adult structures form from an undifferentiated set of tissues called the imaginal discs (7). The metamorphosis stage in subdivided into a half-day pre-pupal stage (pupariation) and about a 4-day long pupal period. There are 10 major pairs of imaginal discs, from which the adult structures, the genitals and reproductive organs are formed.

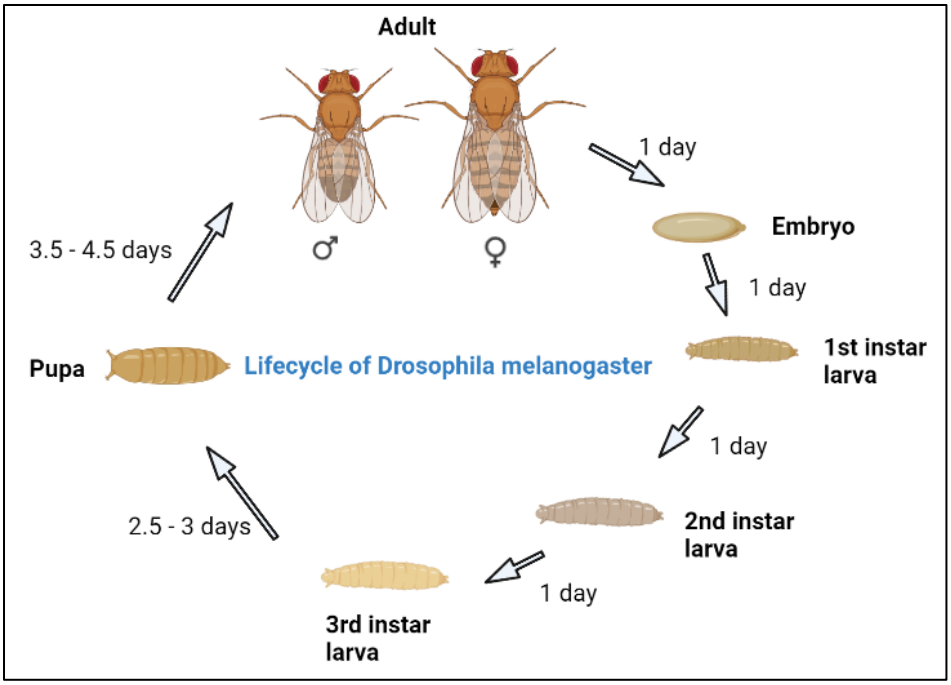

Figure 2: The *Drosophila* lifecycle. The *Drosophila* lifecycle comprises of four stages from the egg to the adult fly (embryo, larva, pupa, adult). The length of generation of all stages is shown in number of days. The fastest generation time is at the temperature of 25 ˚C and humidity of 65% yielding an adult from the egg in approximately 10 days.

1.3 The Fly Wing

The wing in *Drosophila* is derived from the wing imaginal disc which is further divided into a dorsal-ventral (DV) and anterior-posterior (AP) axis, proximal-distal (PD), notum and the primordial germ cells (PGCs). The primordium of the wing disc is formed from a set of 40 cells, which eventually proliferate into about 50,000 cells and gain maturity on differentiation. *Wingless (wg)* and *Decapentaplegic (Dpp)* are genes that contribute towards segment polarity and defining of the DV and lateral stripes of *Wg* and *Dpp*, respectively (8). The differentiation of cells begins when anterior cells and posterior cells segregate at embryogenesis (9). There are three genes responsible for pattern formation along the proximal-distal region of the imaginal discs: *Decapentaplegic*, *Distal-less* (*Dll*) and *rotund* (*rn*). *Rotund* is localized in a sub-distal region along the PD axis needed for proper development of the sub-distal structure and female genitalia (10). Expression of another gene called *vestigial* (*vg*) is found centred on the boundary between the DV region of the wing. Cells in the wing pouch expressing a gene called *apterous* (*ap*) are found on the dorsal region of the wing while cells not expressing *apterous* are given a ventral identity. *Apterous* functions to determine the dorsal fate of the wing. The typical subdivision of the wing disc provides a foundation for specific cell-cell interactions which accentuates the pattern (11). The well described expression of several of these aforementioned patterning genes has been useful in genetic studies described in the results.

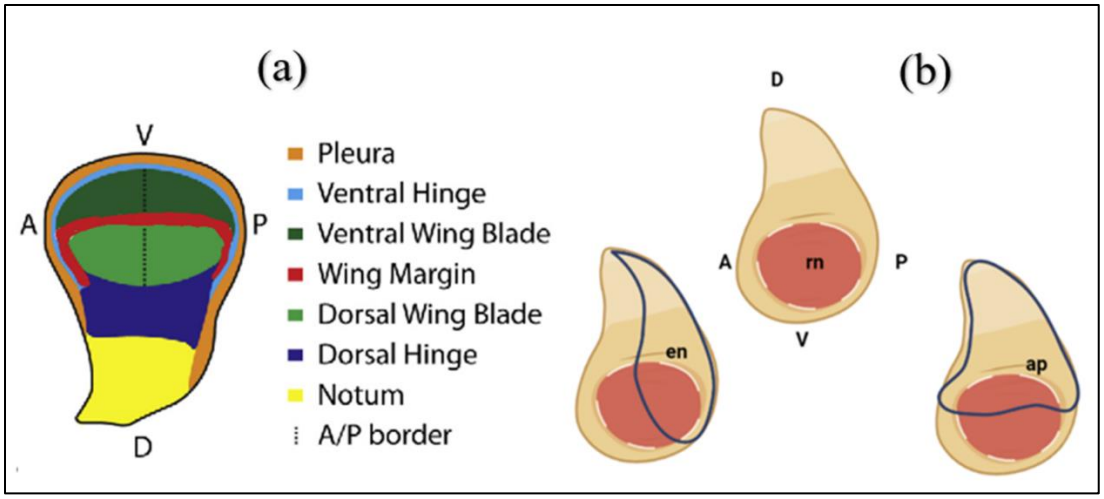

Figure 3: The *Drosophila* wing disc patterns. (a) Shown in the figure is a DV (dorsal/ ventral) and AP (anterior/ posterior) axis of the wing disc and nomenclature in *Drosophila*. (b) Some characteristic patterns shown are for *rotund* (*rn*) expressed in the central and notum of the disc, *engrailed* (*en*) expressed in the posterior region, and *apterous* (*ap*) expressed in the posterior region of the wing pouch. These characteristic patterns are a result of genetically programmed pattern formation and can be harnessed to perform temporal or spatial gene/protein studies in a compartmentalized fashion within specific tissues. Figure (a) obtained from (12) and (b) made in Biorender .

1.4 Investigating gene expression using genetic tools in *Drosophila melanogaster*

Drosophila provides a useful model system to study several human diseases, essentially due to its similarity with the human system. For instance, the central brain (or optic lobes) and the ventral nerve chord in *Drosophila* is analogous to the brain, the spinal cord, and the segmental nerves in humans. Genes that underlie several genetic disorders especially cancer and neurodegenerative diseases conserved through evolution can be studied in *Drosophila* systems (13).

Forward genetics is a popular method used for determining the genetic basis leading to a certain phenotype and is also used in *Drosophila melanogaster* to identify genes involving a particular function, biological process, or phenotype. In the 20th century, Thomas Hunt Morgan and his colleagues discovered a *Drosophila* mutant having the white eye mutation. The white eye was a result of a random and spontaneous mutation event. This proved to be a basis for using random mutations to infer the function of a gene, and thus in turn became the basis of genetic screens using *Drosophila*. These mutations can be made with selected mutagenic agents which are convenient to administer and cause a larger number of mutations, such as ethyl methane sulphonate (EMS). While EMS induces point mutations, other mutagens such as X-ray and gamma irradiation are also used, which yield double-stranded DNA breaks. The latter can prove to be a better tool since it does not cause mosaicism. On the other hand, males which are mutated with EMS can lead to a mosaic progeny (14).

One of the newer techniques being used in fly genetics is insertional mutagenesis, which can either be a single site insertion (site-specific) or multiple insertions (random insertions). Engineered transposable elements called P-elements containing specific markers for eye traits, body colour, and/ or other dominant visible markers can be used in this case (15). A gene which is mutated using P-element insertion can be identified using sequencing (14). However, it's not possible to mutate every gene in the genome using P-element insertion because the technique favours insertion at the 5' noncoding regions (16). The P-element fly lines initially identified and collected by the Berkeley *Drosophila* Genome Project (BDGP) and later also maintained as a library by Bloomington *Drosophila* stock centre consist of enhancer traps which can be used to extract the expression pattern of effected genes (16). One of the most relevant examples of the usefulness of P-element insertions can be illustrated by the GAL4/UAS binary expression system used in this report.

1.5 GAL4/ UAS expression system

The GAL4/ UAS expression system has become an important expression system for gene expression in *Drosophila* allowing activation of specific cloned transgenes in tissues and cells (14). GAL4 is a yeast transcriptional activator and under the control of a tissue specific promoter triggers targeted/specific transcriptional upregulation. In yeast, GAL4 causes transcription of Gal1 and GAL10 through binding to Upstream Activating Sequences (UAS) (four 17 base pair sequences) (15). In Drosophila the GAL4 protein does not affect the native genes in any way as no innate UAS sequence exists. The GAL4/ UAS system separates the transcriptional activator from the gene that is being targeted where both are from a different transgenic line. Once the two lines are crossed the target gene is turned on, making it possible to study phenotypic effects such as a Red-Fluorescent Protein signal (RFP) shown in Figure 4. The target gene is placed under control of the UAS promotor and is activated for transcription on binding of the GAL4 protein (14). For the purpose of this study many lines with tissue specific expression patterns were obtained which were initially generated using P-element based insertion of GAL4 elements into the genome (obtained from the Bloomington Stock library). All of the lines (shown in Table 4) obtained had P-elements with UAS tagged DNA constructs inserted into the genome, for example those expressing RNAi, or reporter proteins. An example of such fly lines is shown in Figure 4.

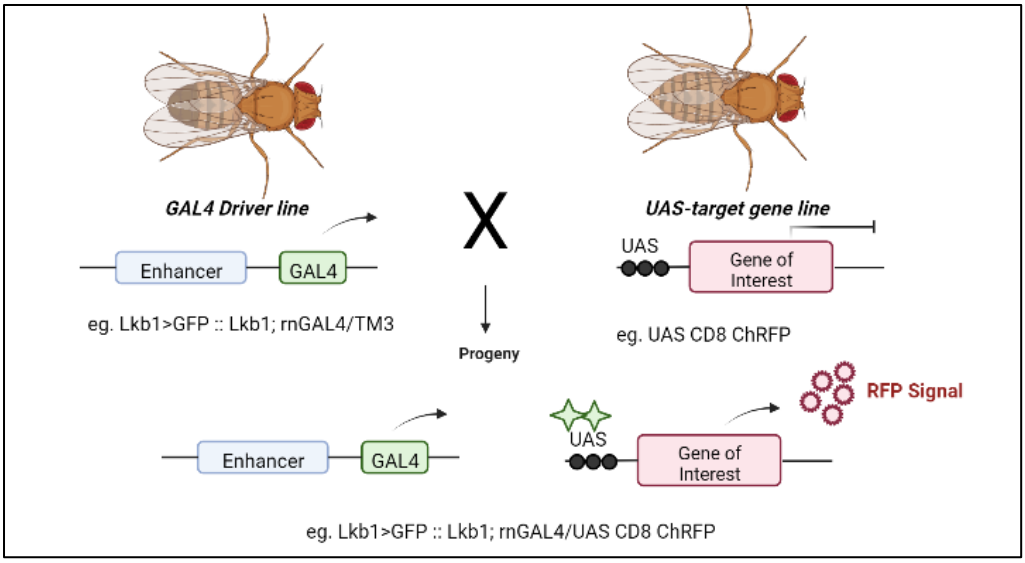

Figure 4: Using the GAL4-UAS lines with fluorescent markers. The transcriptional activator in yeast called GAL4 was used to regulate expression in *Drosophila*. GAL4 (e.g., from lkb1>GFP::Lkb1; rn-GAL4/TM3) binds to the upstream activating sequence (UAS) adjacent to the gene of interest (e.g., UAS (or >) CD8 ChRFP). A genomic enhancer (e.g., tissue specific endogenous enhancer for *rotund*) controls the expression of GAL4 in cells and tissues. Once the two lines in the example above are crossed rn-GAL4 stimulates expression of UAS CD8 ChRFP (gene of interest) which is displayed as an RFP signal in a pattern reflecting the endogenous genomic enhancer for *rotund*. Figure adapted from (14) and made in Biorender.

1.6 RNA induced gene silencing

The mechanism of RNA (RNAi) interference relies upon small fragments of double stranded RNA (dsRNA) with a matching sequence to a specific targeted gene. This causes interference of expression, of the targeted gene at a post transcriptional level, having the overall effect of lowering protein level. The mechanism was first identified in the nematode worm in 1998, and came to be useful for other plants and animals (17). Gene specific RNA interference is used to investigate the function by suppressing the gene expression and subsequently any resulting phenotypic effect. A sequence of about 22 nucleotides called guide sequences, homologous to the gene being expressed is primarily used for the mechanism (18, 19). The guide sequences interact with a nuclease called an RNA-induced silencing complex (RISC) to break down specific messenger RNAs (mRNA) (19). The RNAi process is said to be initiated by a nuclease called dicer (belonging to the RNase III family) which produces guide RNAs by destroying dsRNA. *Drosophila* has several RNAi stock collections each of which target every coding gene in the genome (found in Bloomington stock library). For the purpose of this study, RNAi lines were used for targeted knockdown as shown in Table 5. Other ways to cause lowering of targeted protein activity include expression of dominant negative protein forms, commonly used to disrupt Rab small GTPases and Kinase signaling.

1.7 Liver Kinase B1 (LKB1)

The focus of this study has been the vertebrate Liver kinase B1 (LKB1), also known as STK11 (serine/ threonine kinase 11 and XEEK1 in Xenopus, and is believed to be conserved throughout evolution from worms to mammals (20). The serine/ threonine kinase has been demonstrated to function as a master regulator of several downstream kinases, such as AMP-related protein kinases (21). LKB1 was initially found in the PAR-4 homologue of *Caenorhabditis elegans* and has been identified to play a major role in regulating cellular energy balance (20, 22). This might be important in terms of maintaining cellular polarity, p53 mediated apoptosis, cell growth, acting as a tumour suppressor as well as potentially a contextual oncogene (23). The latter implies that LKB1, owing to its function as a tumor suppressor can control bioenergetics and cell growth through regulation of the mammalian target of rapamycin (mTOR) (24). On the other hand, it also implies that LKB1 has oncogenic function as it can promote tumorigenesis by enhancing nutrient utilization through interaction with AMP-activated protein kinase (AMPK), fuelling energy production and promoting cellular growth (25). However, the role of LKB1 in influencing tumor metabolism is not quite clear.

LKB1 was initially identified as a tumour suppressor (located on chromosome 19p13), and it was found to be mutated in nearly 95% of patients having a disease called the Peutz-Jeghers Syndrome (PJS) (26). In studies in mice, the kinase is constitutively active in a heterotrimeric complex with the mouse protein 25 (MO25) and pseudokinase STE20-related adaptor (STRAD). These two regulators help in determining the localization of the protein. Previous studies have identified that while LKB1 is primarily shown to be overexpressed in the nucleus in mammalian cells, it is also located in the cytoplasm in the heterotrimeric complex (27-29). In addition, it is a key upstream activator of AMPK in turn leading to regulation of crucial cellular events such as apoptosis, metabolism, and cellular energy balance.

The survival of cells is greatly dependent on their access to a sufficient abundance of nutrients that ensure successful cell survival and division. The relationship between cellular metabolism and tumorigenesis has been investigated in the past decades, proceeding the initial discovery by Dr. Otto Warburg that cancer cells have the ability to convert tremendous amounts of glucose into lactic acid, despite scarcity of oxygen (30). The observation later gained popularity as the Warburg effect or aerobic glycolysis and has become an important concept in the context of cancer therapy.

1.7.1 LKB1 structure and localization

All LKB1 protein activity stems from a single gene in humans and the predominant translated protein comprises of a 433 amino acids long sequence with regulatory domains at the C- and N- terminal, as well as a central kinase domain (49 to 309 amino acids). Similarly, single orthologs of LKB1 are found in

Drosophila (dLKB1), Xenopus, Mouse and *Caenorabhditis elegans* (*C. elegans*). dLKB1 is made up of a sequence of 567 amino acids consisting of a protein kinase region, an ATP binding site, and disordered regions. A comparison of hLKB1 and dLKB1 is shown in Figure 5, along with a structure alignment to show structural similarity in space. In vitro studies have shown the activation of LKB1 in a heterotrimeric complex with STRAD and MO25, primarily in the cytosol.

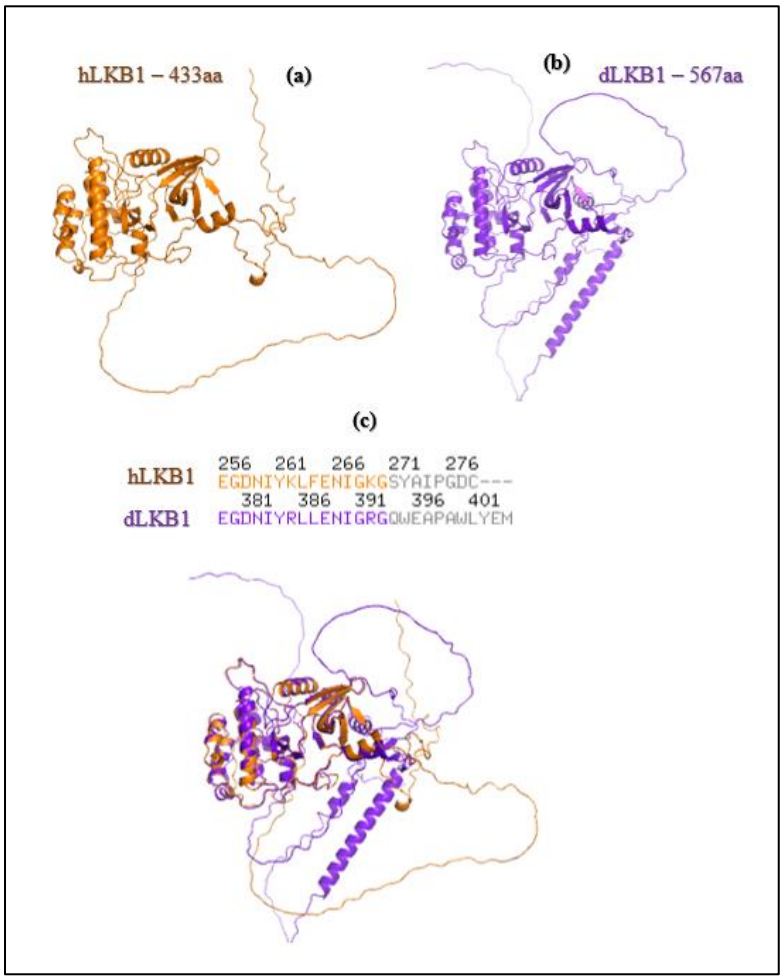

Figure 5: Overview and comparison of hLKB1 and dLKB1. (a) The human LKB1 consists of 433 amino acid residues as compared to (b) *Drosophila* LKB1 which consists of 567 amino acid residues. (c) The sequences are orthologs and show significant alignment when the two structures are superimposed on each other. The sequence shown is of a selected region of high sequence similarity and the grey sequence highlights irregular alignment or disordered regions. Sequences were obtained through UniProt, and AlphaFold predicted structures projected using PyMOL.

The C-terminal of the protein contains three phosphorylation sites: S428, T366, S325. The former two sites are targets of protein kinase A (PKA), ataxia telangiectasia mutated (ATM), and protein kinase C (PKC) (31, 32). ATM regulates phosphorylation of LKB1 at T366, which is involved in B cell proliferation

although not effecting the catalytic activity of LKB1 in any way (33, 34). PKA (cAMP-dependent protein kinase) and p90 (RSK) phosphorylates S428, not affecting the kinase activity of LKB1 but playing a role in suppressing cell growth (35). S325 of LKB1 is a target of extracellular signal-regulated kinases (ERK proteins). The nuclear localization signal (NLS) and an additional phosphorylation site (S31) are all present in the N-terminal (33). Mutations at the autophosphorylation sites T336 or S428 have shown to mitigate the ability of LKB1 to promote G1 arrest in G361 melanoma cells (33, 35). The protein residues in LKB1 either phosphorylated or autophosphorylated by upstream regulators such as kinases are highly conserved in *Drosophila* (36). LKB1 is believed to interact with phospholipids for the purpose of direct binding to membranes. LKB1 contains autophosphorylation sites (T185, 3404, T336, T189) and a prenylation motif at the C-terminal. The motif can be farnesylated (addition of farnesyl group to a Cysteine) in cells within a CAAX box (where C is cysteine, A is any of the aliphatic amino acids and X, any amino acid) generating a lipid membrane localizing signal and promoting membrane targeting (31-33). It has been shown in *Drosophila* germ line that blocking of efficient farnesylation leads to improper cortical binding and also disturbs polarization of the oocyte (37). However, it was found that the farnesylation motif alone in not sufficient for association of LKB1 to the cell cortex as shown by Martin et al. (using last 15 residues of LKB1 fused to GFP) (37). Thus, protein modifications, or membrane binding domains apart from the farnesyl motif in LKB1 are needed for proper cortical association (38).

1.7.2 LKB1 in *Drosophila*

LKB1 in *Drosophila* (dLKB1) was identified in mutants affecting the localization of maternal Staufen protein in germline clones (37). The protein has strong homology with the human tumor-suppressor LKB1 and has an important role in polarity control in follicle cells of the epithelium (37). It was identified through biochemical experiments that demonstrated that LKB1 acts upstream of PAR-1 and tau (39). AMPK is a downstream target of LKB1 under energy stress to control mitosis, growth, and cell polarity. It has been shown in the retina that dLKB1 interacts with PAR-1 and several AMP-related kinases to regulate polarity (40). dLKB1 induces apoptosis and negatively regulates organ size, without having any effect on the cell cycle progression (41). In *Drosophila*, LKB1 mutants are shown to lose cells polarity, also leading to defects on the structure of the cytoskeleton (42). Larval neuroblasts consisting of LKB1 mutations lead to defects in apical polarity. Par-6 is involved in recruitment of aPKC and Bazooka, both of which are important for establishing the apical domain. Thus, loss in polarity is seen through improper localization of Bazooka, Par-6 and aPKC, resulting in polyploid cells in the larval brain (43). It was identified that LKB1 thus has a role in cell polarity, and the regulation of cell responses to energy stress. In fact, LKB1 was initially identified as a tumor suppressor due to its link to PJS (44). Later on, a dual nature of LKB1 was

identified due its ability to promote or halt cancer progression calling it a contextual oncogene with a dual role (45).

1.7.3 LKB1 as a tumour suppressor

Patients with PJS have been proved to have a high susceptibility to developing malignancies, originating from missense mutations of the conserved kinase and regulatory domain of LKB1. These mutations have proved to cause decreased kinase activity of LKB1, in turn affecting its overall function (44). This stressed the importance of investigating the role of LKB1 as a tumor suppressor through studies showing its involvement in halting cancer progression. Several studies show that LKB1 may have a role in inducing inhibitors of cell cycle progression, such as p21, p27 and p16 (46, 47). Introduction of wild type LKB1 into LKB1-null cells halted cell cycle progression at the G1 phase of the cell cycle. The opposite affect was seen when cells were deprived of LKB1 through knockdown. LKB1 causes G1 arrest regulated through a p53-dependent o independent manner (27, 48-50). In the former case, LKB1 might be involved in p53-dependent cellular death through interaction via phosphorylation of p53 (51). In *Drosophila* dLKB1 induces apoptosis through the JNK pathway and in a p53 independent manner (41). Mice, which were homozygous negative for both LKB1 and p53 displayed PJS related phenotypes; characterized by gastric hamartomas, adenomas and carcinomas in the liver and the GI tract (51).The evidence provides a clear proof of interaction of p53 and LKB1 in terms of tumor progression.

Phosphatase tensin homologue (PTEN) is another known tumor suppressor acting upstream of LKB1 and directly inhibits the PI3K/AKT pathway for oncogenic survival. Its nuclear transport is facilitated by LKB1 and is one of the initial steps needed for regulation of the PI3K/AKT pathway (52). Loss of function mutations of both LKB1 and PTEN caused augmented progression of lung squamous cell carcinoma (53). It has been proposed by Liu *et al.* in 2011 that the interaction of PTEN and LKB1 leading to regulation of the PI3K/AKT pathway is independent of the AMPK/mTOR signalling pathway (54). All these studies show a clear role of LKB1 as a tumor suppressor which can further be assessed by different modifications of the LKB1 function to get an insight on risk assessment for cancer. However, there are certain reports which investigate LKB1s involvement in tumorigenesis by increasing viability of cancer cells along with their ability to metastasize (55-57).

1.7.4 Potential oncogenic role of LKB1

The cellular stress regulatory pathway involving interaction of LKB1, and AMPK has been recognized to have a possible oncogenic role. The pathway promotes maintenance of homeostasis and regulates cell metabolism which might aid cancer cells to adapt to hostile conditions and survive under stress (58). A classic example of a survival advantage under stress was shown by Lee *et.al* in 2015; LKB1

polyubiquitination by a ubiquitin ligase called S-Phase Kinase-Associated Protein 2 (Skp2) led to poor outcome in patients of hepatocellular carcinoma (59). A proceeding study showed an augmented activity and expression of LKB1 in spheroids which were obtained from breast cancer cell lines. In addition, if LKB1 activity was blocked it led to anchorage-dependent cell death called anoikis (60). Thus, LKB1 promotes survival of circulating tumor cells. In turn, Katia and colleagues established a link of LKB1 with ERα and ERβ (ligand transcription factors) in, in vitro and in vivo breast tumors (55). It was highlighted that LKB1 as a part of a complex containing metERα/Src/PI3K could lose its properties as a tumor suppressor and promote cancer progression (55). LKB1 also has the ability to promote survival of adult T-cell leukemia/lymphoma (ATLL) by augmenting the expression of miR-34a (45, 61).

The downstream target of LKB1, AMPK has also been investigated as having a role of a contextual oncogene. AMPK causes internalization of lipids which in turn leads to growth of glioblastoma (62). AMPK has a role in increasing AKT oncogenic signaling when under stress, via phosphorylation of Skp2. Resistance of cancer cells to chemotherapy has also been linked directly to increased expression of AMPK by induction of autophagy (63). Having investigated the possible oncogenic role of LKB1 and AMPK they may have important implications as therapeutic targets for cancer.

1.8 Biochemical functions of LKB1

1.8.1 LKB1 involvement in polarity control

LKB1 activates many different members of the AMPK super family by phosphorylation, which eventually contribute to regulating epithelial polarity. These include AMPK, MARK/PAR1 (MAP microtubule affinity regulating kinases found in several species, like mammals, yeast, and *Drosophila*), and MST4 (mammalian STE20-like protein kinase 4). MARK/PAR1 kinases are phosphorylation targets of LKB1 and play a crucial role in asymmetric cell division and cell polarity control (40, 64-70). MST4 is phosphorylated by LKB1 and eventually causes activation of ezrin, a mechanism involved in induction of the apical brush border within cells of the intestine (64, 71, 72). LKB1 has a crucial role in activating the AMPK kinases such that it causes inhibition of the mTOR pathway involved in autophagy and dealing with cell size. Thus, this regulation in the primary cilium and the basal body where LKB1 is localized, helps in maintaining the size of the cell (73). E-cadherin helps in maintaining the localization of LKB1 by binding to STRADα in its heterotrimeric complex, in turn also maintaining the phosphorylation and activation of AMPK in polarized cells in the epithelia (74). The activation of AMPK also helps in polarity maintenance and the formation of tight junctions (TJ), but it is unclear whether LKB1 is the only upstream activator of AMPK. There are other upstream kinases such as Ca2+ calmodulin-dependent protein kinase kinase-β (CAMKKβ) which might cause activation of AMPK for TJ formation (65, 70, 75). Studies have shown a rescue of cell polarity

by introduction of AMPKα in loss of function mutants for LKB1, showing a direct role of LKB1 coordination with AMPK for regulation of epithelial polarity and cellular proliferation (40, 64, 76). In fact, AMPK and MARK kinases both play a role in regulating epithelial polarity together through overlapping coordination of their substrates.

1.8.2 AMPK as a target of LKB1

It has been identified in many mammalian cell lines that AMPK activation is prominently regulated by LKB1 at a specific phosphorylation site in the activation loop (T172) (77). At conditions of low energy, the levels of ADP and AMP augment. The signal interacts with Cystathionine β-synthase (CBS) motifs of the AMPKγ subunit of AMPK (78). The effect causes the activation of the AMPKα subunit by causing a conformational change, eventually leading to phosphorylation of Threonine at the 172 position (79). AMPKα plays a role in restoring energy levels by interacting with other proteins which are involved in metabolism, cell growth and proliferation (80). A serine residue at position 108 (S108) if phosphorylated, leads to further allosteric reconfiguration of AMPK allowing for maximal activation of the kinase (78). Cellular ATP levels are increased in the cell by restoring the catabolic function as opposed to the anabolic function, as a result of AMPK activation.

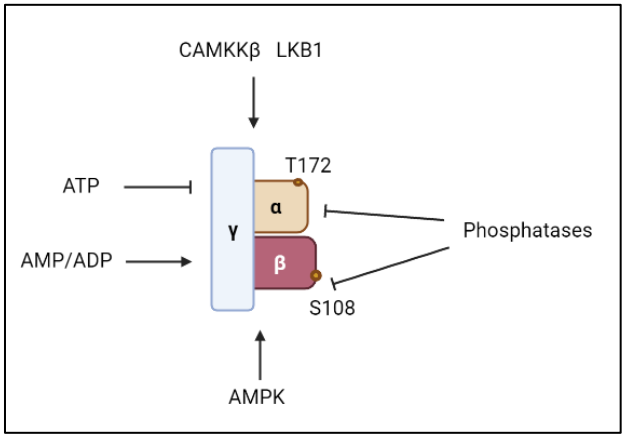

Figure 6: AMPK acts as a heterotrimeric energy sensor. AMPK consists of a catalytic subunit, α (yellow), and two regulatory subunits: β (red) and γ (blue). Binding of adenylates takes place competitively at the γ subunit. As the ratios of AMP/ADP to ATP increase the α subunit gets activated by phosphorylation at T172. AMPK is regulated allosterically by other upstream activators to resist the action of phosphatases. Figure made in Biorender and adapted from (79).

It is believed that the ability of LKB1 to function as a tumor suppresser may be linked to the AMPK activation pathway. The mammalian target of rapamycin (mTOR) is an inhibitory target of AMPK, and regulates important cellular processes such as cell growth, apoptosis and autophagy as shown in Figure 8 (24). The interaction of LKB1 with AMPK has been shown by their co-localization in ciliated MDCK cells

(73). The LKB1-AMPK pathway may have a useful role in promoting tumorigenesis despite LKB1s reputation as a tumor suppressor, leading it to be referred to as a contextual oncogene (60). By regulating metabolic homeostasis, decreasing oxidative stress, and maintaining NADPH levels, LKB1 can protect cells from apoptosis and promote cell survival (81). Thus, LKB1 levels are found to be elevated in many tumors (82). Mutants (null) for AMPK show abnormal cell growth and cell polarity, similar to LKB1 mutants (null), along with a disrupted actin-myosin cytoskeleton (40). Furthermore, AMPK regulates MRLC (myosin II regulatory light chain) through phosphorylation in human epithelial cells and *Drosophila*. The phosphorylation of MRLC is not affected by inhibition of LKB1 and is further increased by inhibition of AMPK in vascular smooth muscle cells (83, 84). This may indicate indirect interaction of AMPK with MRLC leading to regulation of the actin cytoskeleton for polarity control (85). However, the involvement of AMPK towards polarity control is quite unclear still.

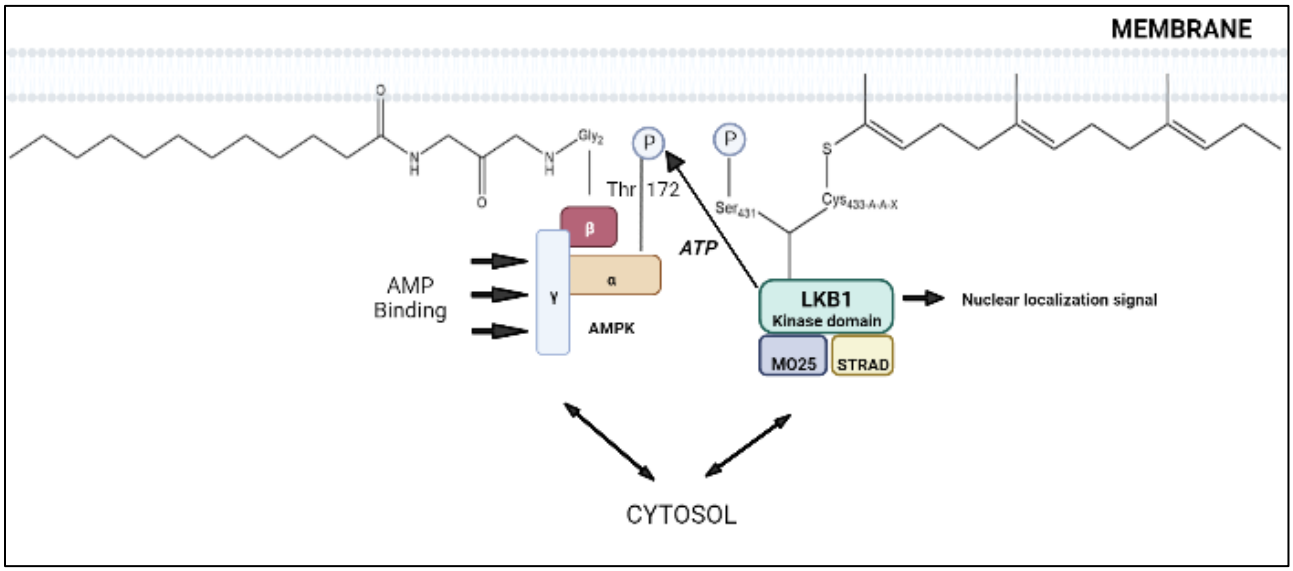

Figure 7: Schematic representation of farnesylation of LKB1 and its interaction with activated AMPK after myristolation. AMPKβ is myristoylated at membranes which allows activation of its catalytic loop, preceding phosphorylation at the Thr172. Similarly, LKB1 in recruited to the membrane through farnesylation at the CAAX box. These lipid modifications localize AMPK and LKB1 to two-dimensional membrane surface making them necessary for membrane association, polarization of oocyte, as well as activation of AMPK. Figure made in Biorender and adapted from (86).

AMPK supposedly has a role in inducing mitophagy (control of mitochondrial health) by recruitment to the mitochondria and association with extracellular membranes, which requires *N*-Myristoylation at AMPKβ by *N*-myristoyltransferase 1 (NMT1) as shown in Figure 7 (87). This in turn promotes cell survival. Myristoylation is essential for recruitment of the AMPK complex in response to mitochondrial damage as shown by Liang *et al*, in H23 cells (87). Myristoylation at the β subunit of AMPK is also important for AMP activation (88). Furthermore, AMPK interaction with ATG16 (autophagy-related) complex is induced

in response to the damage to mitochondria in cells which eventually allows removal of damaged components by autophagy through recruitment to the lysosome. Recently, this has allowed AMPK to become an important therapeutic target for diseases involved in metabolic perturbation, like diabetes, obesity, and cancer. One important example in the context is the use of metformin in type 2 diabetes, which is linked to activation of AMPK and its role in circulating glucose and lipids (89). AMPK activation is suggested to have anticancer properties, although in some cases such as metabolic stress it may promote tumor survival, in turn suggesting the role of AMPK as a contextual oncogene (90, 91).

1.8.3 LKB1 and its interaction partners

AMPK and AMP-related kinases are important interaction partners of LKB1, allowing their activation. However, apart from these several other effectors of LKB1 have been identified in yeast two hybrids using mass spectrometry analysis (20). LKB1 interacts with chaperone proteins (Hsp90, Hsp/Hsc79-CHIP) to help regulate stability and activity. Another target of LKB1 is the LKB1 interacting protein 1 (LIP1), but the effect of the interaction is unclear (21). Brahma related gene 1 (Brg1) and Estrogen receptor α are transcriptional factors (TF) indirectly activated by LKB1 and have a role in regulating growth arrest. The indirect interaction conclusion was made on the basis that there is no proof of these TFs being phosphorylated by LKB1 (92).

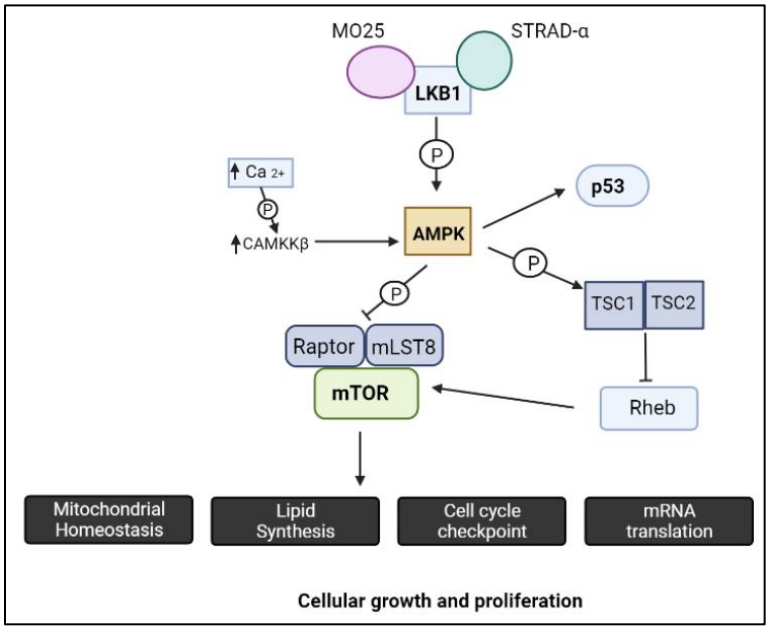

Figure 8: LKB1/AMPK interaction partners. LKB1 is activated in a complex with MO25 and STRAD leading to downstream targeting of AMPK. AMPK is also activated by CAMKK and TGFβ Activated Kinase 1 (TAK1) and inhibits mTOR signaling via two distinct mechanisms: through phosphorylation of TSC and phosphorylation of RAPTOR. Therefore, AMPK negatively regulates translation of proteins, and also inhibits lipid biogenesis by negatively regulating the activity of acetyl CoA carboxylase (20, 90).

As shown in Figure 8, LKB1 acts upstream of AMPK as a tumor suppressor and AMPK acts upstream of the tumor suppressors Tuberous sclerosis complex (TSC) and p53. The activation of AMPK leads to initiation of catabolic metabolism and a switch to processes that restore energy. This leads to a halt of proliferation and increased uptake of glucose by AMPK to maintain homeostasis under conditions of metabolic cellular stress. An imbalance in the AMP/ATP ratio as a response to metabolic stress is essentially normalized by the regulation of AMPK by LKB1 and intracellular Ca^{2+}, by phosphorylation of AMP at a specific site (Thr172) on AMPK at the α subunit. The process is further enhanced by heterotrimeric complex of LKB1 with STRAD and MO25. Calcium/calmodulin-dependent protein kinase kinase (CaMKK) is also able to activate AMPK by increased levels of Ca^{2+} as a response to changes in energy stress in the surroundings.

It has been suggested that LKB1-AMPK regulate TORC1 (target of rapamycin complex 1) at the Ras-related protein 7 (RAB7)/ Lysosomal-associated membrane protein 1 (LAMP1) at the membrane exterior of the lysosome (93, 94). This deduces that membranes play an essential role in providing an appropriate signalling platform for LKB1 as we see in section 1.10.

1.9 Mutated LKB1 and Peutz-Jeghers syndrome (PJS)

PJS is an autosomal dominant disorder by inheritance most often due to germline mutations in STK11/LKB1 (on chromosome 19p13.3) paired with a mutation in the second allele of somatic cells (95). Patients with PJS have characteristic symptoms; hyperpigmentation on the skin, particularly on the hands and lips, formation of hamartomas at an early age which are benign polyps along the gastrointestinal tract and increase in incidence of carcinomas (96, 97). A large proportion of mutations identified are null alleles. These null mutations in the gene were identified as leading to inactivation of LKB1 either due to exonic or complete gene deletions, insertions, or rearrangements (98-100). In turn, only one missense mutation has been identified, in the conserved serine/threonine kinase domain, namely L67P (26, 44).

Figure 9: Hyperpigmentation of a patient with Peutz Jeghers Syndrome. The symptoms are characterized by discoloration of the skin, especially hands and lips and presence of Mucocutaneous pigmentation. Figure retrieved from (101).

The most important health condition associated with PJS is the increased risk of development of cancer (102). The most common malignancy identified in PJS patients are tumors in the breast and gastrointestinal tract. However, the risk of developing cancer in other regions is also considerably high, such as the lung, stomach and pancreas as explained in Table 1 (102-104). The frequency of results from two different studies have been compiled by Giardiello *et al* and Mehenni *et al* (102, 104). The former study was a meta-analysis done across six studies in which a total of 210 patients were observed, showing increase of cancer incidence by age. The latter was a survival study done within a group of 76 males and 73 females (total 149). The study showed low incidence of breast cancer as compared to that performed by Giardiello *et al* for reasons that are unclear, however the risk of cancer is seen to considerably increase across both studies after the age of 50.

Table 1: Incidence of cancer in Peutz-Jeghers Syndrome by cancer site (105). The yellow highlighted columns show the results of the meta-analysis done by Giardiello *et al* including 210 patients from six studies of different ages (102). The green highlighted column shows incidence of cancer as examined by Mehenni *et al* in a total of 149 patients, 73 of which were female and 76 were male (104).

Site/ Cancer	Frequency (%)	Mean Age (years)	Cancer Frequency (fraction)
Breast	54	37.0	1/149
Colorectal	39	45.8	11/149
Pancreas	36	40.8	-
Stomach	29	30.1	-
Lung	15	-	-
Small bowel	13	41.7	4/149
Testis	9	8.6	-
Gynaecological	9	-	7/149
Gastro-oesophageal	0.5	67	6/149

Immunostaining studies of LKB1 have shown moderately high levels in the epithelium of the small intestine, breast, colon, and the stomach of human embryos. Most studies in PJS patients have identified the presence of LKB1 mutations in the germline in 80-94% of the individuals. Polyps identified in PJS are only found in 50% of patients (105).

LKB1 is known as being a suppressor of sporadic cancer through loss of function mutations found frequently in non-small cell lung carcinomas (up to 17% of cases in population studies performed). Inactivating mutations as reported in 5% of cancers of the pancreas, cervix, prostrate and melanomas (25, 33, 106). The characteristic of a hemizygous loss of function of 19p of LKB1 is identified in many cancers, which implies a haploinsufficient function of LKB1 as a tumor suppressor. Some cancers such as breast and testicular cancers show inactivation of LKB1 epigenetically, through promoter hypermethylation (107). There is relatively frequent occurrence of negative mutation analysis in LKB1, up to 28%, which could be due to de novo mutations (frequent in children) with a position unknown in the gene loci or as a result of mosaicism (95). An important aspect to note here is that the levels of LKB1 and not only loss of its function are important to investigate. Mechanisms of controlling levels of signalling are therefore relevant, but currently lacking.

1.10 Endosomal and lysosomal regulation of LKB1

It has been suggested that LKB1 in *Drosophila* and human cells associates with endosomes and is regulated by endocytic trafficking. LKB1 passes from RAB5 to RAB7 compartments (which facilitates the maturation of Rab5 vesicles to Rab7) and CIII-PI3K inactivation causes increased LKB1 signalling and in turn epithelial disruption (108).

Axin is a scaffolding protein and has been shown to directly interact with LKB1 and AMPK directly and cause phosphorylation of the latter in an AMP-dependent manner. Insufficient AMPK activation occurs if Axin is knocked down in mice models, in turn resulting in accumulation of fat in the liver (109). It has been shown in mouse embryonic fibroblasts that the scaffold of Axin, LKB1 and AMPK reaches the late endosome to form a complex with the lysosomal v-ATPase-Regulator complex (93). The formation of the complex aids LKB1 in the activation of AMPK. If the formation of the complex is halted by knocking down one of its components called LAMTOR1, AMPK is no longer activated (93). Moreover, Metformin, a treatment used for type 2 diabetes is shown to cause the formation of the Axin-LKB1-AMPK-v-ATPase-Regulator complex and stimulate the activation of AMPK in the lysosomal dependent manner. In fact, stimulation by metformin has also been shown to increase lifespan in *Caenorhabditis elegans* (*C. elegans*) (110).

It is not known that Axin is a general activator of the function of LKB1 or specifically aids in its downstream substrate recognition or phosphorylation of AMPK. However, what is an established fact is that Axin is a

core component of the Wnt pathway (an important target in tumor cells) as being part of the β-catenin destruction complex (111). Thus, it is speculated that Axin might have a role in the interaction between the Wnt/ β-catenin- and LKB1/AMPK signalling pathways.

While LKB1 can be activated in an endosomal dependent manner, it has also been demonstrated in epithelial cells that dLKB1 and hLKB1 can be negatively regulated (112). On the endosomal membrane the class III phosphatidylinositol-3-OH kinase (CIII-PI3K) comprises of a catalytic subunit called vps34 and regulatory subunits called vps15 and Beclin-1. CIII-PI3K is involved in two different mechanisms namely autophagy and endocytosis distinguished by the presence of ATG14 or UVRAG respectively. CIII-PI3K associates with RAB5 for association with early endosomes and later vesicle maturation leads to RAB7 positive endosomes (113, 114). Production of phosphatidylinositol 3-phosphate (PtdIns(3)P) by PI3K makes a binding site for WD repeat and FYVE domain-containing 2 (WDFY2). WDFY2 regulates LKB1 function and the activation of AMPK which maintains epithelial integrity. In human epithelial cells (Caco-2) normal cyst formation was disrupted when CIII-PI3K was pharmacologically inhibited (112). The inhibition of LKB1 by CIII-PI3K-WDFY2 is important as the loss of this inhibition leads to the oncogenic traits of LKB1 (112).

1.11 LKB1 as an indirect regulator of autophagy

Autophagy is a process which involves several steps conserved through evolution to allow intracellular self-degradation. The housekeeping function of the process allows it to remove proteins and organelles from cells under basal conditions. Autophagy induced on starvation upon metabolic stress can allow to maintain homeostasis by degradation of substrates for energy production (115). Defects in autophagy have been proved to be involved in cancer, neurodegeneration, as well as aging (115).

Autophagy is induced and regulated in response to energy stress, on activation of AMPK (116). AMPK has been conserved through evolution as an energy sensor and regulates homeostasis by restoration of energy through regulation of downstream pathways, such as negative regulation of lipid biogenesis and protein translation (as shown in Figure 10). AMPK, being a downstream target of LKB1 negatively regulates the serine/ threonine kinase mTOR, involved in nutrient sensing, proliferation, and growth (24). Since AMPK is directly involved in the control of the central energy checkpoint in the cell, it can be said that LKB1 indirectly plays a role in energy metabolism in the cell. Furthermore, LKB1 mediates the effect of low energy on the viability of cells, which means that cells which lack or are deprived of LKB1 undergo apoptosis during metabolic stress since the checkpoint is flawed, and cells are unable to detect low energy levels (77). In *C. elegans* dauer it has been shown that LKB1/AMPK signalling is needed for long term survival of cells (117). On the other hand, mice embryos that were mutant for LKB1 or double mutants for LKB1 and AMPK have proved to show early lethality, due to inability to detect metabolic stress leading to

apoptosis (118). AMPK is a negative regulator of mTOR signalling, thus the LKB1/AMPK pathway is believed to promote autophagy by regulating the activity of mTOR (119). The classic way of initiating autophagy is through RNAi knockdown of Chico, an important substrate of insulin receptor, or through starvation in low nutrient conditions as shown in Figure 10 (120). The LKB1-AMPK regulation of mTOR is directly linked to autophagy but AMPK can also directly regulate autophagy through a mechanism involving the phosphorylation of Unc-51 like autophagy activating kinase 1/ Atg1 (ULK1/Atg1)(121). LKB1 itself may also lead to direct stimulation of autophagy by regulating p27 but the exact mechanism of a starvation-induced autophagy through LKB1 signalling in vertebrates is still unknown (122).

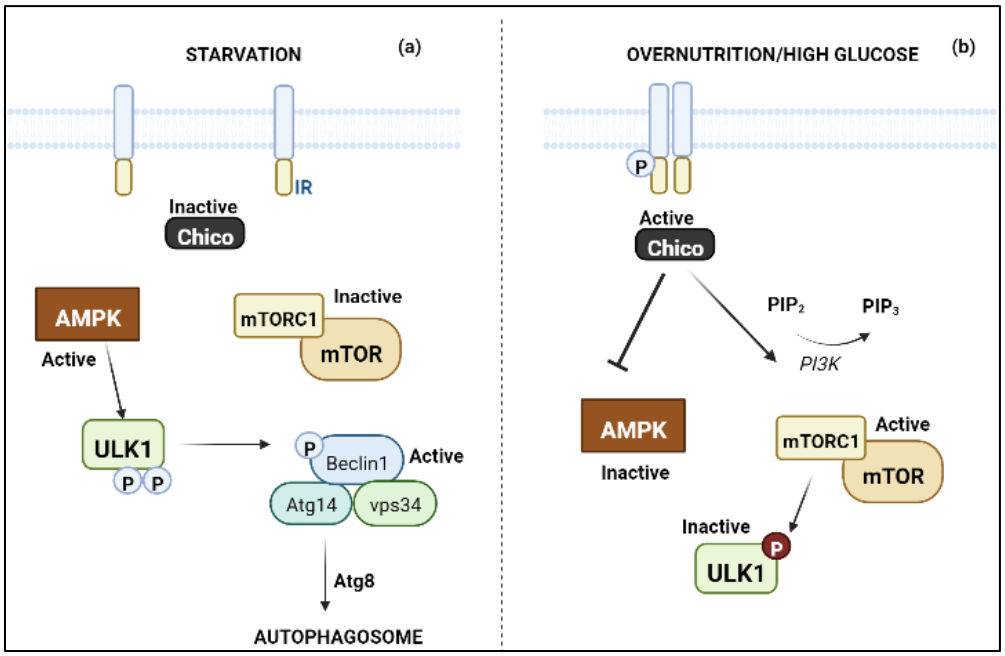

Figure 10: Regulation of autophagy by insulin signaling and starvation. (a) The conventional activation of autophagy happens through starvation when insulin signaling is blocked. In low nutrient conditions or genetic starvation where Chico, an insulin receptor substrate is inactivated, AMPK is activated which phosphorylates ULK1, at two different sites. ULK1 phosphorylates Beclin1 which works along with other components to first form a phagophore and then conjugate through Atg-dependent pathways (Atg5-Atg12) to an autophagosome. (b) In the case of overnutrition, or overexpression of Chico, PI3K is activated, which eventually allows activation of mTOR and inactivation of AMPK. The TORC1-mTOR complex inactivates ULK1 so mammalian autophagy cannot be induced. Figure adapted from (123) and made in Biorender.

It has been shown in previous studies that LKB1 interacts with AMPK on endosomes as a result of lipid modification (108). LKB1 has a functional CAAX box where prenylation happens and AMPK is myristolated, both being present on the membranes. Furthermore, it has been shown by O'Farrell *et al*. that LKB1 associates with Rab5 and Rab7 vesicles near to the plasma membrane. Blocking the effect of vps34 or Rab changes the localization of LKB1 and leads to augmented activation of AMPK (112). Another

research group claimed that basic lysine residues if mutated in LKB1 are important for localization on vesicles (124). However, the journey of LKB1 from the plasma membrane to its destination is not clear, in terms of questions of whether it is sorted, recycled, or associated with other organelles. Also, the role of LKB1 in autophagy has also not been investigated, which should be positively regulated with AMPK.

2. Aims and Objectives

The primary aim of the study is to map out the localization of LKB1 and its activity under normal conditions and when modulating trafficking regulators, while also taking interest in the localization and activity of AMPK. To accomplish this, we will disrupt normal trafficking to identify key regulatory steps. Finding out whether LKB1 recycles to membranes or to the lysosome or both and whether AMPK as a downstream target of LKB1 has an overlapping route.

Specific Objectives:

- A major objective is to develop tools capable of monitoring LKB1 location in control and marked tissue side-by-side within the same tissue. Develop three recombinant fly lines with overlapping usefulness capable of labelling an area within a field of cell expressing GFP-tagged LKB1 (recombinant fly lines shown in appendix II).
- To confirm the validity of the approach, several lines of control experiments were needed – LKB1 non-localizing mutant, LKB1 RNAi and disruption of known LKB1 trafficking regulators, such as Wdfy2 and vp34 designed to reveal delocalization or inactivation of LKB1, by monitoring GFP expression.
- Inducing autophagy through genetic starvation, by disrupting insulin signaling regulators such as Chico and see its effect on the localization and levels of LKB1 as an effect of autophagy.

3. Materials and Methods

3.1 Working with flies

Flies were bred at 25˚C or 18˚C and a humidity of 65% at the typical conditions of food, unless otherwise required. The former temperature allowed the fastest generation time of about 9 to 10 days until the emergence of the adult while the later temperature increased the generation time by about 2 to 3 days. Flies kept at 25˚C were maintained once every week by substituting vials having old food with vials having newer food.

3.1.1 Fly Food

The standard medium was made with 80 g agar, 300 g dry yeast, 360 g instant potato mash, 660 g sugar, 22 g of Nipagin in 50 mL of ethanol, 50 mL of propionic acid solved in 11 L of water. Culture vials of 28.5ml were used to fill up with fly food.

3.1.2 Anaesthesia for flies

Carbon dioxide was used to anaesthetize flies for the purpose of examination. The container for flies was emptied onto a rectangular pad connected to a carbon dioxide outlet to anaesthetize the flies.

3.1.3 Virgin collection

All crosses that were set-up with male and female flies were set with virgin flies (♀) of known genotype. Once the virgin female is fertilized after the event of mating she can lay eggs for many days, since she has the ability to store the sperm in the spermathecae and seminal receptal. The characteristic features of the virgin female include a dark meconium in the gut and translucent body, which is visible through the ventral abdominal wall. Within 5 hours of emerging from the pupal case the female is consider immature, hence repeated emptying of vials is key to quickly collecting virgins. A watercolour brush of size 6 or 4 was used to move around the flies and observe the flies and spot the virgins.

Figure 11: *Drosophila* virgin fly. The virgin female has a translucent body and visible presence of food/ meconium in the gut.

3.1.4 Identification of markers for distinguishing genotypes

The fly stocks which were used consisted of distinguishable phenotypes, either present in balancer chromosomes as markers or otherwise, through P-element insertion. Selection of virgin females and males was done on the basis of these markers for the purpose of our genetic crosses of interest (refer to Appendix III, for visual representation of markers). Table 2 summarizes the key markers that were used to distinguish and select fly populations of interest. A watercolour brush of size 6 or 4 was used to move around the flies and observe the flies and spot the virgins.

Table 2: *Drosophila* fly genetic markers and phenotype. Balancers used in study along with their characteristic markers are shown. For visual representation of the genetic markers observed during the study, please refer to the appendix.

Selection Marker – presence in balancers	Phenotype
***Tubby* (Tb) – present in TM3, TM6c**	Tubby larvae and adults, with shorter body segments and reduced size of the fly overall.
***Stubble* (Sb) – present in TM3 and TM6c**	Flies characterized by shorter bristles
***Curly* (Cy) – present in CyO**	The wings curl away from the body such that the flight is sometimes affected
***Drop* (Dr)**	The size of the eye is severely reduced and contains less than 30 ommatidia. The shape of the mutant eye resembles an inverted drop
***Serrate* (Ser)**	Repression of wing so it shows as if it is sliced and also discoloured
***Sternoplural* (Sp/sp)**	Can exist as loss of function and gain of function. Effects the number of bristles.
w+ (X-linked marker)	Red eye
w- (X-linked marker)	White eye

Table 3: Selection of markers from a genetic cross. This particular genetic cross was performed in order to cross with our double balanced recombinant stocks of interest (refer to Schemes in Appendix II), to eventually make stable stocks for experiments related to localization of intracellular trafficking regulators with LKB1. The table shows a few of the many possibilities of the AB cross. Our desired genotype was (c), and that could be obtained by selection against sp (*sternopleural*) characterized by an increased number of bristles. An interesting point to note here is that (b) will die due to presence of double balancer emerging together on the 3rd chromosome making the fly lethal. In such a cross the expected percentage of getting the correct outcome (c) was 25%.

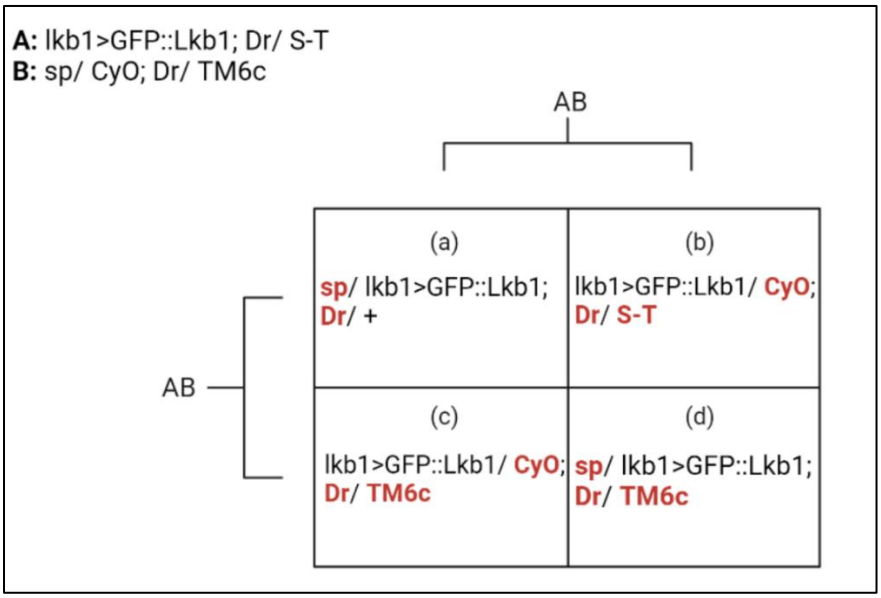

3.2 Larvae Dissection and collection of wing imaginal discs

Wing discs were extracted from larvae at the 2nd instar or 3rd instar stage. The larvae were put on a drop of 1XPBS (8 g NaCl, 0.2 g KCl, 0.24 g KH_2PO_4 in 800 mL of distilled H_2O, 1.44 g Na_2HPO. The pH was adjusted to 7.4 with HCl. And the volume made up to 1 L with H_2O) and dissected using forceps (Dumont # 5) and a syringe under a light microscope. The wing discs along with the other discs are attached to the trachea and the brain. The wings were fixed in 4% formaldehyde (in 1XPBS) in a 12-well plate for 20 minutes followed by two washes with 1XPBS for 20 minutes each. After that they were stained as required with 1ug/ml of Hoechst for nuclear staining and mounted on to a slide using n-Propyl gallate (NPG) for imaging. The wings were imaged using transmitted light microscopy or confocal microscopy.

3.2.1 Fixation and antibody staining of wing discs

After dissection of larvae to extract the wing imaginal discs, they were fixed in 4% formaldehyde and then rinsed three times in PBT (1XPBS and 0.1% Triton X). Following that three washing steps were performed in PBT with a 20-minute incubation each. The discs were permeabilized by incubating them with PBS with 0.1% Triton X and 0.5% BSA for 20 minutes. The primary antibody (diluted 1:300) was added in PBS with

0.1% Triton X and 0.5% BSA and the sample was kept overnight at 4°C on a rocker. The next day, the primary antibody was removed, and the discs were washed three times in PBS with 0.1% Triton X and 0.5% BSA for 20 minutes each. Following that, the secondary antibody was applied (diluted 1:500) in PBS with 0.1% Triton X and 0.5% BSA for two hours at room temperature, or overnight at 4°C on a rocker. Afterwards the discs were washed three times with PBS with 0.1% Triton X and 0.5% BSA for 20 minutes each. Subsequently, the discs were stained with Hoechst (10ug/ml) for 20 minutes (Hoechst solution 1: 10,000 in PBT) and washed once with PBT. Finally, the discs were mounted onto a microscope slide in NPG.

3.3 Fly stocks

Fly lines were either made by site-specific insertion or random insertion using P-elements. These were taken from different sources as shown in Table 4.

Table 4: Fly lines and sources.

Stock	Map (Chromosome)	Description	Reference
rn-Gal4/ TM3	Chr 3	Gal4 driver line. Expressed in a ring in the leg disc, in an antennal portion in the eye disc, a central region of the haltere disc and in the central and notum of the wing imaginal disc.	Bloomington #8142
sp; >ChSNF1a/ S-T	Chr 2, Chr 3	mCherry-tagged SNF1A/AMP-activated protein kinase expressed under control of UAS promoter	Bloomington #32182
> mCD8ChRFP	Chr 3	Cherry RFP fused to mouse CD8 extracellular and transmembrane domains under control of a UAS promoter	Bloomington #27391

**Remaining contents of the table, on the next page*

en-Gal4, ChAtg8/ S-T	Chr 2, Chr 3	Expresses Gal4 in the posterior compartment of embryonic segments. Expresses mCherry-tagged Atg8 a nuclear localization sequence under UAS control.	Bloomington #1460
lkb1>GFP::Lkb1; Dr/ S-T	Chr 2, Chr 3	GFP driven LKB1 expression in the cell membrane.	
sp/ CyO; Dr/ TM6c	Chr 2, Chr 3	Double balancer stock	
lkb1>GFP::Lkb1; rn-Gal4/ TM3	Chr 2, Chr 3	GFP driven LKB1 expression in the cell membrane. Gal4 expressed in a ring in the leg disc, in an antennal portion in the eye disc, a central region of the haltere disc and in the central and notum of the wing imaginal disc.	
ap-Gal4; ChWdfy2/ S-T	Chr 2, Chr 3	Expresses Gal4 in the dorsal compartment of embryonic segments. Expresses mCherry-tagged Wdfy2 in the endosomes under UAS control.	
> ChWdfy2	Chr 3	Expresses mCherry-tagged Wdfy2 in the endosomes under UAS control.	

3.3.1 Wild type LKB1 stock

The original stock was obtained from Dogliotti *et al* and was generated using phiC31-mediated germline transformation on attp40. The expression of LKB1 was obtained as a result of an endogenous promoter to express GFP-tagged LKB1. The cDNA of wild-type LKB1 was cloned into pENTR using a standard polymerase chain reaction (PCR) on a full-length EST clone as a template (*Drosophila* Genomics Research Centre). The forward and backward primers used are as follows; LKB1-F: 5'-CACCATGCAATGTTCTAGCTCTCGG-3', LKB1-R: 5'- CTACGAAGTTCGGCAGTGG-3'. Expression of LKB1 from its endogenous promoter was done by inserting a genomic fragment into pENTR (placed 1kbp downstream of the stop codon and 2.8kbp upstream of the translation start site). The following primers were using for the insertion; LKB1gen-F: 5'-GGCTCCCACTAGCGTAATTTGACGG-3', LKB1gen-R: 5' CTCGAGCAGCCAGTACGGTCATCTC-3'. The start codon was replaced by an XbaI cutting site in a PCR with the following primer: LKB1gen-XbaI-F-

GGCTCCGCGGAGGTTTTCTAGACAATGTTCTAGCTCT-3'. GFP was inserted using PCR and standard ligation after being inserted into the XbaI site.

3.3.2 Balancer stock

A double-balanced (DB) stock was conveniently used to introduce balancers to flies. Presence of two balancers in the stock ensured a high chance of maintaining the genotype of flies being made.

	Chromosome	
	2nd	3rd
Double Balancer Stock (DB)	$\frac{sp}{CyO}$	$;\frac{Dr}{TM6c}$

3.3.3 Stocks used for RNAi experiments

Table 5: RNAi fly lines used for knockdown of controls.

Stock Number	RNAi lines
1216	>LKB1IR (on the 3rd chromosome)
1236	>LKB1IR/ S-T
1150	>WDFY2IR/S-T
1211	>apvps34IR/S-T

3.3.4 RNAi line used for starvation experiments

For knockdown of Chico $\frac{lkb1 > GFP :: Lkb1}{CyO} ; \frac{> ChicoIR}{TM6c}$

3.4 Collection of recombinants

The genetic crosses and schemes needed for generation of our three fly-lines can be found in the Appendix II. In order to generate recombination, it was ensured that an unbalanced virgin female was crossed to our double-balanced stock. The larvae at the 2nd and 3rd instar stage and pupa were observed under a light microscope using a green light beam (510 – 540nm) with an 600nm long-pass RFP filter. Larvae displaying

fluorescence in imaginal discs, and pupa displaying fluorescence in the wing region were selected and allowed to grow into adults. Adults were examined for balancer phenotypes to ensure they were balanced.

In the case where fluorescence was not visible through a light microscope, two different methods were followed. The first method involved, selection of random pupa, and observation on a high-powered microscope through arranging carefully on a slide with the pupa sandwiched in between the cover slip and the slide using a double-sided tape. The second method involved identification of recombinants through high colour of adult flies.

3.5 Confocal and Wide-field Microscopy

Whole mount images of the *Drosophila* larval wing disks were captured in the Olympus Fluoview FV3000 confocal laser scanning microscope using 10X, 20X and 40X objective (with silicon). The software used was ImageJ with Olympus plugin. The same images were also captured in the Leica DMI60000B Wide-field microscope at an objective of 10X and 20X. Pupa were also examined to spot recombinants in the later microscope using 10X as objective.

Structural prediction modelling was done in PyMOL, Molecular Visualizing System and through ColabFold: AlphaFold2 using MMseq2.

3.6 Reagents

Table 6: Antibodies and mountants used

Name/ Catalog number	**Supplier**	**Application**
Rabbit anti-GFP polyclonal antibody, A-11122	Thermo Fisher Scientific	Antibody staining of wing discs
Fluorescein (FITC) AffiniPure Goat Anti-Rabbit IgG (H+L), AB_2337972	Jackson ImmunoResearch	Antibody staining of wing discs
Propyl gallate, Cat. No. 02370	Sigma-Aldrich	Mounting wing imaginal discs
ProLong™ Glass Antifade Mountant with NucBlue™, P36985	Thermo Fisher Scientific	Mounting wing imaginal discs

Table 7: Other buffers and reagents

Chemical/Stock	Composition/ Supplier	Application	Catalog Number
Potassium Chloride (KCl)	Merck	Component of PBS	1.04936
Sodium Chloride (NaCl)	Sigma-Aldrich	Component of PBS	31434N
PBS (phosphate buffer saline) 1 liter	0.2 g KCl 0.24 g KH2PO4 1.44 g Na2HPO4 6 g NaCl 800 mL Milli-Q water pH adjusted to 7.4 with HCL Milli-Q water to a total of 1 L	Larval Dissection and Dilution of reagents used for antibody staining	-
Hoechst Solution (10 ug/ml)	1:10,000 Dilution with 1X PBS/ Thermo Fisher Scientific	Nuclear Staining	33342
Triton X-100 (0.1%)	Diluted in 1X PBS	Antibody staining protocol	9036-19-5
PBT (Phosphate buffer saline Tween)	1XPBS, 0.1% Triton X-100	Antibody staining protocol	-
PBSBT	1XPBS, 0.1% Triton X-100, 0.5% BSA (Bovine Serum Albumin)	Antibody staining protocol	-
Formaldehyde (4%)	Diluted in 1XPBS/ Sigma-Aldrich	For fixation of wing discs	11-0735
n-propyl gallate	90mM propyl gallate in 90% glycerol and 10% PBS, pH 7.4	Mounting wing imaginal discs	-
BSA (Bovine Serum Albumin)	Sigma-Aldrich	Antibody staining protocol	A8531

3.7 Statistical Analysis

ImageJ with Olympus plugin was used to extract raw data from confocal images (for rectangular regions selected nearly two-cells apart) and were analysed on Microsoft Excel and ImageJ analysis functions to

find two parameters: slope average, and average total intensity. A two-tailed t test was done to concur the difference between parameters, where the null hypothesis stated that there was no difference in means between parameters (NS-Not Significant). P values obtained from the statistical test with $p<0.05$ were considered to be significant, and $p<0.005$ were considered to be very significant.

3.7.1 Calculation of Slope Average

The values of intensity against distance in microns was copied on excel. As shown in Figure 12, cell C2 was used to get the difference of intensity values, cells B2 and B1, and the same was done for the rest of the intensity values to get a column C. Cell D2 was used to get the difference of distance values, cells A2 and A1, and the same was done for the rest of the distance values to get a column D. Column E was used to get values for all the ascending and descending peaks occurring (differentiating them from troughs/ noise) for intensity against the distance in microns for which the following condition was used: IF(AND(C3<0,C2>0),1,0). The condition gave a value of 1 to all ascending and descending peaks and a value of 0 to all the troughs in column E. All the values of intensity difference and distance difference having a value of 0 were filtered out and only those with a value of 1 were used for calculation of the slope average (average for gradient of peaks). The gradient or 'slope' was calculated as intensity difference divided by distance difference (Gradient=Intensity difference/Distance difference=y_2-y_1/x_2-x_1) in Column F. An average of the slope could then be calculated.

(a)

	A	B	C	D	E
	Distance	**Intensity**			**Condition for filtering**
1	0.0	4957.4			
2	1.2	4864.7	B2-B1	A2-A1	IF(AND(C3<0,C2>0),1,0)
3	2.8	4880.7	16.0	1.6	0
4	3.7	4892.9	12.2	0.9	1
5	5.3	4650.6	-242.3	1.6	0
6	5.9	4850.3	199.7	0.6	1
7	6.8	4589.7	-260.6	0.9	0
8	8.4	4647.3	57.6	1.6	1
9	9.0	4459.6	-187.7	0.6	0
10	9.6	4458.1	-1.5	0.6	0

(b)

Peaks obtained

	A	B	C	D	E	F
1	0.0	4957.4				GRADIENT
4	3.7	4892.9	12.2	0.9	1	=C4/D4
6	5.9	4850.3	199.7	0.6	1	321.292
8	8.4	4647.3	57.6	1.6	1	37.07472
11						
12					SLOPE AVERAGE->AVERAGE OF COLUMN F	123.81

Figure 12: Calculation of slope average in Microsoft excel. Column A and B represent Distance in microns and Intensity, respectively. Column C represents the intensity difference and column D represents the distance difference. (a) Represents condition specified for extraction of peak values. (b) Represents peaks filtered and Column C and Column D used for calculation of the gradient or slope. The slope average was calculated as highlighted in yellow, a value of 123.81 in the given example. The values in the table are not from a real data set and are quoted as an example.

3.7.2 Calculation of Total Intensity

Two different methods were used for the measurement of total intensity for a selected region of a wing disc. Method (1) was using ImageJ software to get a plot profile for a particular area and then using the 'Analyse particles' function in ImageJ to get the area under the plot. Method (2) used Microsoft excel to plot the extracted peaks obtained by the same method as in Figure 13 and obtaining a trendline (polynomial type) for the plot. An integral of the equation obtained from the trendline was used to measure the area under the graph (for the plot obtained with the troughs/ noise filtered out as in Figure 12 and consisting of only the peaks) as shown in Figure 13.

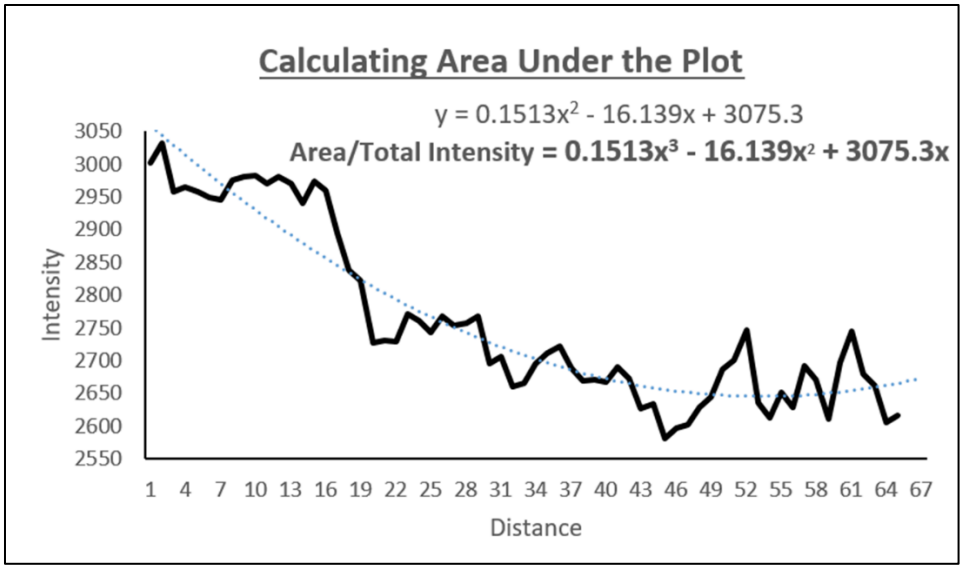

Figure 13: Calculating Total Intensity as area under the plot. A trendline (blue dotted line) was for obtained for the plot of intensity against distance. The integral of the equation of the trendline was taken to calculate area under the plot.

4. Results

4.1 Genetic recombination can be induced in *Drosophila Melanogaster*

In accordance with our major aim, we wanted to construct tools which could be used for the purpose of observing LKB1 localization in different regions of the wing disc and which could be later used to compare control and marked tissue side-by-side within the same disc. We used the fact that recombination events occur only in females in *Drosophila* to our advantage for the construction of these recombinant tools. We started with a stock consisting of red-eyed (w+) flies with *rotund* on the 3rd chromosome along with GAL4 driver and a TM3 balancer with *Stubble* (*Sb*) as an obvious physical marker, and also the *Serrate* marker (*Ser)*, rnGAL4/TM3. These flies were crossed with UAS (symbol used for UAS '>') adjacent to gene of interest sequences either Cherry tagged (Ch) or consisting of RFP; (1) >CD8ChRFP, (2) ChSNF1a, (3) ChWdfy2. mCD8 would prove as a marker on the cell membrane and could be used to see co-localization with LKB1. ChSNF1 also known as AMPKα-subunit could be used to map down its interaction with LKB1 by checking for co-localization and for marking the kinase domain region. Wdfy2 localizes on the endosomes and is also found to interact with LKB1 so its co-localization with LKB1 could potentially give information about the localization of LKB1 on endosomes (38). After documenting normal localization of LKB1 with these RFP components, RNAi screening could be performed to disrupt localization and hence determine which factors are normally important in this context.

The schemes (Scheme 1, 2 and 3) as shown in the appendix (II) were used for the construction of stable recombinant stocks. The wild-type GFP-LKB1 stock was double balanced by crossing with the DB stock. For the initial cross of gene of interest with rnGAL4/TM3 there was a distinct probability of obtaining flies which had rn-GAL4 along with gene of interest on the 3rd chromosome across different lines: 33% for obtaining rn-GAL4/>ChSNF1a, 50% for obtaining rn-GAL4/>ChWDFY2 and 50% for obtaining rn-GAL4/>mCD8ChRFP. Of that there was another 50% chance of the flies being female (crosses 2, 4 and 6 in Appendix I) as shown in Figure 14. We checked that RFP was visible at the first cross stage prior to looking for recombinants. Consequently, virgin females were selected at this stage due to their ability to cause recombination (as shown in cross 3,5 and 7) in Appendix I. The following stage was crucial for selection of recombinants which usually showed a florescent pattern on adjacent precursor wings at the larval and pupal stage (as shown in Figure 14a). Recombinants for >CD8ChRFP were visible in a light microscope using an RFP filter, but not for ChWdfy2 and ChSNF1a. The frequency of recombination for the latter two cases seemed less and the fluorescent properties were weaker in comparison to >CD8ChRFP. For obtaining recombinants of ChWdfy2 and ChSNF1a random selection of larvae and pupa were done. These were allowed to grow into adults and the final step of the scheme completed, followed by dissection and observation of an RFP signal in the *rotund* region of the wing disc (wing pouch) to see if a recombinant

was selected as the first place. Flies negative for RFP signal were discarded and the selection was repeated several times.

An alternative used for identifying recombinants in >ChSNF1a was to do selection by eye color of the adult. For that purpose, instead of w+(red-eyed) rnGAL4/TM3 line, a w- (white-eyed) rnGAL4/TM6c line was used. If >ChSNF1a flies were yellow eyed and when mated with white-eyed flies and having induced recombination would give orange-eyed adults. However, this method and the method of random selection did not work for the >ChSNF1a line. We were successful in making two double-balanced recombinant fly lines for >CD8ChRFP and >ChWdfy2 as shown in Figure 14(b) (Scheme 2 and 3 in Appendix II). These lines could then be crossed to double-balanced GFP-LKB1 stock to obtain two recombinant fly lines with GFP-LKB1 on the second chromosome and recombinant gene of interest of the third chromosome. These stocks were suitable for subsequent screening. A summary of selection for and against physical markers and possibilities of genotypes for generations is shown in Figure 14(b).

(a)

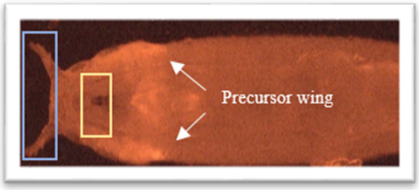

(b)

Scheme	Cross	Marker/ Balancer (Selection For or Against)	Desired Genotype - Probability
1	2	Against Ser and Stubble/ Against TM3 and S-T	rnGAL4/>ChSNF1a ♀ - 16.5%
	3	For Sp, Curly (CyO), Tubby/ Stubble (Tm6c) and against Drop	sp/CyO;rnGAL4 | >ChSNF1a/Tm6c
2	4	Against Ser and Stubble/ Against TM3 and S-T	rnGAL4/>ChWdfy2 ♀ - 25%
	5	For Sp, Curly (CyO), Tubby/ Stubble (Tm6c) and against Drop	sp/CyO;rnGAL4 | >ChWdfy2/Tm6c
	9	Against Sp and Drop, and for Stubble (TM6c) and Curly (CyO)	lkb1>GFP::Lkb1/CyO; rnGAL4 | >ChWdfy2/Tm6c **Stock Number: 250**
3	6	Against Ser and Stubble/ Against TM3 and S-T	rnGAL4/>CD8ChChRFP ♀ - 25%
	5	For Sp, Curly (CyO), Tubby/ Stubble (Tm6c) and against Drop	sp/CyO;rnGAL4 | >CD8ChRFP/Tm6c
	10	Against Sp and Drop, and for Stubble (TM6c) and Curly (CyO)	lkb1>GFP::Lkb1/CyO; rnGAL4 | >CD8ChRFP/Tm6c **Stock Number: 150**

Figure 14: Genetic recombinants can be obtained in *Drosophila* through planned crossing schemes and selection criteria. (a) The 3rd instar larvae shown shows RFP signal in adjacent precursor wing region behind the mouth hooks and either side of the trachea. (b) Shown is a summary of the selection criteria and probability of occurrence to eventually obtain the desired recombinant genotype. Refer to the Appendix I and II for crosses and crossing schemes.

Wing discs from fly lines 150 and 250 were dissected and the presence of the GFP signal and RFP signal for LKB1 and CD8ChRFP or ChWDFY2 respectfully (in the *rotund* region), was confirmed. The images were taken at 40X on a confocal microscope and are shown in Figure 15. An estimate of the membrane localization of GFP and RFP represented proteins was done by selecting three different regions for n=1 for 150 and 250 recombinant fly lines. ImageJ with an Olympus plugin was used to obtain a plot profile for a particular region selected like the one shown in a white rectangular region in Figure 15. This raw data gave values of Intensity against Distance in microns. The raw data extracted from these regions was used to calculate three essential parameters; **total intensity** (area under the plot) which gave information about the magnitude of the signal or the expression level, **number of peaks** (which would relate to the signal present in either the cell membrane or cytoplasm in the number of cells within the region selected), and **slope average** of peaks (which would give information about the proximity of the signal intensity to the cell membrane). The steep peaks or a higher slope average represented close proximity to the membrane. Broader peaks with a low slope average represented presence of signal in the cytoplasm (including endosomes and nucleus).

The slope average (for 3 regions) obtained for LKB1-GFP was 120.1 for fly line 150 and 125.3 for fly line 250 respectively as shown in Figure 15. The slope average for CD8ChRFP (localized on the membrane) obtained was 246.3 and that for ChWDFY2 (localized in the cytoplasm and endosomes) was 116.5 respectively. The total intensity was measured using the 'Analyse particles' function on ImageJ and also using an integral of a polynomial line to find the area under the plot in Microsoft excel. It was found that the second method in Microsoft excel was more appropriate for our study and thus was used for the rest of the experiments. A high total intensity and slope average was seen for mCD8 which confirmed its expression in close proximity to the membrane. Lower levels of WDFY2 were observed in general compared to mCD8 as shown by a low total intensity.

Although information for the localization and levels of proteins represented by the RFP signal could be estimated by the slope average and total intensity values for RFP respectively, the same for LKB1 needed to be confirmed in the wild-type LKB1 stock (lkb1>GFP::Lkb1; Dr/ S-T).

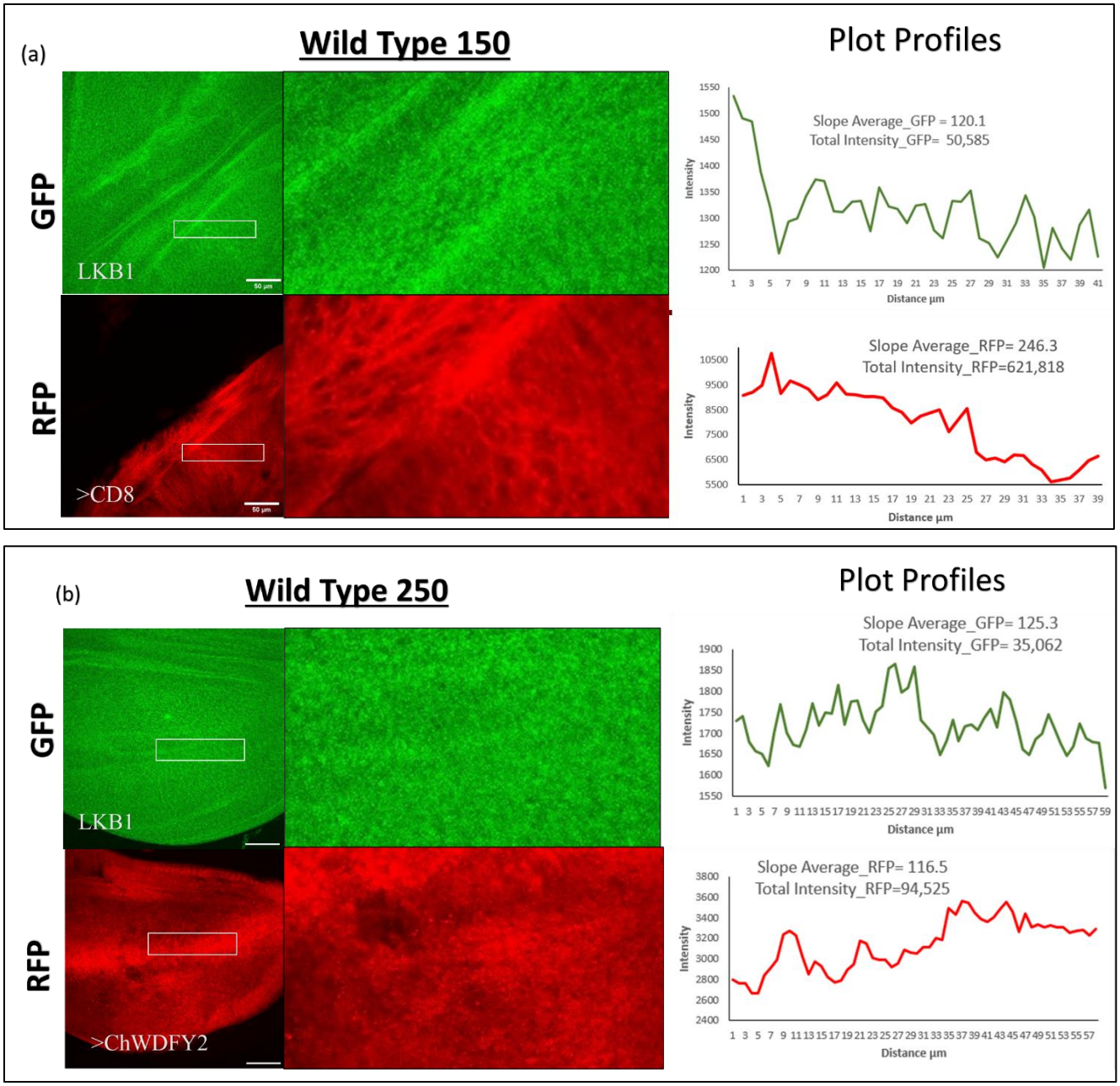

Figure 15: Relative comparison of protein localization in fly line 150 and 250. GFP represents LKB1 localization and levels, and RFP represents mCD8 and ChWDFY2 localization and levels using slope average and total intensity, respectively. Three different regions for one disc were selected and an average of parameters taken for both fly lines 150 and 250 (a) mCD8 represented by RFP consisted of steep peaks with a high slope average and visually seen to have a membrane-like signal. (b) 250 consisted of the WDFY2 represented by Cherry-tagged signal, consisting of broader peaks with a low slope average. Inset X-Z section (4-6µm) and the line intensity graph is through the indicated region in white rectangular selection in RFP (red) and GFP (green) sections represented. Scale bars used in all images, 50µm.

4.2 Expression of GFP-tagged wild-type LKB1 from its endogenous promoter is found on the cell membrane

To investigate previously uncharacterised LKB1 localisation in wing disc epithelial cells, we investigated expression and localisation in *Drosophila* wing imaginal discs. Wing discs were dissected from tubby larvae from lkb1>GFP::Lkb1; Dr/ S-T stock as well as the lkb1>GFP::Lkb1/CyO; Dr/Tm6c stock (obtained from Cross 1 in Appendix I) and observed for GFP signal using an EGFP (enhanced-GFP) filter and Hoechst nuclear filter on a high-powered brightfield microscope as well as a confocal microscope. In the initial observations a low signal of GFP was observed for repeated experiments (n=3). Thus, the process was instead done using an antibody against GFP and the experiment repeated two times (n=2). A stronger GFP signal was observed with anti-GFP antibody as compared to without the antibody; average intensity total (AIT) for anti-GFP antibody with value of 257,200 and AIT for without antibody of 53,450 (80% of increase in signal magnitude of the GFP). GFP expression showed membrane localization which was representation of the fact that endogenous wild-type LKB1 mostly localizes to the (lateral) membrane of the *Drosophila* wing imaginal disc.

As shown in Figure 16, an estimate of the membrane localization of endogenous LKB1 was done by selecting several regions in the disc for two separate experiments (n=2) and obtaining a plot profile which gave values of Intensity against Distance in microns. The steep peaks were representative of close proximity of LKB1 to the cell membrane while broader and less steep peaks represented probable localization in the cytoplasm. An overall slope average obtained for 5 regions for n=2 for GFP-LKB1 wild type (using antibody staining) was 178.7.

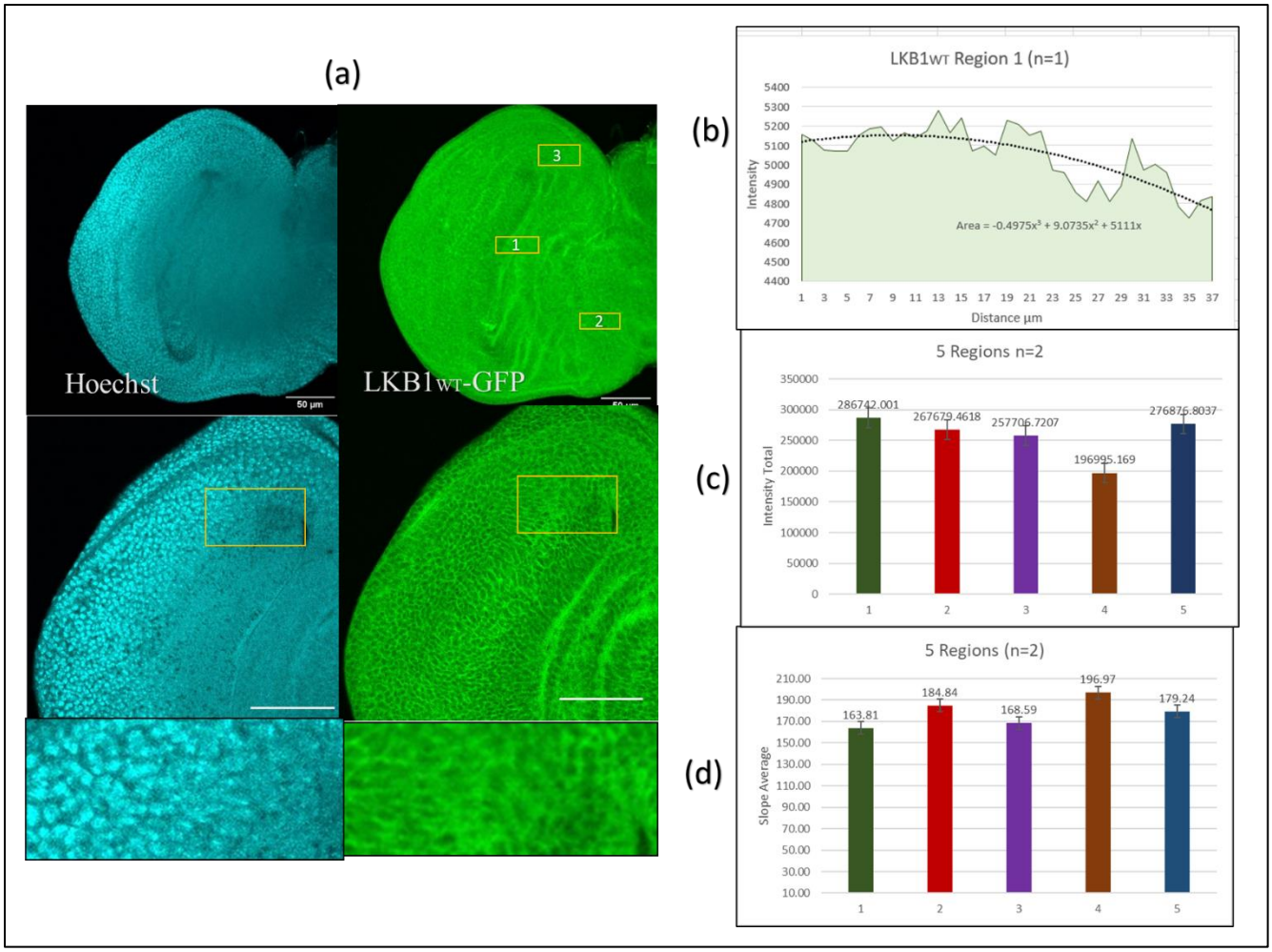

Figure 16: Endogenous GFP-LKB1 localizes to the plasma membrane in *Drosophila* wing discs. (a) For experiments repeated two times (n=2) using anti-GFP antibody, LKB1 was found to localize mostly in the (lateral) cell membrane. The blue signal is the Hoechst nuclear signal, and the green signal is for $LKB1_{WT}$-GFP (b) The yellow rectangular region in (a) highlight regions randomly selected to retrieve raw data on ImageJ (5 regions selected in two separate discs) for intensity against distance (µm). The area highlighted in light green gave the area under the graph to intensity total for Region 1 of n_1 (c) A bar graph was plotted for total intensity obtained for 5 regions for n=2. The AIT was 257200. (d) A bar graph of the slope average was obtained for 5 regions for n=2. The total slope average was calculated as 178.7. The error bars shown represent standard error. Scale bar is 50µm in (a).

4.3 Mutation in LKB1 CAAX box region and LB domain disrupts its cellular localization

It has been discussed that LKB1 leaves the nucleus to form a heterotrimeric complex and then finds its way to the cytoplasm. We worked with the wild-type endogenous LKB1 construct which was formed through site-directed P-element insertion and confirmed it to be mostly present on the cell membrane. As a

comparative control of LKB1 membrane localisation, we compared a mutant LKB1 version with mutations in the CAAX (Cysteine to Adenine at 564 position) box region and the lipid binding (LB) domain (Lysine to Adenine at positions 539-541, 546, 550-551 and Arginine to Alanine at positions 547-548); LKB1 ΔLBCA, to see if the effect of the mutation is a change of localization of LKB1 as it had been documented to be in (108) in *Drosophila* and mammalian cell culture. Wing discs were extracted from tubby larvae from lkb1>GFP::Lkb1 LBCA/ S-T stock and observed for GFP. In this case as well, similar to wild-type LKB1 initially a weak signal for GFP was seen (with at AIT of 41,500). To increase the signal intensity an anti-GFP antibody was used which increased the AIT to 195828 (80% of increase of signal magnitude for 5 regions and n=2), calculated as area under the plot as shown in Figure 17(a) (shown for Region 1 of n_1). As shown in Figure 17(a,b) the GFP signal seemed to be disrupted for LKB1 ΔLBCA mutant.

The peaks obtained for LKB1 ΔLBCA were broader and less steep representing lesser localization in the cell membrane and probably more in the cytoplasm as compared to endogenous LKB1 wild type (Figure 17d). The slope average for LKB1 ΔLBCA came out to be **116.3** which was reduced as compared to LKB1 WT which was **178.7** (comparison in Figure 17d). This was representation of the fact that LKB1 localization in the (lateral) membrane was reduced significantly (although not completely) due to the mutations in the CAAX box region (farnesylation- deficient) and lipid binding domain.

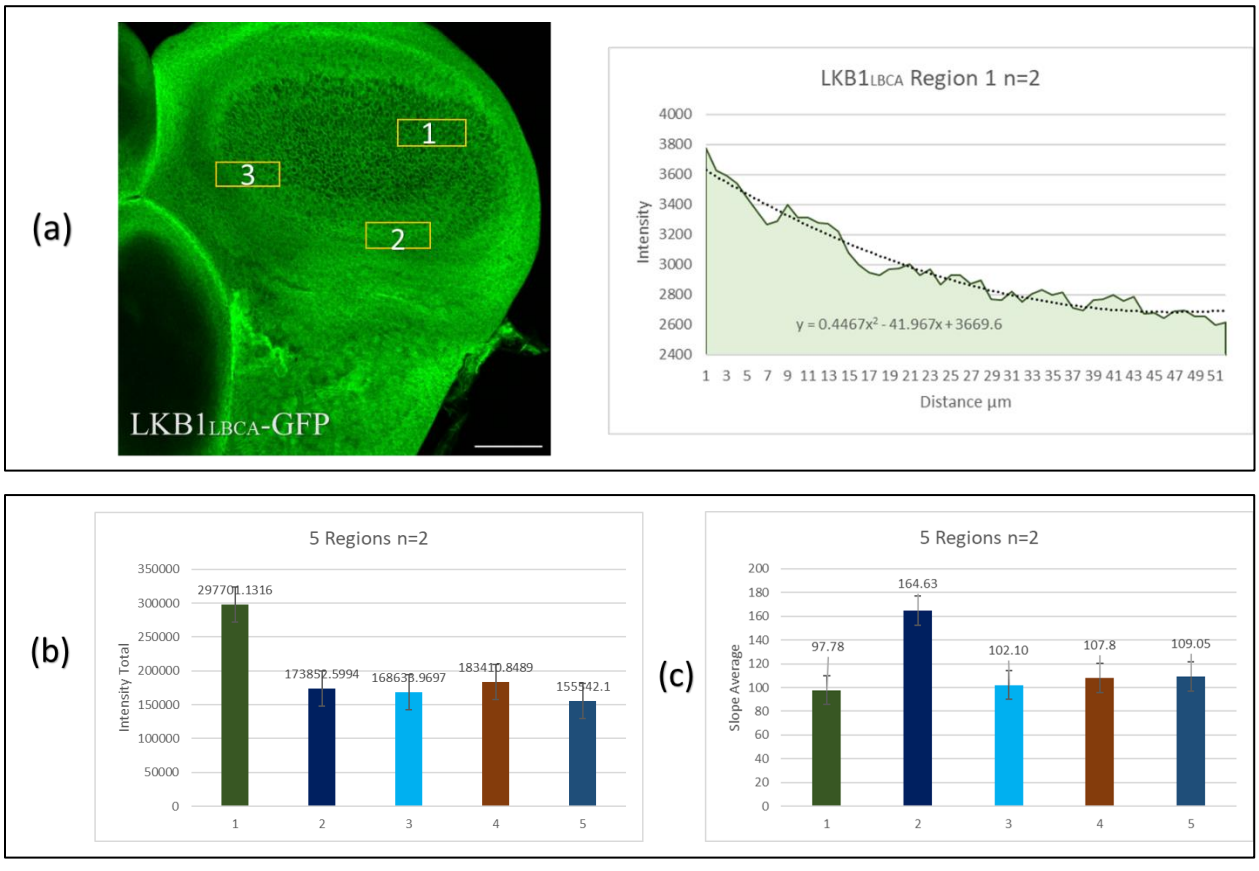

**Remaining contents of the figure, on the next page*

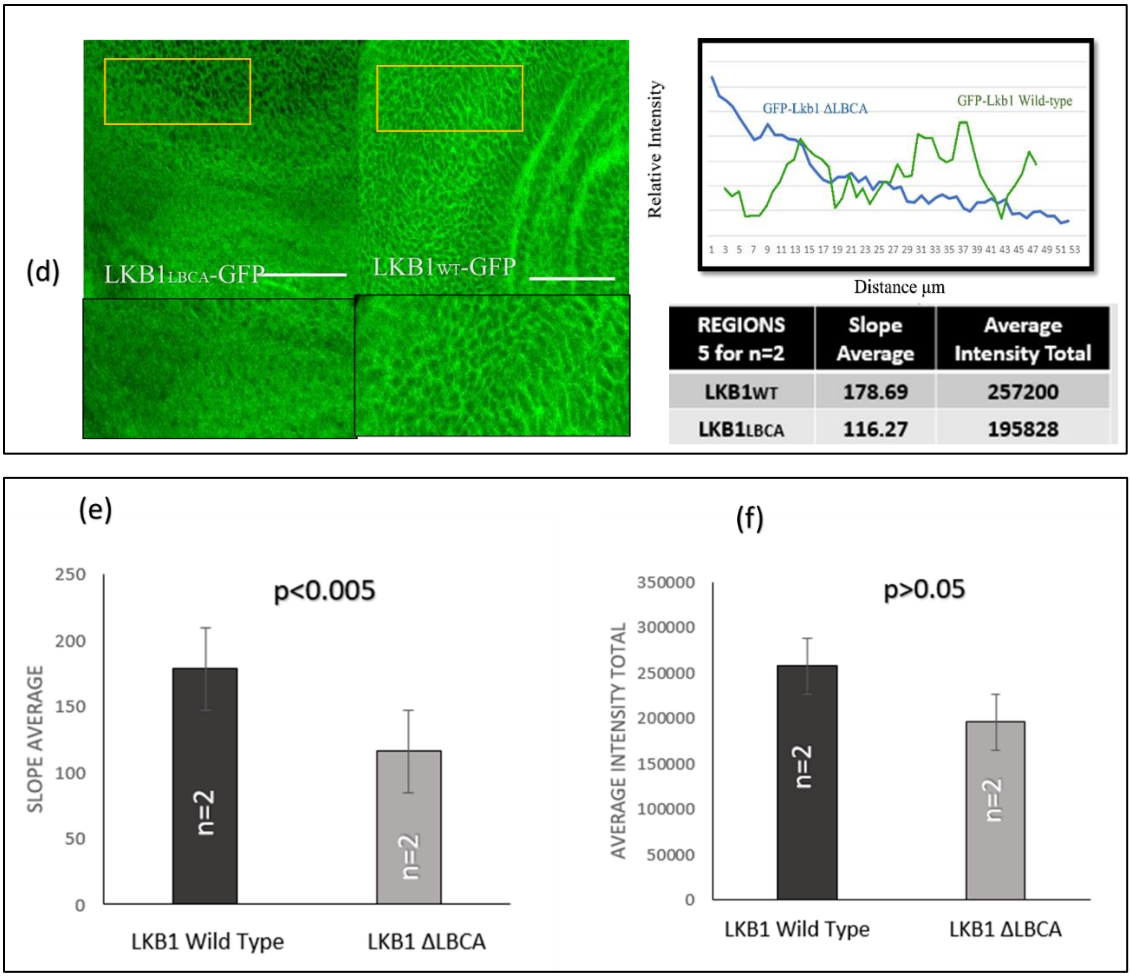

Figure 17: Mutation in CAAX box and LB domain disrupts membrane localization of LKB1. (a) The wing discs extracted from LKB1 ΔLBCA showed a reduced GFP signal in the cell membrane and between cell-to-cell contacts when observed in two separate experiments (n=2). The yellow rectangular region highlighted was selected for random regions to retrieve raw data in ImageJ (5 regions selected in two separate discs) for intensity against distance (µm). The area highlighted in light green gave the area under the graph or intensity total for Region 1 of n_1 (b) A bar graph was plotted for total intensity obtained for 5 regions for n=2. (c) A bar graph of the slope average was obtained for 5 regions for n=2. (d) Shows a comparison between LKB1 WT and LKB1 ΔLBCA localization.. (e) Shown is a comparison of slope average for LKB1 wild type and LKB1 ΔLBCA. (f) Shown a comparison of average total intensity for LKB1 wild type and LKB1 ΔLBCA. The error bars shown represent standard error and statistical significance was determined using t-test. Scale bar is 50µm in (a).

Since we observed decrease in localization of LKB1 in the cell membrane (lateral) for LKB1 ΔLBCA as shown in Figure 17d we proceeded by doing structure prediction modelling to find whether the CAAX and lipid binding domain mutations affect the tertiary structure of LKB1, and via that the effect on levels or localisation of LKB1 (which is not addressed in previous studies). Figure 18a highlights in red the regions which were mutated to retrieve the primary sequence of LKB1 ΔLBCA and that was projected into the 3D

structure seen in 18c using ColabFold by AlphaFold. When comparing 18b (LKB1 wildtype) and 18c (LKB1 ΔLBCA) we observed a change in orientation of α helices in the protein core. This might have an effect on the binding pocket of the protein affecting LKB1 interaction with MO25 and STRADα to form a heterotrimeric complex, in turn affecting its localization or stability.

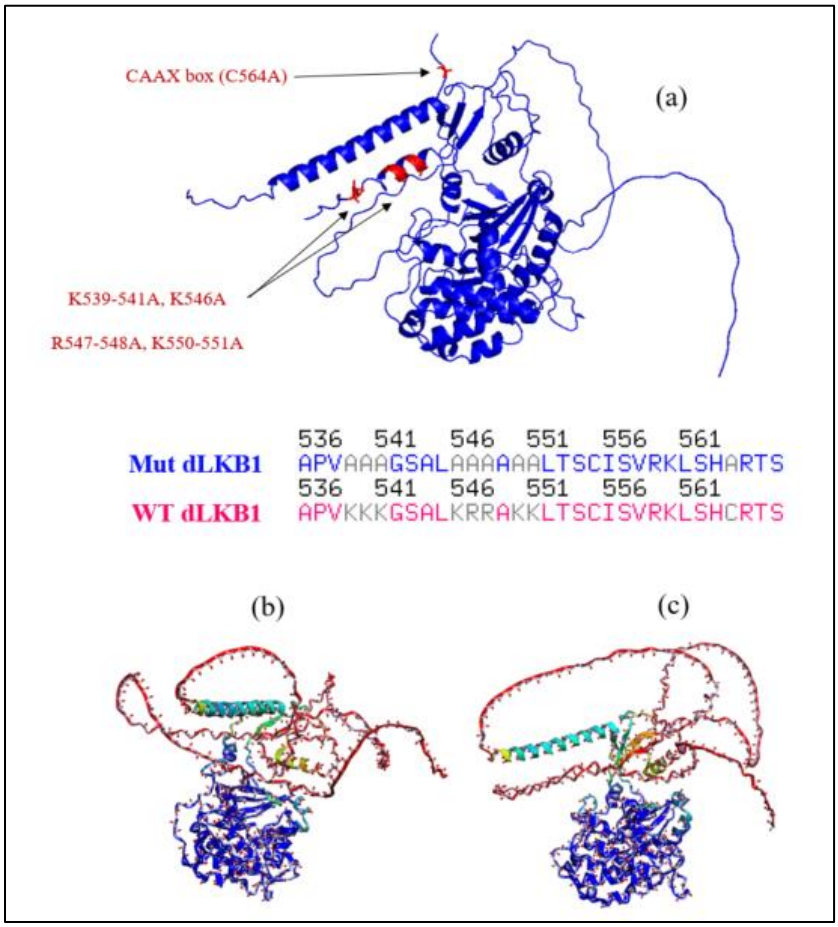

Figure 18: Structure prediction of LKB1-WT and LKB1 ΔLBCA using software prediction modelling. (a) Represents WT dLKB1 in blue where mutations leading to Mutant dLKB1 (ΔLBCA) are marked in red; CAAX box (C546A), and LB domain (K546A, R547A, R548A, K550A, K551A, K539A, K540A, K541A). The grey residues in the sequence comparison in (a) show the LB and CAAX box mutations. The LKB1-WT structure in (a) was projected in PyMOL by retrieving from an AlphaFold structure prediction on UniProt. (b) The structure of WT dLKB1 was also predicted using ColabFold: AlphaFold2 using MMseq2, with side chains shown. (c) In order to predict the effect of mutations on the structure of dLKB1 the mutations were manually added in the original wild-type sequence for (b), and the structure predicted using ColabFold.

4.4 Recombinant fly lines can be used for screening of cellular trafficking regulators

Recombinant fly lines were used as tools, which were crossed to RNAi lines to cause disruption of normal trafficking regulators such as vps34 catalytic subunit of PI3K-III and Wdfy2 and also performing knockdown of LKB1 to visually see the affect side-by-side in the same tissue. In order to ensure that selection was done in larvae in which the knockdown construct had been incorporated in our recombinant line the following genotype was selected (red line used to indicate recombination event).

Selection of Non-tubby larvae

$$\frac{lkb1{>}GFP{::}Lkb1}{CyO};\frac{rnGAL4\,|{>}CD8ChRFP}{RNAi} \quad \text{or} \quad \frac{lkb1{>}GFP{::}Lkb1}{CyO};\frac{rnGAL4\,|{>}ChWdfy2}{RNAi}$$

Non-tubby larvae were selected to increase the probability of selecting the right genotype to see the effect of knockdown and that on localization of LKB1. Three different areas of the wing disc were observed spanning through the DV to AP division of the wing disc. The wing pouch was the focus of observation. Expression for *rotund* was observed between the wing margin separating the wing pouch from the dorsal hinge. Expression for *apterous* was observed in the dorsal region of the wing or the dorsal wing blade. Expression of *engrailed* was observed in the anterior region of the wing or anterior-dorsal wing blade and anterior-ventral wing blades.

4.4.1 Knockdown of LKB1 decreases its localization in the lateral membrane

The LKB1 line was under the control of an endogenous promoter and found to be localized in the lateral membrane. A knockdown of LKB1 was performed to see whether the localization and stability of the protein is affected with the aims to investigate if it in turn effects the localization and function of other trafficking regulators. Two different RNAi lines were used for knockdown of LKB1 in our recombinant stocks 150 and 250: (1) Lkb1IR – no. 1216 (homozygous on the 3rd chromosome), (2) Lkb1IR/S-T – no. 1236 (on the 3rd chromosome). The probability of selecting the right non-tubby larvae in 1216 was **50%** and the probability of selecting the right non-tubby larvae in 1236 was **25%.** The wild-type 150 and 250 from Figure 19 lines were used for comparison to the knockdown effect as shown in Figure 20. Two parameters were calculated in this case between the dorsal wing blade (where GAL4 is expressed and knockdown possible) and the dorsal hinge (control region immediately abutting): difference in slope average (Diff_SlopeAverage_GFP) and difference in AIT (Diff_AIT_GFP) for the GFP region representing LKB1 localization and levels, respectively. Diff_SlopeAverage_GFP was calculated between slope average

of dorsal wing blade and slope average of dorsal hinge. Diff_AIT_GFP was calculated as difference in AIT of dorsal wing blade and AIT of dorsal hinge. Negative value represented a decrease in membrane localization or protein levels. Values of 'difference' obtained in Figure 19 between the dorsal wing blade (*rotund* region) and dorsal hinge were considered to be natural variation between the two regions for localization and levels of LKB1. The parameters obtained for wild-type 150 and 250 as shown in Figure 19 were used as positive control to compare the effect on LKB1 localization and levels as a result of its knockdown.

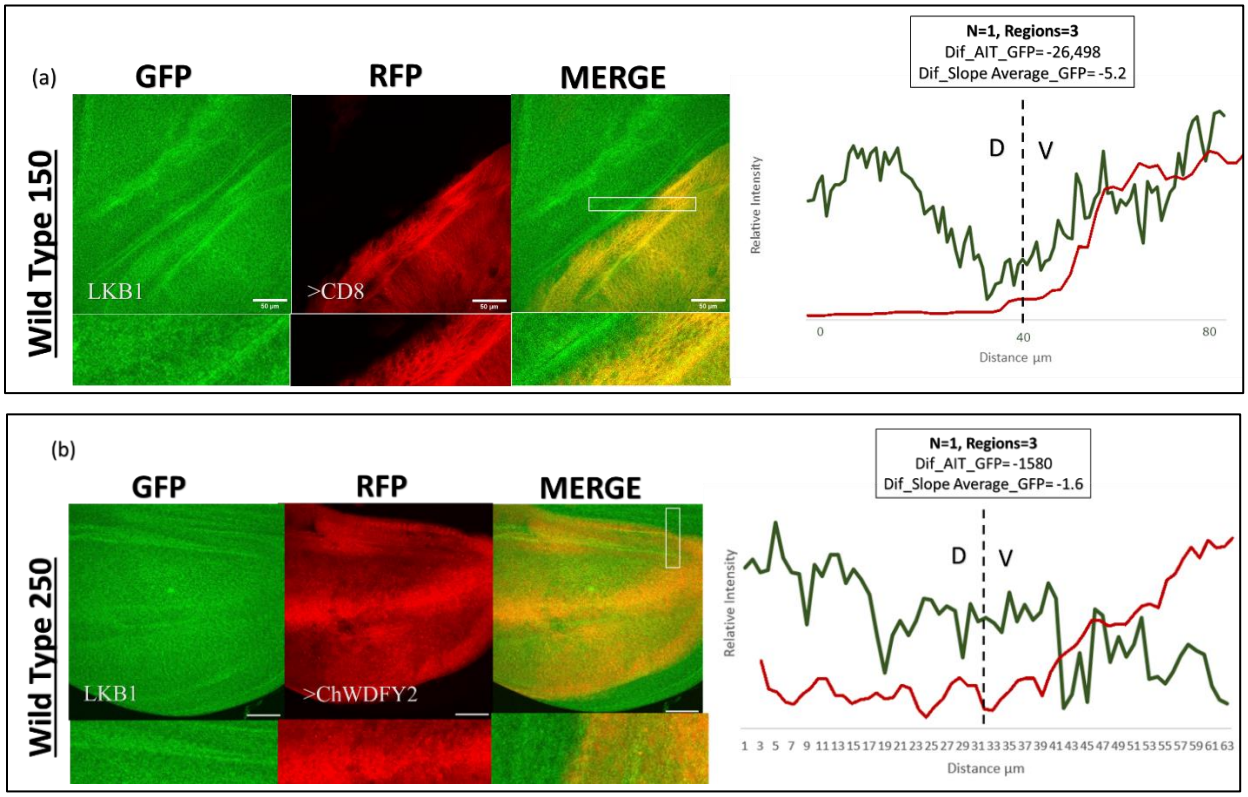

Figure 19: LKB1 localization and levels observed in wild-type 150 and 250 fly lines. A comparison of the dorsal wing blade, represented as V in the line intensity plot and D in the dorsal hinge is shown. (a) For line 150 GFP represents LKB1, and RFP represents mCD8. A difference in slope average of -5.2 was seen for the GFP signal and a different in AIT of -26,498 was seen between the two regions. (b) For line 250 GFP represents LKB1, and RFP represents ChWdfy2. A difference in slope average of -1.6 was seen for the GFP signal and a difference in AIT of -1,580 was seen between the two regions. Inset X-Z section (0.9-8µm) and the line intensity graph is through the indicated region in merged panels with RFP (red) and GFP (green) represented. Scale bars used in all images, 50µm.

The effect of the knockdown on the localization of LKB1 was observed in the *rotund* region, spanned by a Cherry-tagged or RFP signal. Knockdown was effective using the 1216 fly line where majority of LKB1 membrane localization decreased in the *rotund* region (Figure 20a, b). Knockdown using 1236 only gave satisfactory results and it was not as effective as RNAi line 1216 (Figure 20c). The values obtained for LKB1 knockdown were negative values, representing decrease in localization and levels of GFP-LKB1 in the *rotund* region as compared to dorsal hinge. When using RNAi line 1216 the Diff_SlopeAverage_GFP was calculated to be -12.1 and -21.3 for 150 and 250, respectively. The Diff_SlopeAverage_GFP for both cases was increased with a negative value, when compared to the wildtype. A greater Diff_SlopeAverage_GFP was seen for 250 knockdown with 1216 RNAi line, and it showed a greater decrease in slope average for dorsal wing blade region as compared to 150 knockdown. Thus, membrane localization for LKB1 was seen to reduce more for 250 than for 150. When 1236 RNAi line was used for knockdown of LKB1 in 150 the membrane localization of LKB1 was seen to reduce the least with a difference in slope average of only -6.3 (Figure 20c). Thus, it was concluded that the RNAi knockdown of LKB1 using 1216 reduced the membrane localization of LKB1 more than that of 1236.

The AIT for the GFP signal was measured between the dorsal wing blade and dorsal hinge and the Diff_AIT_GFP calculated for 150 and 250, using RNAi line 1216 was -83,029 and -86,378 respectively. This showed reduced magnitude of signal in the dorsal wing blade and reduced levels of LKB1 due to knockdown. The protein stability or the effectiveness of the kinase domain of LKB1 was seen to decrease for 150 by 6-fold (compared to wild type in Figure 20a) than that of 250 which was nearly by 20-fold (compared to wild type in Figure 20b), in RNAi knockdown using 1216. So, the levels of LKB1 in 250 were decreased significantly more than 150 using 1216 RNAi line. For LKB1 knockdown in 150 using RNAi line 1236 Diff_AIT_GFP was measured to be -26,444 as shown in Figure 20c and was lesser as compared to 19b or 19a. This showed that the stability of LKB1 protein or effectiveness of its kinase domain was reduced more when LKB1 knockdown was performed in 150, as compared to 250, and using RNAi line 1216 rather than 1236.

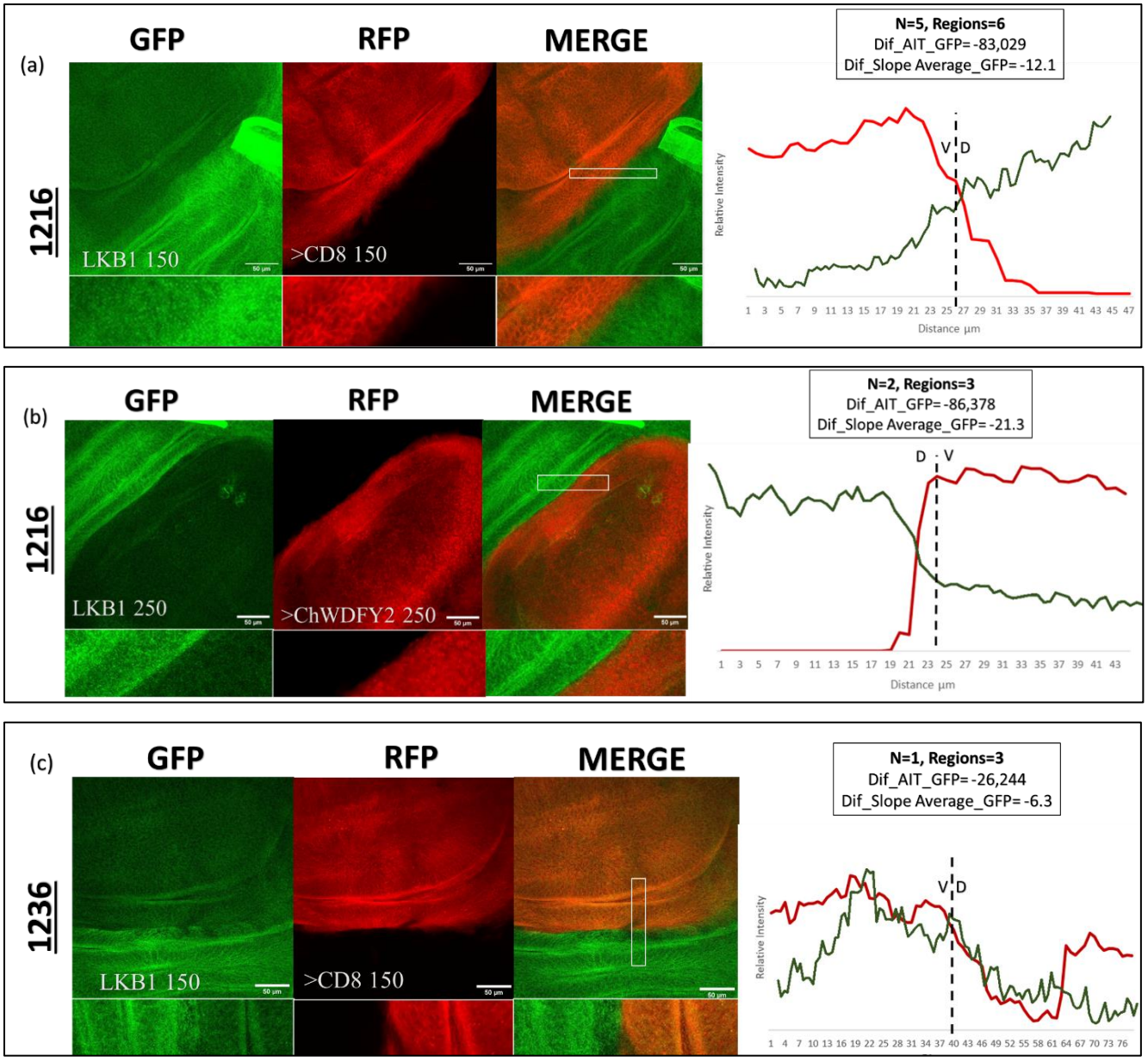

Figure 20: Knockdown of LKB1 in 150 and 250 reduces localization of LKB1 in the lateral membrane of *rotund* expression region. Inset X-Z section (0.9-8µm) and the line intensity graph is through the indicated region in merged panels with RFP (red) and GFP (green) represented. (a) RNAi 1216 used to cause knockdown in 150. The RFP signal is for CD8 glycoprotein. (b) RNAi 1216 used to cause knockdown in 250. The RFP signal is for WDFY2. Knockdown was compared in the region dorsal to *rotund* region. (c) The second RNAi line called 1236 was used to knockdown LKB1 in 150. The dorsal hinge and the dorsal wing blade regions were observed to see the knockdown effect. All images are confocal projections originally consisting of 8-10 stacks of a distance of 1-1.8µm. Scale bars used in all images, 50µm.

It has already been identified in previous studies and our own observation that LKB1 localizes in the lateral membrane (108). We were curious to see whether RNAi knockdown affected the localization and stability

of LKB1 in the apical membrane. We performed knockdown of LKB1, to see the effect of its localization in the lateral membrane as compared to the apical membrane. For the purpose, the following line was used to cross with RNAi line 1216, and non-tubby (selection against S-T) were selected for extraction of wing disc; lkb1>GFP::Lkb1; rnGAL4/S-T. The chance of selecting the right non-tubby larvae was 100%. As shown in Figure 21 the GFP signal represents apical membrane localization of LKB1 for two separate discs. The slope average(s) between regions shown as A and B, and C and D do not look considerably different. Here, A and C represent the dorsal hinge and B and D represent the dorsal wing blade. Thus, the slope average values compared between the dorsal hinge and dorsal wing blade stayed approximately the same. This showed that the knockout of LKB1 in the apical membrane is not effective and thus apical localization of LKB1 stays nearly undisturbed using RNAi line 1216. A slight decrease in AIT was seen in region B and D shown in Figure 21, which showed that even though the apical localization of LKB1 (shown by unaffected slope average) was not affected by the knockdown, the levels of LKB1 were reduced. In addition, a phenotype difference was also observed in adult flies with LKB1 knockdown, having wings which were more bent as compared to wild type (Figure 21d).

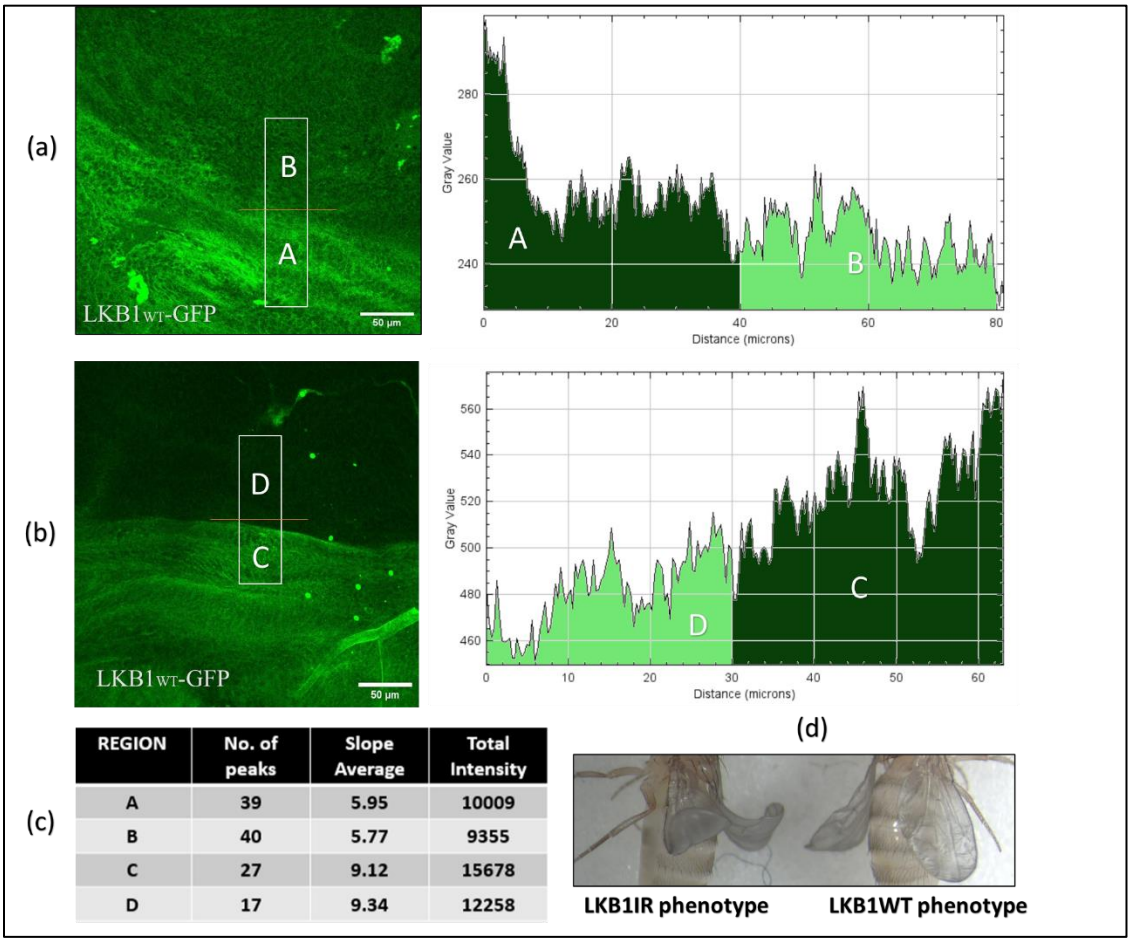

REGION	No. of peaks	Slope Average	Total Intensity
A	39	5.95	10009
B	40	5.77	9355
C	27	9.12	15678
D	17	9.34	12258

*Remaining contents of the figure, on the next page

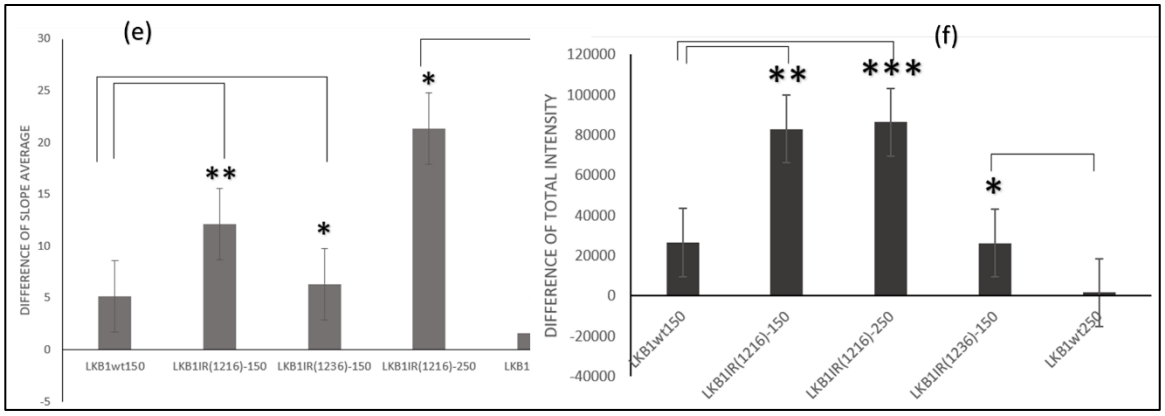

Figure 21: Knockdown of LKB1 does not affect apical membrane localization but reduces the lateral membrane and cytoplasmic levels. lkb1>GFP::Lkb1; rnGAL4/S-T was used to knockdown LKB1 in the *rotund* expression region. Two different discs represented for the same cross (n=2) (a) and (b) highlight region A, B, C or D, where A or C represent the dorsal hinge while B or D represent the dorsal wing blade in the *rotund* region. (c) Gives a summary of the measurements of slope average, total intensity, and no. of peaks for regions in (a) and (b). The peaks in the plot represent apical membrane localization. (d) Knockdown of LKB1 induced wing bending demonstrating a decrease in stability of LKB1. (e/f) Shown a comparison of difference in slope average and difference in AIT for LKB1 after knockdown using fly line 1216 and 1236 in recombinant lines 150 and 250. Error bars represent standard error and statistical significance was determined using t-test:*** P<0.0005, ** p<0.005, * P<0.05. Scale bar used, 50µm.

4.4.2 Knockdown of Wdfy2 increases membrane and endosomal localization of LKB1

It had been identified by O'Farrell *et al.* that WDFY2, an effector of PI3K- III is a regulator of LKB1 in *Drosophila* tissues and human organoid, also proving that LKB1 is involved in PI3K- III regulated endosomal signaling (112). In order to confirm the interaction of LKB1 with WDFY2 at the endosomes and make a speculation about its role in endosomal signaling we performed WDFY2 knockdown in fly lines 150 and 250, respectively. This would allow us to see any effect on lateral membrane localization and levels of LKB1, as well as its effect on localization on the endosomes. A single RNAi line was used for knockdown of Wdfy2 in our recombinant stocks 150 and 250; WDFY2IR/S-T – no. 1150. Selection was done against tubby larvae for the purpose of dissection. The probability of selecting the right genotype amongst non-tubby larvae was 25%. The effect of the knockdown on the localization/levels of LKB1 were observed in the *rotund* region, spanned by a Cherry-tagged or RFP signal. Knockdown was effective in fly line 150 where LKB1 membrane localization increased in the *rotund* region when compared with the wild type from Figure 19 as shown in Figure 22. The slope average for GFP signal in the dorsal wing blade increased as compared to the wild type. Thus, the difference in slope average between the dorsal hinge and the dorsal wing blade in the *rotund* region was increased positively when compared to the wild type (Figure 19a, showing no knockdown) (from -5.2 in wildtype in Figure 19a to 2.3 in Figure 22, a 3-fold increase).

In addition, the difference in AIT in the dorsal wing blade also increased positively as compared to wild type speculating increase in the levels/ activity of LKB1 as well due to WDFY2 knockdown. Thus, LKB1 membrane localization and stability or levels increases with knockdown of WDFY2 in 150.

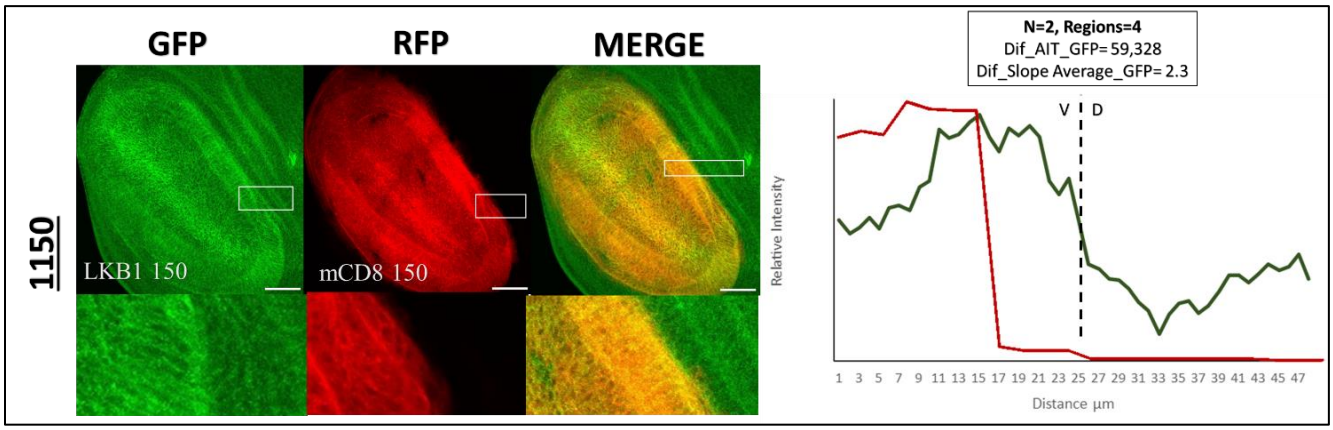

Figure 22: Knockdown of Wdfy2 in fly line 150, increases membrane localization of LKB1. Represents wild type 150 stock with difference in AIT and difference in slope average calculated for the dorsal hinge and the dorsal wing blade in the *rotund* region. (b) Represents WDFW2 knockdown in 150 stock. Inset X-Z section (5µm) and the line intensity graph is through the indicated region in merged panel with RFP (red) and GFP (green) represented. Scale bars used in all images, 50µm.

Wdfy2 knockdown effect on LKB1 levels and localization was also observed in fly line 250. However, we could not assess the effectivity of the knockdown in the RFP region as Wdfy2 in fly line 250 is an overexpression shown by RFP and will not show a reduced RFP signal to WDFY2IR. Knockdown of Wdfy2 corresponding to the Cherry-tagged signal was not visually decreased in the *rotund* region as shown in Figure 23 highlighting the wing margin.. However, some visual increase of LKB1 membrane localization was indicated in the ventral and dorsal wing blade as marked by white rectangular regions in Figure 23 but was not comparable with any signs of decreased expression of RFP in the same region due to Wdfy2 knockdown, for the latter reason. The slope average and total intensity for >ChWDFY2 obtained in the *rotund* region was 117.9 and 96,344 for Figure 23a (n_1, average of 3 regions), and 116.1 and 93,989 for Figure 23b (n_2, average of 3 regions) respectively. This showed that the parameters for the RFP signal for both the wing discs were comparable to the wild type in Figure 19b, showing nearly no decrease in either localization or levels of WDFY2. An increase in slope average was seen in the dorsal wing blade as compared to the dorsal hinge for GFP-LKB1 as shown in Figure 23. Two different discs are shown and a positive increase in Diff_SlopeAverage_GFP was seen for both, with a greater increase seen for N_2. However, Diff_AIT_GFP for both discs was seen to increase positively by a significant amount as compared to wild type in Figure 19b where the difference was a negative value. These numbers showed that LKB1 membrane localization increased on WDFY2 knockdown, and the levels of LKB1 or the stability

of the kinase domain increased using fly line 250. This experiment of knockdown of Wdfy2 with fly line 250 showed some signs of LKB1 and Wdfy2 co-localization in the endosomes. Shown in Figure 23 is possible colocalization of LKB1 and WDFY2, where yellow might represent higher localization and orange lower localization (marked by white arrows).

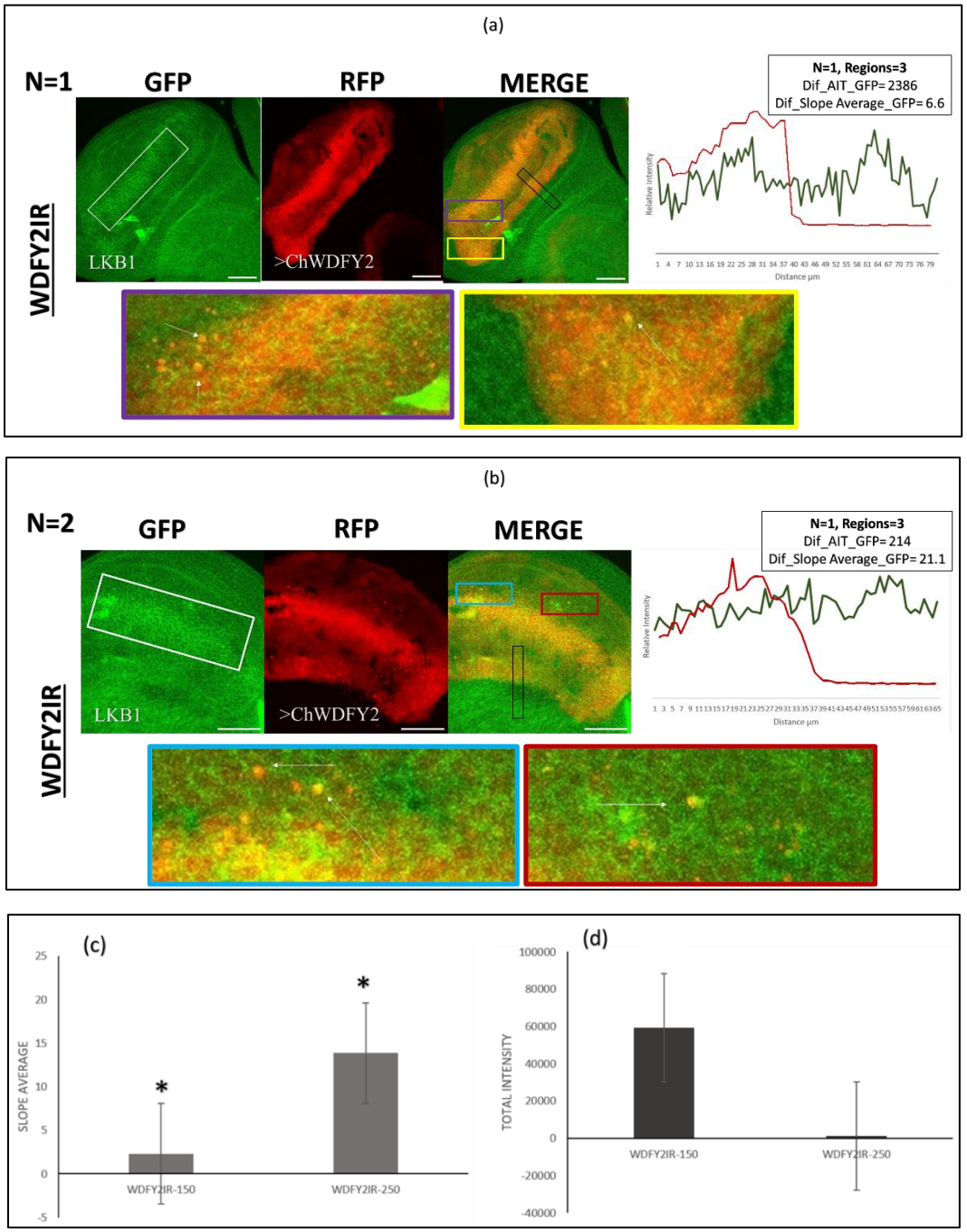

Figure 23: LKB1 co-localizes with WDFY2 on endosomes. Inset X-Z section (6-8µm, projection of the z stack) and the line intensity graph is through the indicated region in a black rectangle in merged panel with RFP (red) and GFP (green) represented. The knockdown of WDFY2 for fly line 250 is shown in two separate wing discs (a) and (b). In

the wing margin and some regions of the ventral wing blade visually an increase in GFP signal corresponding to increased membrane localization of LKB1 is seen, marked by white rectangular regions. The merge image in (a) is zoomed in and shown in purple and yellow rectangular selection representing puncta marked by white arrows. The merge image in (b) is zoomed in and shown in blue and red rectangular selection also representing puncta marked by white arrows. (c/d) Shown a comparison of difference in slope average and difference in AIT for LKB1 after knockdown using WDFY2IR in recombinant lines 150 and 250. Error bars represent standard error and statistical significance was determined using t-test * $P<0.05$, $P>0.05$. Scale bars used in all images, 50μm.

4.4.3 Knockdown of vps34 increases membrane localization of LKB1

LKB1 is a downstream interacting partner of PI3K-III and associates with Rab5 and Rab7 endosomes as shown by O'Farrell *et al*. in both flies and humans. Vps34 is the catalytic domain of PI3K-III and its inactivation by the same is shown to increase LKB1 signaling causing epithelial disruption (112). In order to confirm this observation, we used our recombinant tools. The knockdown of vps34, catalytic domain of PI3K-III in recombinant fly lines 150 and 250 was done using the following RNAi line: 1211, ap>vps34IR/ S-T. Selection was done against tubby larvae for the purpose of dissection. The probability of selecting the right genotype amongst non-tubby larvae was 25%. The effect of the knockdown on the localization of LKB1 was observed in the *apterous* region, spanned by a Cherry-tagged or RFP signal (difference in parameters calculated for the dorsal wing blade and the ventral wing blade). Knockdown was effective in 150 recombinant fly line as it resulted in increase in LKB1 membrane localization in the *apterous* region or dorsal wing blade as compared to the ventral wing blade, as the slope average was seen to increase from 87.3 to 102.6 (difference in slope average of 15.3) as shown in Figure 24a. However, the RFP signal in the *apterous* region was seen to leak from the dorsal wing blade to the ventral wing blade (shown by arrows in Figure 24). The leaky expression was seen more evidently for >CD8ChRFP recombinant (fly line:150) as compared to >ChWdfy2 recombinant (fly line: 250) marked by white arrows. We assumed that the leak could be due to some interaction between the *apterous* and *rotund* expressions, which is a phenomenon not observed in *Drosophila* wing imaginal disc before. However, nearly no difference in slope average was seen for vps34 knockdown in fly line 250 as shown in Figure 24b. The difference in AIT for 150 was increased between the two regions observed with a value of 74337 due to knockdown indicating increased levels of LKB1 in the cell membrane (4 times increased as compared to wildtype). As compared to 150, the knockdown of vps34 in 250 showed lesser levels and membrane localization of LKB1 (10 times lesser levels and 4 times lesser membrane localization). It would have been useful to compare Figure 24 knockdown effect with a wild type with no knockdown in the *apterous* region but that was not available. The phenotype of the wing of the adult fly when originated was observed, and it was seen that the wing had been discolored, shrunk, and destroyed.

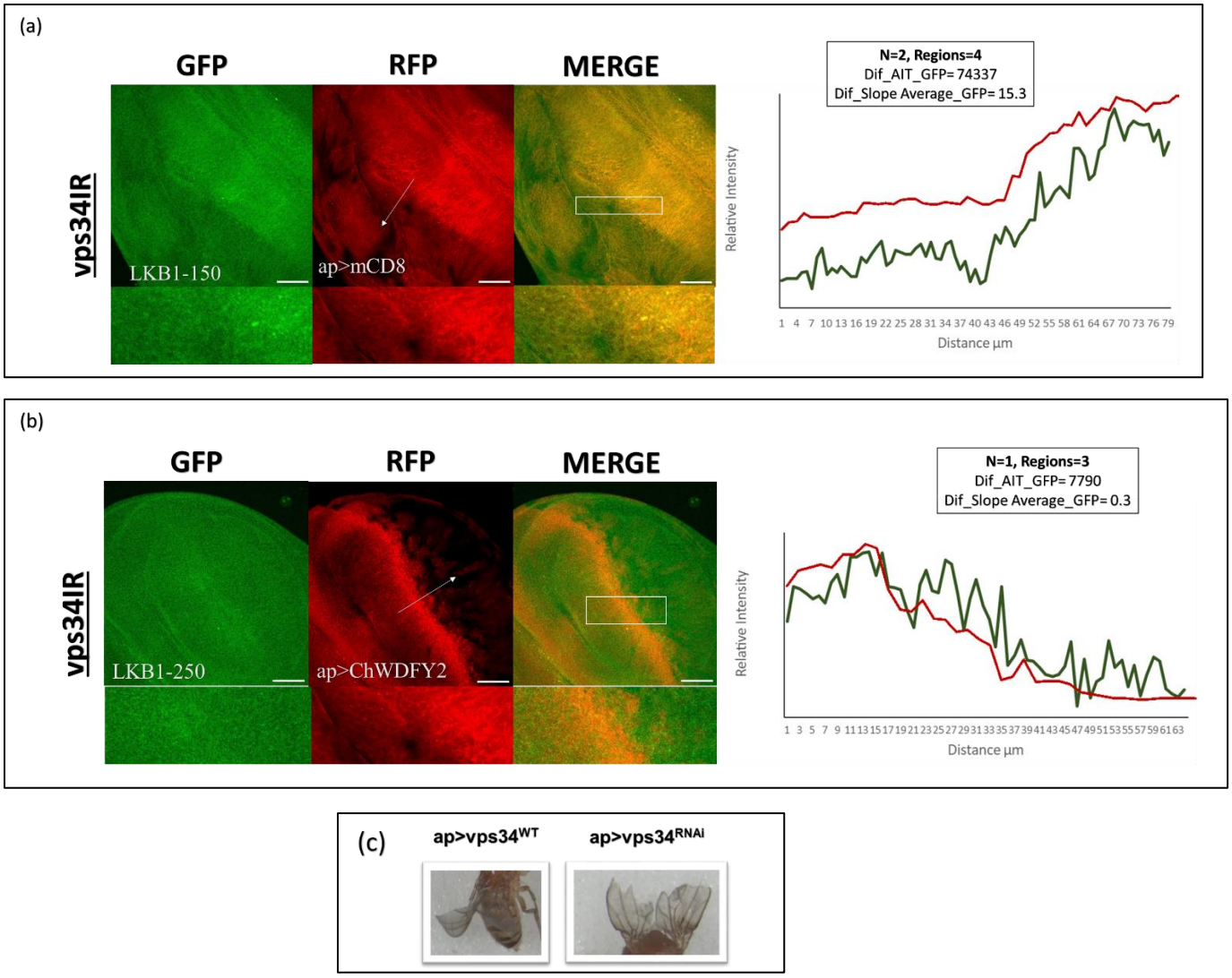

Figure 24: Membrane localization of LKB1 increases in 150 fly line on vps34 knockdown. (a) The knockdown effect of fly line 150 is shown in which difference in AIT and difference in slope average was calculated for n=2 and 4 separate regions. (b) The knockdown for fly line 250 is shown in which difference in AIT and difference in slope average was calculated for n=1 and 3 separate regions. The RFP signal in the *apterous* region was seen to leak from the dorsal wing blade to the ventral wing blade shown by white arrows. Inset X-Z section (6-8µm) and the line intensity graph is through the indicated region in merged panel with RFP (red) and GFP (green) represented. (c) A crumpled wing phenotype for ap>vps34^{RNAi} was observed as compared to the wild type. Scale bars used in all images, 50µm.

In order to confirm that the leaky signal between apterous region and the ventral wing blade did not affect the GFP signal, we performed knockdown of vps34 in LKB1 wildtype stock (lkb1>GFP::Lkb1/CyO; Dr/Tm6 – fly line 500). The results obtained are shown in Figure 25. The difference in slope average between the dorsal wing blade and the ventral wing blade positively increased. In addition, the difference

in AIT also positively increased to a lesser level as compared to knockdown in 150 (Figure 24a) and to a greater level when compared to the knockdown in 250 (Figure 24b).

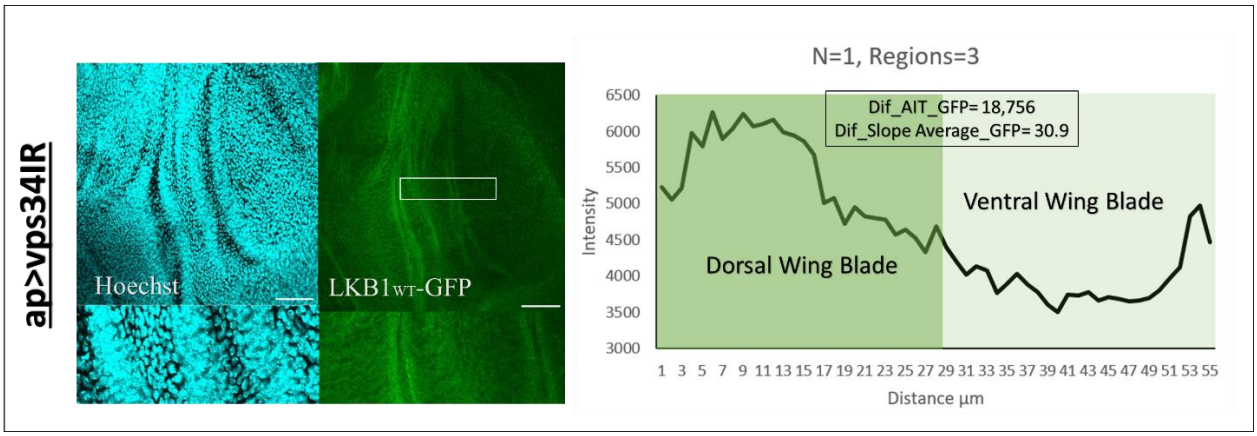

Figure 25: Membrane localization of LKB1 increases in LKB1-WT stock on vps34 knockdown. The dorsal wing blade consisting of the *apterous* expression, and the ventral wing blade were compared for the effect of ap>vps34IR on LKB1 localization and levels. The difference in AIT and the difference in slope average between the two regions for n=1 and three rectangular selections like the one shown were measured. Inset X-Z section (6µm) and the line intensity graph is through the indicated region in white rectangular selection in GFP (green) section represented. Scale bars used images, 50µm.

4.5 Induction of starvation decreases localization of LKB1

LKB1 is known to regulate autophagy via AMPK but little is known about mechanisms to shut this pathway off. Additionally, LKB1 association with the endosomal system including regulation by vps34 (required also for autophagy) lead us to investigate the effects of genetic starvation used to induce autophagy and in turn to see its effect on LKB1 localization. For that purpose, Chico an important part of the insulin signaling pathway was knocked down to block TOR signaling, in enGAL4,>ChAtg8/S-T fly line (stock number: 1460) and observe the affect in the *engrailed* region (posterior region of the disc). The Chico RNAi line used for the experiment was lkb1>GFP::Lkb1/CyO;>ChicoIR/Tm6c (initially double-balanced and made into a stable stock using DB stock). The cross was kept at 18˚C to allow more stability in a slower development mode (as a temperature of 25˚C proved to be toxic for the animal). As a negative control w1118 flies were also crossed to fly line 1460. Non-tubby larvae which emerged were dissected for wing discs for imaging, and of these non-tubby larvae, there was 25% change of getting the right disc. Cherry tagged Atg8 protein, involved in the steps leading to conjugation of the autophagosome was used as a reporter in the *engrailed* (posterior) region of the wing disc. Change in LKB1 localization across the posterior anterior border of the wing disc was observed in the *engrailed* region (posterior boundary of the disc) as compared to the rest of the disc (Figure 26). This was concluded by measuring the difference in GFP signal between the posterior-anterior border of the wing disc using slope average and AIT. The

difference in slope average for GFP signal was 6.3 (higher in the *engrailed* region as compared to the rest of the disc) and the difference in AIT for GFP signal was -20,286 (2 times lower in the *engrailed* region as compared to the rest of the disc) as shown in Figure 26b. This showed that the knockdown of Chico in the *engrailed* region had increased membrane localization but reduced levels of LKB1, respectively. The enGAL4,>ChAtg8/S-T fly line was also crossed to w1118 flies as a negative control where no GFP signal was expected to be seen as shown in Figure 26a. Any GFP signal seen was a background. In order to confirm the knockdown, it would have been useful to compare Figure 26b knockdown effect with a wild type with no knockdown (positive control) in the *engrailed* region but that was not available.

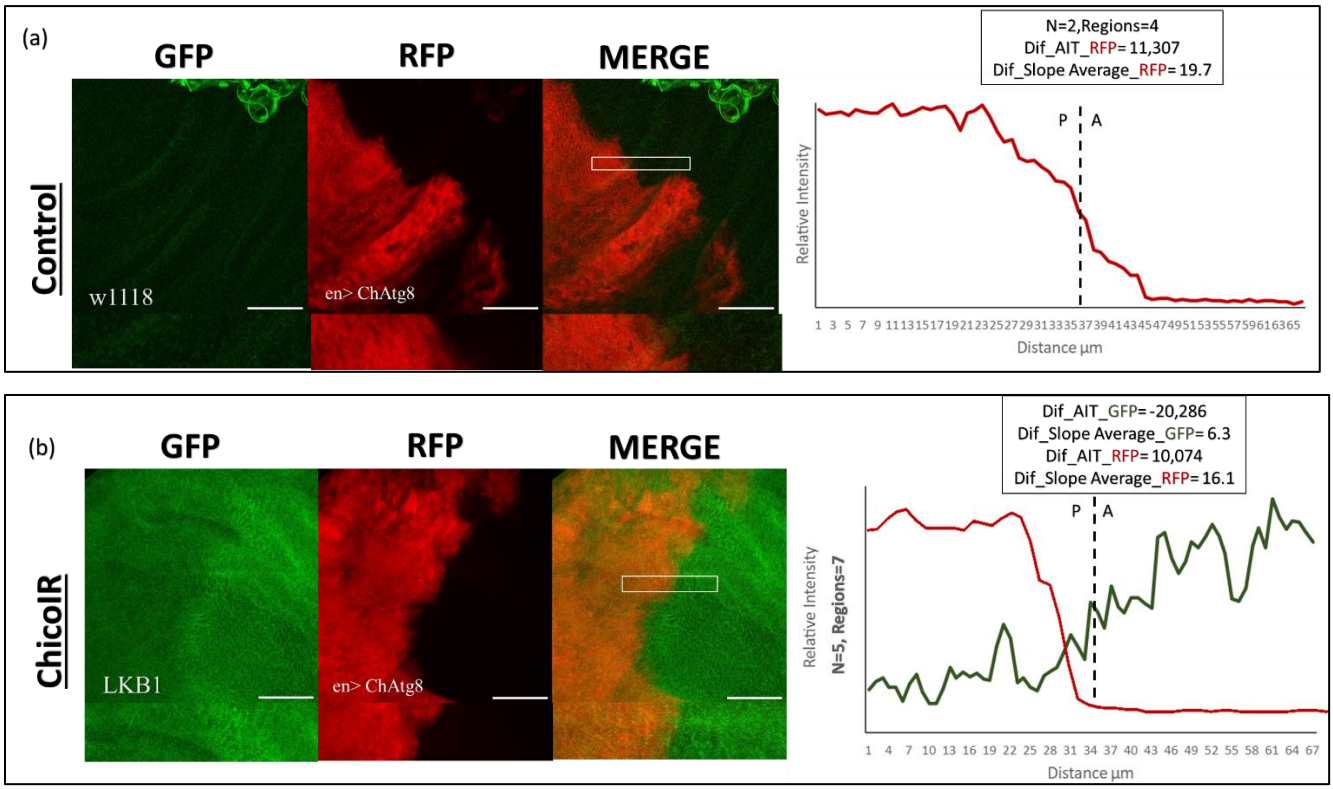

Figure 26: LKB1 membrane localization is decreased in starvation induced autophagy. (a) As a positive control, w1118 flies were crossed with enGAL4,>ChAtg8/S-T (1460) where no GFP was observed as expected and an RFP signal for Atg8 was seen in the anterior boundary of the wing. (b) Chico was knocked down in fly line 1460 in which ChAtg8 localization was seen in the *engrailed* (across anterior to posterior boundary) region as an RFP signal. Inset X-Z section (6-7µm) and the line intensity graph is through the indicated region in merged panel with RFP (red) and GFP (green) represented. Scale bars used in all images, 50µm.

5. Discussion

5.1 Methodological considerations and limitations

While setting up crosses for construction of recombinant tools some challenges were faced in terms of getting a stable stock with no contamination with flies from the wrong genotype. These challenges were faced with fly lines lkb1>GFP::Lkb1/CyO;rnGAL4|>CD8ChRFP/Tm6c (150) and lkb1>GFP::Lkb1/CyO;rnGAL4|>ChWDFY2/Tm6c (250). Along the course of the experiment, these lines were seen to lose the TM6c balancer, observed by the non-*stubble* phenotype in flies (longer bristles instead of shorter bristles). It was also identified that some flies had lost their w+ genotype (red-eyed) and had become w- (white-eyed). Since the rnGAL4/TM3 stock and >CD8ChRFP (used for 150) and >ChWDFY2 (used for 250) were all w+ this indicated that losing the TM6c balancer had caused the third chromosome to recombine and lose the recombinant we were maintaining, to eventually become white-eyed. This problem was solved by discarding these contaminated stocks and setting up new crosses (Cross 9 and 10 from Appendix I). Furthermore, it was observed while maintenance of flies that some stocks had stopped producing larvae. It was identified that this was due to the fact that the same flies were being flipped (introduced into a fresh food medium) instead of allowing them to produce adult offspring before flipping. Since the female *Drosophila* fly typically lays 100-600 eggs during its lifetime, eventually it becomes unfertile, thus it was made sure to flip-over the newer generations or set-up new crosses for collection to allow the cross to keep going. Another threat to *Drosophila* food medium was possibility of fungal contamination or mite infestation which had to be taken care of since the issue could harm the culture. Midst the research we found some stocks in which development was halted due to fungal contamination in the food, thus eggs did not develop further. This was avoided by regular flipping and keeping the environment clean.

The aim of the study was to construct 3 recombinant fly lines to observe with LKB1 localization side-by-side: one with >CD8ChRFP, the second with >ChWDFY2 and the third with >ChSNF1a. However, we were unsuccessful in construction of a recombinant fly line incorporating >ChSNF1a. The main challenge of this occurred at the stage of recognizing recombinants in a light microscope as shown in Figure 14a. The easiest was to identify recombinant larvae and pupae for >CD8ChRFP, where a larger number of recombinants, with a clear RFP signal in the precursor wings were identified. However, a clear signal was not seen for >ChWDFY2 or >ChSNF1a. We decided that this could be due to two reasons. The first reason could be the chance of recombination depending on the inserted position of the gene of interest or the recombination frequency. In fact, recombination might also be affected by chromosomal rearrangements such as inversions, fissions, fusions, and translocations (125). If the genes of interest are far apart from each other, they have a higher chance of recombining or crossing over, as was in the case of >CD8ChRFP and

rnGAL4 (150 stock). On the other hand, if the genes are closer to each other or to the centromeric region, they have a lesser chance of recombining, as maybe was in the case of >ChWDFY2 and >ChSNF1a (126). The frequency of recombination for >CD8ChRFP and rnGAL4 was 3-4% (An average of 6 larvae or pupae identified on average in a vial containing 3 females and assuming they produced an average of 50 embryos). Random selection at the pupal stage for recombinants and eventual dissection of adults yielded us a stable recombinant stock for >ChWDFY2 and rnGAL4 (250 stock). However, since random selection did not work for >ChSNF1a the method of selection by eye colour was done. The >ChSNF1a stock (fly line 1227) consisted of the mini white gene (mini-w+), a miniature form of the w+ with yellow-eyed phenotype. The mini-white gene has a range of eye colour phenotype which may range from pale yellow to red, and this is dependent on the position at which the gene is inserted in the genome(127-129). The 1227 had a pale-yellow eye phenotype due to its position through non- specific P-element insertion. Knowing that the mini-white gene is sensitive to chromosomal position effects, we had hypothesised that a recombinant event with rnGAL4 would change the position of the gene and cause a change in eye colour to perhaps orange. The change of eye colour would not be visible when using w+; rnGAL4/TM3 (8142 fly line) due to its red-eyed background. Thus, another line with a white-eyed background was used: w-; rnGAL4/Tm6c. However, we were unable to spot a change in eye colour using a w- background as well, perhaps due to low frequency of recombination or no visible change in phenotype (unlike the predicted hypothesis) due to recombination.

Dissection, fixation, and microscopy were important techniques which were used throughout the study. While dissecting larvae it was important to make sure that as much of the trachea possible was removed from the wing disc to avoid it from overlapping the discs while imaging. This was usually done after having transferred them into formaldehyde (4%) for fixation. This is preferred for two reasons. Firstly, if the wing discs are kept in PBS for too long (longer than 20 minutes) there is a risk of the live cells to degrade. Since we wanted to check for localization of the membrane or cytosol, we had to fix the cells while they were still alive (preserving the structure of the tissue while it is still alive). Secondly, removing the trachea in formaldehyde (4%) is easier as it is a more viscous solution than PBS keeping the discs from moving around much. Formaldehyde (4%) no longer than two weeks old was used to avoid unsuccessful fixation. Another issue that occurred for imaging was appearance of blurry discs. This was an indication of contamination of the mounting medium. NPG consists of glycerol and bacteria use it as a carbohydrate source (130). It was made sure to use fresh NPG stocks when a cloudy solution was noticed which indicated possible contamination. The amount of the mountant added before putting on the cover slip was also important. If too much was added it would give a chance for wing discs to overlap or turn over. If too less was added it would cause a lot of air bubbles while mounting the cover slip. Both of these issues created problems for imaging, so adding an optimal amount was practiced.

The localization of endogenous LKB1 has not been explored much in previous studies, perhaps due to challenges of lower expression of the protein and lack of appropriate antibodies for the purpose (74). It was identified by Sebbagh *et al.* that endogenous LKB1 localizes in the cytosol and the membrane in MDCK cells, but not in the nucleus (74). It was suggested by Dogliotti *et al.* that endogenous LKB1 is particularly present between cell-to-cell contacts in polarized epithelial cells (both in various *Drosophila* cell types in vivo as well as MDCK cells in vitro) (108). We were able to document the same in vivo in epithelial cells of the wing imaginal disc as shown in Figure 16. After n=2 attempts it was seen that lesser levels of LKB1 were present in the disc as seen by a low total intensity (magnitude) of the GFP signal. Furthermore, the GFP signal did not seem as membrane-like as we expected, and it was identified that this was due to the issue of the nuclear signal leaking into the GFP channel. When the wing disc was exposed to a strong 410 nm light, Hoechst was photoactivated and the florescence for EGFP seen at 488 nm was stronger than the actual/real GFP signal. Eventually, a bleached GFP signal was seen after exposure at 488 nm following initial exposure to Hoechst at 410 nm. Thus, exposure at 410 nm first was bleaching the GFP signal. In order to eradicate this issue, in the third attempt it was practiced viewing GFP first on the microscope, turning the intensity of the 410 nm light down and increasing the exposure time. However, this practice too did not help, and the problem persisted. Thus, it was decided to improve the magnitude of the GFP signal, for better visualization of localization, by using anti-GFP antibody. This improved the GFP signal by a factor of 8. The indirect method of immunostaining was used which allowed to maintain stability of the primary antibody, however it was a time-consuming process requiring several steps, and this proved to be a disadvantage . This increased the chances of damaging or losing the wing discs collected while exchanging the medium, and during the washing steps (131). Another cost of using antibody against GFP was the risk of non-specific binding. This was especially seen when after using an antibody against GFP the slope average was seen to increase from 120 (Figure 15) to 178 (Figure 16). The antibody staining was only expected to increase the signal magnitude (shown by increase of total intensity), however it should have not shown a change (increase) in localization of LKB1. This non-specific binding may have occurred from binding to endogenous Fc receptor (FcRs), protein present on the surface of certain cells, or certain mutual effect of ionic and hydrophobic interactions (132). According to Buchwalow *et al.* amending the protein blocking steps in the traditional antibody staining protocol may improve the problem of non-specific binding (132). In addition, using a different combination of primary and secondary antibodies to determine localization of LKB1 might prove to be useful.

In the context of statistical analysis, we mentioned earlier that in order to calculate the total intensity the method of area under plot of extracted peaks was preferred (method (2) from section 3.7.2) rather than the 'Analyze particles' function in ImageJ (method (1) from section 3.7.2). This was because the analyze particles function also took into account the 'noise' or troughs in the plot. While on the other hand, Figure

13, which used method (2) calculated area under graph from a plot in which noise was filtered out. Since we were obtaining plot profiles with only the peaks extracted from which the slope average was calculated (Figure 12), we decided it would be more appropriate to calculate the intensity total using a trendline of the same plot. This was an attempt to standardize the method (plot with peaks with noise filtered out) from which the two important parameters in the study were calculated: slope average and total intensity. Furthermore, on calculating the total intensity using both the methods, it was seen that the ratio of difference between two regions being compared was nearly the same. The plot profiles (raw/ unfiltered for peaks) in Figure 21(a) and (b) show total intensity calculated by method (1) (directly from Image J) and also by using method (2). The ratio difference using both methods was 1.0 when comparing regions, A and B, and 1.25 when comparing regions C and D.

5.2 General Discussion

It had already been shown by Dogliotti *et al.* that mutation in the CAAX box (using $LKB1_{C564A}$ mutant) does not affect lateral membrane localization of LKB1 in epithelial cells of embryonic epidermis (108). However, CAAX box and lipid binding domain mutant, LKB1 ΔLBCA did show a prominent change in localization in the lateral membrane of the Drosophila wing imaginal disc. This is seen by presence of broader peaks for LKB1 ΔLBCA as compared to steeper peaks in LKB1 wildtype in Figure 17d. However, presence of some steeper peaks is still seen thus some membrane localization still remains, as visually seen after mutation of the CAAX box and lipid-binding domain. The differences in slope average and total intensity obtained for LKB1 wild type and LKB1 mutant were significant as shown in Figure 17e and f, with the P-values<0.05. Thus, the differences in localization and levels/ stability of the kinase domain of LKB1 between the wild-type and mutant were real. An interesting observation was comparison of the slope average of LKB1 ΔLBCA (in Figure 17) and that of WDFY2 in Figure 15b. The value for slope average obtained for both was approximately 116. Since we know that WDFY2 localizes in the cytosol (endosomes and cytoplasm), this could help us conclude that the ΔLBCA mutation, in fact reduces membrane localization of LKB1, to the extent that most of it has the same localization pattern as WDFY2.

Furthermore, we decided to make a stable stock for LKB1 ΔLBCA double balanced and with the >ChWDFY2 recombinant (i.e., LKB1 ΔLBCA/CyO; rnGAL4|>ChWDFY2/Tm6c). We were hoping that this would help us conclude better if the localization of LKB1 ΔLBCA is the same as >ChWDFY2 (in the *rotund* region) side-by-side in the same disc. However, due to the interest of time the experiment was not completed. On our existing findings it was concluded that only mutants which are deficient of both the farnesylation mutant and lipid binding domain may affect LKB1 membrane localization as compared to only farnesylation-deficient mutants (which have no effect as shown by Dogliotti *et al.*) (108). Since the average total intensity of LKB1 ΔLBCA was lower than LKB1 WT we also speculated that the stability of

LKB1 in the mutant was lesser than its wild-type counterpart (AIT for LKB1 WT of 257200, AIT for LKB1 ΔLBCA of 195828). This speculation was made on the basis that both the constructs are inserted at the same site with the same endogenous enhancer for both LKB1 WT and LKB1 ΔLBCA. Furthermore, the mutation of the CAAX box and lipid binding domain cause a change in the tertiary structure of the protein, as shown by the structural prediction model in Figure 18, comparing the three-dimensional structure of wildtype and mutant protein. The ΔLBCA mutations cause the secondary structure to fold differently, such that perhaps it may affect the binding site of LKB1 where it binds MO25 and STRAD-alpha, to form a heterotrimeric complex. Unable to form a heterotrimeric complex due to the binding site being affected, does not allow it to be transported to the cytoplasm from the nucleus, thus affecting its localization.

Figure 20 shows knockdown of LKB1 using RNAi line 1216 and 1236. The knockdown reduces membrane localization of LKB1 as well as its levels on the membranes. The knockdown effect in 250 was more than in 150. If the membrane localization of LKB1 reduces, the leftover levels seen were perhaps of cytosolic LKB1. The membrane association of LKB1 is important for the stability of the protein and is needed for polarization of the oocyte, survival, and development of the *Drosophila* fly (108). Reduction of protein levels on the membrane indicates lower stability of the kinase domain.

Figure 21 helped us identify apical membrane localization of LKB1 wildtype stock. An LKB1 knockdown using the effective fly line 1216 (penetrance on 50-60% as shown in Figure 1 in Appendix IV) did not show knockdown of apical LKB1. This was shown by unaffected values for slope averages in Figure 21 when compared to dorsal wing blade (rotund region) and dorsal hinge within the same disc. However, a decrease in the total intensity in the dorsal wing (*rotund* region) is seen in comparison to the dorsal hinge. This indicates that even though the slope average of GFP-LKB1 stayed unaffected, the levels of GFP-LKB1 decreased due to knockdown. The unaffected values of slope average might correspond to apical localization of LKB1 while the decrease in LKB1 levels might correspond to the value caused by knockout of lateral membrane localized LKB1. This helped us conclude that the LKB1IR line 1216 was successful in reducing lateral membrane localization but not apical membrane localization.

In Figure 22 (fly line 150) we see increase in membrane localization and levels of LKB1 due to WDFY2 knockdown. LKB1 associates with WDFY2 on the endosomes. WDFY2 also causes LKB1 mediated activation of AMPK, needed for epithelial integrity (133). When the cytosol is deficient of WDFY2 it can no longer associate with the endosomes and instead associates to the membrane (or closer to it) through the farnesylation motif in its CAAX box. This increases its membrane localization/proximity and levels. The same pattern was seen in Figure 23 (fly line 250) for LKB1 where the membrane localization was seen to increase, however, the levels of LKB1 were not affected. The variation of the same affect across different fly lines may be due to the natural variability of stability of the kinase domain. LKB1 also colocalizes with WDFY2 and that may visually be seen by an overlap of the GFP and RFP signal, as represented in yellow

and orange in the merge panels in Figure 23. However, in order to investigate and confirm colocalization more complex colocalization studies and statistical tests of the two proteins are needed (134).

PI3K-III interacts with LKB1 downstream which allows LKB1 to associate with Rab5 and Rab7 endosomes as shown by O'Farrell *et al*. in flies and humans. If vps34 is disrupted it was believed to cause the same effect as that seen in WDFY2IR. PI3K-III is important for association of LKB1 with the endosomes thus knockdown of its catalytic will affect its function and interaction with LKB1. If LKB1 cannot associate with the endosomes since the successful maturation of Rab5 to Rab7 vesicles does not happen, it would instead associate with the membranes due to its farnesylation motif. The same was seen in Figure 24 where membrane localization of LKB1 increased on vps34 knockdown. We observed a leakage of the RFP signal from the *apterous* region into the rest of the nearby regions and made a speculation about possible interaction between *rotund* and *apterous*. A phenotype of crimpled wings was seen in Drosophila adults for these flies confirming the possible speculation (in Figure 24c). Furthermore, vps34 knockdown was also seen in LKB1 wildtype to confirm if the knockdown affect was real and not a result of an unknown interaction between the patterning genes. In Figure 25 we saw a similar pattern of increased LKB1 localization and levels, and with a greater affect. PI3K-CIII generates PtdIns(3)P creating a binding site for WDFY2 on the endosomes. This is where LKB1 associates with the endosomes. Thus, WDFY2 allows the activation of AMPK through LKB1, needed for epithelial integrity. Association of LKB1 on the endosomes through the PI3K-CIII and WDFY2 pathway, inhibits LKB1 and regulates its activity. Loss of this regulation, as in the case of our WDFY2 and vps34 knockdown, give rise to oncogenic activities of LKB1 (112). In order to improve the results of the experiment for vps34 knockdown it would have been useful to compare the knockdown effect of LKB1 with a wildtype version of LKB1 with no knockdown effect.

We also investigated the effect of starvation on LKB1 localization and activity (Figure 26). This was done by knockdown of Chico, an insulin receptor substrate which caused induction of autophagy. Under high glucose conditions as shown in Figure 10, Chico is active, and in response to insulin signaling causes inactivation of AMPK and activation of mTOR through PI3K. When AMPK is active on induction of starvation it causes phosphorylation of Ulk1 and Beclin1 which work towards initiating the formation of the phagophore and conjugate through Atg8 (and other Atg-dependent pathways) to form an autophagosome and eventually the autolysosome (135). In Figure 26 we saw reduced levels of LKB1 (as shown by a negative value for difference in AIT between the engrailed/posterior and anterior boundary) and increased membrane localization (shown by positive value for difference in slope average between the engrailed/posterior and anterior boundary) as a result of starvation induced autophagy. This could help us speculate that that cytoplasmic LKB1 was turned over quickly while membrane localized LKB1 was saved from turnover. Thus, decreased levels of LKB1 could show that it was either on the endosomes or part of the autolysosome for recycling. The reduction in levels of LKB1 could be a probable indication of the latter.

This is because when in the lysosome (for degradation), the expression of LKB1 is sequestered within the double-membrane autophagophore (135). The significance of using Atg8 was that it is commonly used as a reporter for autophagy since it moves from the cytoplasm to the punctate autophagosomal structures (136). Since LKB1 levels were seen to reduce in our experiment, Atg8 could not be used for the purpose (i.e., to see expression of LKB1 in the puncta). It would be interesting to see the effect of starvation induced autophagy on LKB1 localization and levels in LKB1 ΔLBCA mutant. A change in cytoplasmic LKB1 in that context would help us gain a better understanding of the pathway of LKB1. It would also have been useful to have a wildtype version of enGAL4,>ChAtg8 showing expression of LKB1 without the knockdown affect for a better comparison. In that context, constructing the following fly line would have helped: lkb1>GFP::Lkb1/CyO;enGAL4>ChAtg8/Tm6c. This would also give us a chance to compare the change on levels of Atg8. Since we are aware that autophagy is regulated through the LKB1-AMPK-mTOR pathway it would be interesting to see how the localization and activity of AMPK is affected alongside LKB1. In addition, an AMPK independent regulation of autophagy through LKB1 and p27 has also been suggested by Liang *et al* (122). We could further investigate this for phenotypic effects in the wing using knockdown of p27 after starvation induced autophagy and observe the reduction in the number of puncta (autophagosomes).

6. Conclusion

The study was successful in using the knowledge of balancer chromosomes and occurrence of recombination in *Drosophila* females to construct recombinant tools for identifying the localization and activity of LKB1 in control and marked tissue of wing imaginal discs. Additionally, we made ways to measure its proximity to membrane. Our findings have shown that endogenous GFP-LKB1 is present on the lateral membrane and on knockdown shows lesser turn over in the cytoplasm, as compared to the lateral membrane. This could be suggestive of the fact that lesser levels of LKB1 are found closer to the membrane than the rest of the cell and also that, once LKB1 is endocytosed it becomes active. We confirmed that recombinant fly lines lkb1>GFP::Lkb1/CyO; rnGAL4|>CD8ChRFP/Tm6c (150) and lkb1>GFP::Lkb1/CyO; rnGAL4|>ChWDFY2/Tm6c (250), can be used to knockdown intracellular trafficking modulators such as CIII-PI3K and WDFY2, which have an important role in the endosomal pathway and in turn effect localization and activity of LKB1. Disruption of the endosomal system elevated LKB1 activity levels which disrupted epithelial integrity (which can lead to an oncogenic fate). Furthermore, we were able to examine the effect of starvation-induced autophagy on LKB1 activity which was suggestive of the movement of LKB1 to the lysosome to decrease (or potentially halt) its activity and in turn also cause disruption of polarization. It would be useful to have a rescue of starvation by using another approach for inducing starvation (reduced nutrition), and re-feeding to see how it effects LKB1 activity and epithelial integrity.

Previous studies discuss the role of LKB1 in activation of AMPK to allow cancer cell survival under nutrient stress, or hypoxia and also that LKB1 and AMPK are both associated with the endo-lysosomal pathway (86, 112). Therefore, it would be interesting to see how the activity of both of these proteins are affected as a result of disrupting intracellular trafficking regulators. Construction of a recombinant fly line using Cherry-tagged AMPK, co-expressed with LKB1 would prove to be useful to see how disruption of specific steps in the pathway effect the localization and activity of both proteins side-by-side. In addition, using an antibody against AMPK (consisting of a fluorescence tag different than Cherry or RFP such as yellow fluorescent protein, YFP) after blocking certain steps in the endo-lysosomal pathway in recombinant fly lines could be useful in the same context. This will help it to be distinguished from the Cherry or RFP signal of >CD8ChRFP and >ChWDFY2 in recombinant lines and allow it to be observed side-by-side along with these proteins, as well as GFP-LKB1. In addition, it would be interesting to see how autophagy is positively regulated by AMPK using the same approach which would indirectly give more information about LKB1 regulation and a possible corelation. Other RNAi lines can be used for knockdown of the same controls as used in this study for improved comparison, or other already documented regulators could be

disrupted to see the effect on LKB1: such as Rab5, Rab7, vps15 and scaffolding protein AXIN. Lastly, the results in *Drosophila* could be further examined in mammalian cell culture as well.

Finally, we were able to take the first step towards the pathway of LKB1 through the endosomal system and to assess how disruptions within this system can contribute to cancer in the context of PJS. Thus, LKB1 presents a feasible therapeutic target due to its reputation as a contextual oncogene whose localization and activity contributes to cancer cell survival, as a result of downstream cellular and endosomal signalling.

References

1. Adams MD, Celniker SE, Holt RA, Evans CA, Gocayne JD, Amanatides PG, et al. The genome sequence of Drosophila melanogaster. Science. 2000;287(5461):2185-95.
2. Ugur B, Chen K, Bellen HJ. Drosophila tools and assays for the study of human diseases. Dis Model Mech. 2016;9(3):235-44.
3. Rubin GM, Lewis EB. A brief history of Drosophila's contributions to genome research. Science. 2000;287(5461):2216-8.
4. Su TT, O'Farrell PH. Chromosome association of minichromosome maintenance proteins in Drosophila endoreplication cycles. J Cell Biol. 1998;140(3):451-60.
5. Gramates LS, Agapite J, Attrill H, Calvi BR, Crosby MA, Dos Santos G, et al. FlyBase: a guided tour of highlighted features. Genetics. 2022;220(4).
6. Fly pushing : the theory and practice of Drosophila genetics. 2nd ed. New York: Cold Spring Harbor Laboratory Press ; [Oxford : Lavis Marketing, distributor]; 2004.
7. Jiang C, Baehrecke EH, Thummel CS. Steroid regulated programmed cell death during Drosophila metamorphosis. Development. 1997;124(22):4673-83.
8. Cohen B, Simcox AA, Cohen SM. Allocation of the thoracic imaginal primordia in the Drosophila embryo. Development. 1993;117(2):597-608.
9. Wieschaus E, Gehring W. Clonal analysis of primordial disc cells in the early embryo of Drosophila melanogaster. Dev Biol. 1976;50(2):249-63.
10. Agnel M, Roder L, Griffin-Shea R, Vola C. The spatial expression ofDrosophila rotund gene reveals that the imaginal discs are organized in domains along the proximal-distal axis. Rouxs Arch Dev Biol. 1992;201(5):284-95.
11. Diaz-Benjumea FJ, Cohen SM. Interaction between dorsal and ventral cells in the imaginal disc directs wing development in Drosophila. Cell. 1993;75(4):741-52.
12. Hartl TA, Scott MP. Wing tips: The wing disc as a platform for studying Hedgehog signaling. Methods. 2014;68(1):199-206.
13. Fortini ME, Skupski MP, Boguski MS, Hariharan IK. A survey of human disease gene counterparts in the Drosophila genome. J Cell Biol. 2000;150(2):F23-30.
14. St Johnston D. The art and design of genetic screens: Drosophila melanogaster. Nat Rev Genet. 2002;3(3):176-88.
15. Bellen HJ, Levis RW, Liao G, He Y, Carlson JW, Tsang G, et al. The BDGP gene disruption project: single transposon insertions associated with 40% of Drosophila genes. Genetics. 2004;167(2):761-81.
16. Spradling AC, Stern DM, Kiss I, Roote J, Laverty T, Rubin GM. Gene disruptions using P transposable elements: an integral component of the Drosophila genome project. Proc Natl Acad Sci U S A. 1995;92(24):10824-30.
17. Fire A, Xu S, Montgomery MK, Kostas SA, Driver SE, Mello CC. Potent and specific genetic interference by double-stranded RNA in Caenorhabditis elegans. Nature. 1998;391(6669):806-11.
18. Hamilton AJ, Baulcombe DC. A species of small antisense RNA in posttranscriptional gene silencing in plants. Science. 1999;286(5441):950-2.
19. Hammond SM, Caudy AA, Hannon GJ. Post-transcriptional gene silencing by double-stranded RNA. Nat Rev Genet. 2001;2(2):110-9.
20. Sebbagh M, Olschwang S, Santoni MJ, Borg JP. The LKB1 complex-AMPK pathway: the tree that hides the forest. Fam Cancer. 2011;10(3):415-24.
21. Smith DP, Rayter SI, Niederlander C, Spicer J, Jones CM, Ashworth A. LIP1, a cytoplasmic protein functionally linked to the Peutz-Jeghers syndrome kinase LKB1. Hum Mol Genet. 2001;10(25):2869-77.
22. Shackelford DB, Shaw RJ. The LKB1-AMPK pathway: metabolism and growth control in tumour suppression. Nat Rev Cancer. 2009;9(8):563-75.
23. Alessi DR, Sakamoto K, Bayascas JR. LKB1-dependent signaling pathways. Annu Rev Biochem. 2006;75:137-63.
24. Shaw RJ. LKB1 and AMP-activated protein kinase control of mTOR signalling and growth. Acta Physiol (Oxf). 2009;196(1):65-80.
25. Ji H, Ramsey MR, Hayes DN, Fan C, McNamara K, Kozlowski P, et al. LKB1 modulates lung cancer differentiation and metastasis. Nature. 2007;448(7155):807-10.
26. Hemminki A, Avizienyte E, Roth S, Loukola A, Aaltonen LA, Jarvinen H, et al. [A serine/threonine kinase gene defective in Peutz-Jeghers syndrome]. Duodecim. 1998;114(7):667-8.

27. Tiainen M, Vaahtomeri K, Ylikorkala A, Makela TP. Growth arrest by the LKB1 tumor suppressor: induction of p21(WAF1/CIP1). Hum Mol Genet. 2002;11(13):1497-504.
28. Nezu J, Oku A, Shimane M. Loss of cytoplasmic retention ability of mutant LKB1 found in Peutz-Jeghers syndrome patients. Biochem Biophys Res Commun. 1999;261(3):750-5.
29. Boudeau J, Baas AF, Deak M, Morrice NA, Kieloch A, Schutkowski M, et al. MO25alpha/beta interact with STRADalpha/beta enhancing their ability to bind, activate and localize LKB1 in the cytoplasm. EMBO J. 2003;22(19):5102-14.
30. Warburg O, Posener K, Negelein E. The metabolism of cancer cells. Biochem Z. 1924;152:319-44.
31. Collins SP, Reoma JL, Gamm DM, Uhler MD. LKB1, a novel serine/threonine protein kinase and potential tumour suppressor, is phosphorylated by cAMP-dependent protein kinase (PKA) and prenylated in vivo. Biochem J. 2000;345 Pt 3:673-80.
32. Xie Z, Dong Y, Zhang M, Cui MZ, Cohen RA, Riek U, et al. Activation of protein kinase C zeta by peroxynitrite regulates LKB1-dependent AMP-activated protein kinase in cultured endothelial cells. J Biol Chem. 2006;281(10):6366-75.
33. Sapkota GP, Boudeau J, Deak M, Kieloch A, Morrice N, Alessi DR. Identification and characterization of four novel phosphorylation sites (Ser31, Ser325, Thr336 and Thr366) on LKB1/STK11, the protein kinase mutated in Peutz-Jeghers cancer syndrome. Biochem J. 2002;362(Pt 2):481-90.
34. Sherman MH, Kuraishy AI, Deshpande C, Hong JS, Cacalano NA, Gatti RA, et al. AID-induced genotoxic stress promotes B cell differentiation in the germinal center via ATM and LKB1 signaling. Mol Cell. 2010;39(6):873-85.
35. Sapkota GP, Kieloch A, Lizcano JM, Lain S, Arthur JS, Williams MR, et al. Phosphorylation of the protein kinase mutated in Peutz-Jeghers cancer syndrome, LKB1/STK11, at Ser431 by p90(RSK) and cAMP-dependent protein kinase, but not its farnesylation at Cys(433), is essential for LKB1 to suppress cell vrowth. J Biol Chem. 2001;276(22):19469-82.
36. Jansen M, Ten Klooster JP, Offerhaus GJ, Clevers H. LKB1 and AMPK family signaling: the intimate link between cell polarity and energy metabolism. Physiol Rev. 2009;89(3):777-98.
37. Martin SG, St Johnston D. A role for Drosophila LKB1 in anterior-posterior axis formation and epithelial polarity. Nature. 2003;421(6921):379-84.
38. Dogliotti G, Kullmann L, Dhumale P, Thiele C, Panichkina O, Mendl G, et al. Membrane-binding and activation of LKB1 by phosphatidic acid is essential for development and tumour suppression. Nat Commun. 2017;8:15747.
39. Wang JW, Imai Y, Lu B. Activation of PAR-1 kinase and stimulation of tau phosphorylation by diverse signals require the tumor suppressor protein LKB1. J Neurosci. 2007;27(3):574-81.
40. Lee JH, Koh H, Kim M, Kim Y, Lee SY, Karess RE, et al. Energy-dependent regulation of cell structure by AMP-activated protein kinase. Nature. 2007;447(7147):1017-20.
41. Lee JH, Koh H, Kim M, Park J, Lee SY, Lee S, et al. JNK pathway mediates apoptotic cell death induced by tumor suppressor LKB1 in Drosophila. Cell Death Differ. 2006;13(7):1110-22.
42. Hezel AF, Bardeesy N. LKB1; linking cell structure and tumor suppression. Oncogene. 2008;27(55):6908-19.
43. Bonaccorsi S, Mottier V, Giansanti MG, Bolkan BJ, Williams B, Goldberg ML, et al. The Drosophila Lkb1 kinase is required for spindle formation and asymmetric neuroblast division. Development. 2007;134(11):2183-93.
44. Jenne DE, Reimann H, Nezu J, Friedel W, Loff S, Jeschke R, et al. Peutz-Jeghers syndrome is caused by mutations in a novel serine threonine kinase. Nat Genet. 1998;18(1):38-43.
45. Avtanski DB, Nagalingam A, Bonner MY, Arbiser JL, Saxena NK, Sharma D. Honokiol activates LKB1-miR-34a axis and antagonizes the oncogenic actions of leptin in breast cancer. Oncotarget. 2015;6(30):29947-62.
46. Liang X, Wang P, Gao Q, Xiang T, Tao X. Endogenous LKB1 knockdown accelerates G(1)/S transition through p53 and p16 pathways. Cancer Biol Ther. 2010;9(2):156-60.
47. Liang X, Wang P, Gao Q, Tao X. Exogenous activation of LKB1/AMPK signaling induces G(1) arrest in cells with endogenous LKB1 expression. Mol Med Rep. 2014;9(3):1019-24.
48. Zeng PY, Berger SL. LKB1 is recruited to the p21/WAF1 promoter by p53 to mediate transcriptional activation. Cancer Res. 2006;66(22):10701-8.
49. Xie X, Wang Z, Chen Y. Association of LKB1 with a WD-repeat protein WDR6 is implicated in cell growth arrest and p27(Kip1) induction. Mol Cell Biochem. 2007;301(1-2):115-22.
50. Scott KD, Nath-Sain S, Agnew MD, Marignani PA. LKB1 catalytically deficient mutants enhance cyclin D1 expression. Cancer Res. 2007;67(12):5622-7.

51. Karuman P, Gozani O, Odze RD, Zhou XC, Zhu H, Shaw R, et al. The Peutz-Jegher gene product LKB1 is a mediator of p53-dependent cell death. Mol Cell. 2001;7(6):1307-19.
52. Korsse SE, Peppelenbosch MP, van Veelen W. Targeting LKB1 signaling in cancer. Biochim Biophys Acta. 2013;1835(2):194-210.
53. Xu C, Fillmore CM, Koyama S, Wu H, Zhao Y, Chen Z, et al. Loss of Lkb1 and Pten leads to lung squamous cell carcinoma with elevated PD-L1 expression. Cancer Cell. 2014;25(5):590-604.
54. Liu JL, Mao Z, Gallick GE, Yung WK. AMPK/TSC2/mTOR-signaling intermediates are not necessary for LKB1-mediated nuclear retention of PTEN tumor suppressor. Neuro Oncol. 2011;13(2):184-94.
55. Bouchekioua-Bouzaghou K, Poulard C, Rambaud J, Lavergne E, Hussein N, Billaud M, et al. LKB1 when associated with methylatedERalpha is a marker of bad prognosis in breast cancer. Int J Cancer. 2014;135(6):1307-18.
56. Tan X, Liao Z, Liang H, Chen X, Zhang B, Chu L. Upregulation of liver kinase B1 predicts poor prognosis in hepatocellular carcinoma. Int J Oncol. 2018;53(5):1913-26.
57. Dahmani R, Just PA, Delay A, Canal F, Finzi L, Prip-Buus C, et al. A novel LKB1 isoform enhances AMPK metabolic activity and displays oncogenic properties. Oncogene. 2015;34(18):2337-46.
58. Jeon SM, Hay N. The dark face of AMPK as an essential tumor promoter. Cell Logist. 2012;2(4):197-202.
59. Lee SW, Li CF, Jin G, Cai Z, Han F, Chan CH, et al. Skp2-dependent ubiquitination and activation of LKB1 is essential for cancer cell survival under energy stress. Mol Cell. 2015;57(6):1022-33.
60. Trapp EK, Majunke L, Zill B, Sommer H, Andergassen U, Koch J, et al. LKB1 pro-oncogenic activity triggers cell survival in circulating tumor cells. Mol Oncol. 2017;11(11):1508-26.
61. Sharma VK, Raimondi V, Ruggero K, Pise-Masison CA, Cavallari I, Silic-Benussi M, et al. Expression of miR-34a in T-Cells Infected by Human T-Lymphotropic Virus 1. Front Microbiol. 2018;9:832.
62. Rios M, Foretz M, Viollet B, Prieto A, Fraga M, Garcia-Caballero T, et al. Lipoprotein internalisation induced by oncogenic AMPK activation is essential to maintain glioblastoma cell growth. Eur J Cancer. 2014;50(18):3187-97.
63. Wurstle S, Schneider F, Ringel F, Gempt J, Lammer F, Delbridge C, et al. Temozolomide induces autophagy in primary and established glioblastoma cells in an EGFR independent manner. Oncol Lett. 2017;14(1):322-8.
64. Baas AF, Kuipers J, van der Wel NN, Batlle E, Koerten HK, Peters PJ, et al. Complete polarization of single intestinal epithelial cells upon activation of LKB1 by STRAD. Cell. 2004;116(3):457-66.
65. Zheng B, Cantley LC. Regulation of epithelial tight junction assembly and disassembly by AMP-activated protein kinase. Proc Natl Acad Sci U S A. 2007;104(3):819-22.
66. Shelly M, Cancedda L, Heilshorn S, Sumbre G, Poo MM. LKB1/STRAD promotes axon initiation during neuronal polarization. Cell. 2007;129(3):565-77.
67. Barnes AP, Lilley BN, Pan YA, Plummer LJ, Powell AW, Raines AN, et al. LKB1 and SAD kinases define a pathway required for the polarization of cortical neurons. Cell. 2007;129(3):549-63.
68. Spicer J, Ashworth A. LKB1 kinase: master and commander of metabolism and polarity. Curr Biol. 2004;14(10):R383-5.
69. Fu D, Wakabayashi Y, Ido Y, Lippincott-Schwartz J, Arias IM. Regulation of bile canalicular network formation and maintenance by AMP-activated protein kinase and LKB1. J Cell Sci. 2010;123(Pt 19):3294-302.
70. Zhang L, Li J, Young LH, Caplan MJ. AMP-activated protein kinase regulates the assembly of epithelial tight junctions. Proc Natl Acad Sci U S A. 2006;103(46):17272-7.
71. ten Klooster JP, Jansen M, Yuan J, Oorschot V, Begthel H, Di Giacomo V, et al. Mst4 and Ezrin induce brush borders downstream of the Lkb1/Strad/Mo25 polarization complex. Dev Cell. 2009;16(4):551-62.
72. Gloerich M, ten Klooster JP, Vliem MJ, Koorman T, Zwartkruis FJ, Clevers H, et al. Rap2A links intestinal cell polarity to brush border formation. Nat Cell Biol. 2012;14(8):793-801.
73. Boehlke C, Kotsis F, Patel V, Braeg S, Voelker H, Bredt S, et al. Primary cilia regulate mTORC1 activity and cell size through Lkb1. Nat Cell Biol. 2010;12(11):1115-22.
74. Sebbagh M, Santoni MJ, Hall B, Borg JP, Schwartz MA. Regulation of LKB1/STRAD localization and function by E-cadherin. Curr Biol. 2009;19(1):37-42.
75. Martin-Belmonte F, Perez-Moreno M. Epithelial cell polarity, stem cells and cancer. Nat Rev Cancer. 2011;12(1):23-38.
76. Forcet C, Billaud M. Dialogue between LKB1 and AMPK: a hot topic at the cellular pole. Sci STKE. 2007;2007(404):pe51.
77. Shaw RJ, Kosmatka M, Bardeesy N, Hurley RL, Witters LA, DePinho RA, et al. The tumor suppressor LKB1 kinase directly activates AMP-activated kinase and regulates apoptosis in response to energy stress. Proc Natl Acad Sci U S A. 2004;101(10):3329-35.
78. Hardie DG. AMPK and autophagy get connected. EMBO J. 2011;30(4):634-5.

79. Carling D. The role of the AMP-activated protein kinase in the regulation of energy homeostasis. Novartis Found Symp. 2007;286:72-81; discussion -5, 162-3, 96-203.
80. Carling D, Mayer FV, Sanders MJ, Gamblin SJ. AMP-activated protein kinase: nature's energy sensor. Nat Chem Biol. 2011;7(8):512-8.
81. Jeon SM, Chandel NS, Hay N. AMPK regulates NADPH homeostasis to promote tumour cell survival during energy stress. Nature. 2012;485(7400):661-5.
82. Rowan A, Churchman M, Jefferey R, Hanby A, Poulsom R, Tomlinson I. In situ analysis of LKB1/STK11 mRNA expression in human normal tissues and tumours. J Pathol. 2000;192(2):203-6.
83. Hezel AF, Gurumurthy S, Granot Z, Swisa A, Chu GC, Bailey G, et al. Pancreatic LKB1 deletion leads to acinar polarity defects and cystic neoplasms. Mol Cell Biol. 2008;28(7):2414-25.
84. Horman S, Morel N, Vertommen D, Hussain N, Neumann D, Beauloye C, et al. AMP-activated protein kinase phosphorylates and desensitizes smooth muscle myosin light chain kinase. J Biol Chem. 2008;283(27):18505-12.
85. Mirouse V, Billaud M. The LKB1/AMPK polarity pathway. FEBS Lett. 2011;585(7):981-5.
86. Houde VP, Ritorto MS, Gourlay R, Varghese J, Davies P, Shpiro N, et al. Investigation of LKB1 Ser431 phosphorylation and Cys433 farnesylation using mouse knockin analysis reveals an unexpected role of prenylation in regulating AMPK activity. Biochem J. 2014;458(1):41-56.
87. Liang J, Xu ZX, Ding Z, Lu Y, Yu Q, Werle KD, et al. Myristoylation confers noncanonical AMPK functions in autophagy selectivity and mitochondrial surveillance. Nat Commun. 2015;6:7926.
88. Oakhill JS, Chen ZP, Scott JW, Steel R, Castelli LA, Ling N, et al. beta-Subunit myristoylation is the gatekeeper for initiating metabolic stress sensing by AMP-activated protein kinase (AMPK). Proc Natl Acad Sci U S A. 2010;107(45):19237-41.
89. Zhou G, Myers R, Li Y, Chen Y, Shen X, Fenyk-Melody J, et al. Role of AMP-activated protein kinase in mechanism of metformin action. J Clin Invest. 2001;108(8):1167-74.
90. Svensson RU, Parker SJ, Eichner LJ, Kolar MJ, Wallace M, Brun SN, et al. Inhibition of acetyl-CoA carboxylase suppresses fatty acid synthesis and tumor growth of non-small-cell lung cancer in preclinical models. Nat Med. 2016;22(10):1108-19.
91. Saito Y, Chapple RH, Lin A, Kitano A, Nakada D. AMPK Protects Leukemia-Initiating Cells in Myeloid Leukemias from Metabolic Stress in the Bone Marrow. Cell Stem Cell. 2015;17(5):585-96.
92. Marignani PA, Kanai F, Carpenter CL. LKB1 associates with Brg1 and is necessary for Brg1-induced growth arrest. J Biol Chem. 2001;276(35):32415-8.
93. Zhang CS, Jiang B, Li M, Zhu M, Peng Y, Zhang YL, et al. The lysosomal v-ATPase-Ragulator complex is a common activator for AMPK and mTORC1, acting as a switch between catabolism and anabolism. Cell Metab. 2014;20(3):526-40.
94. Sancak Y, Bar-Peled L, Zoncu R, Markhard AL, Nada S, Sabatini DM. Ragulator-Rag complex targets mTORC1 to the lysosomal surface and is necessary for its activation by amino acids. Cell. 2010;141(2):290-303.
95. Tacheci I, Kopacova M, Bures J. Peutz-Jeghers syndrome. Curr Opin Gastroenterol. 2021;37(3):245-54.
96. Jeghers H, Mc KV, Katz KH. Generalized intestinal polyposis and melanin spots of the oral mucosa, lips and digits; a syndrome of diagnostic significance. N Engl J Med. 1949;241(26):1031-6.
97. Westerman AM, Entius MM, de Baar E, Boor PP, Koole R, van Velthuysen ML, et al. Peutz-Jeghers syndrome: 78-year follow-up of the original family. Lancet. 1999;353(9160):1211-5.
98. Olschwang S, Boisson C, Thomas G. Peutz-Jeghers families unlinked to STK11/LKB1 gene mutations are highly predisposed to primitive biliary adenocarcinoma. J Med Genet. 2001;38(6):356-60.
99. Aretz S, Stienen D, Uhlhaas S, Loff S, Back W, Pagenstecher C, et al. High proportion of large genomic STK11 deletions in Peutz-Jeghers syndrome. Hum Mutat. 2005;26(6):513-9.
100. Volikos E, Robinson J, Aittomaki K, Mecklin JP, Jarvinen H, Westerman AM, et al. LKB1 exonic and whole gene deletions are a common cause of Peutz-Jeghers syndrome. J Med Genet. 2006;43(5):e18.
101. Duan FX, Gu GL, Yang HR, Yu PF, Zhang Z. Must Peutz-Jeghers syndrome patients have the LKB1/STK11 gene mutation? A case report and review of the literature. World J Clin Cases. 2018;6(8):224-32.
102. Giardiello FM, Brensinger JD, Tersmette AC, Goodman SN, Petersen GM, Booker SV, et al. Very high risk of cancer in familial Peutz-Jeghers syndrome. Gastroenterology. 2000;119(6):1447-53.
103. Hearle N, Schumacher V, Menko FH, Olschwang S, Boardman LA, Gille JJ, et al. Frequency and spectrum of cancers in the Peutz-Jeghers syndrome. Clin Cancer Res. 2006;12(10):3209-15.
104. Mehenni H, Resta N, Park JG, Miyaki M, Guanti G, Costanza MC. Cancer risks in LKB1 germline mutation carriers. Gut. 2006;55(7):984-90.

105. Beggs AD, Latchford AR, Vasen HF, Moslein G, Alonso A, Aretz S, et al. Peutz-Jeghers syndrome: a systematic review and recommendations for management. Gut. 2010;59(7):975-86.
106. Koivunen JP, Kim J, Lee J, Rogers AM, Park JO, Zhao X, et al. Mutations in the LKB1 tumour suppressor are frequently detected in tumours from Caucasian but not Asian lung cancer patients. Br J Cancer. 2008;99(2):245-52.
107. Esteller M, Avizienyte E, Corn PG, Lothe RA, Baylin SB, Aaltonen LA, et al. Epigenetic inactivation of LKB1 in primary tumors associated with the Peutz-Jeghers syndrome. Oncogene. 2000;19(1):164-8.
108. Dogliotti G, Kullmann L, Dhumale P, Thiele C, Panichkina O, Mendl G, et al. Author Correction: Membrane-binding and activation of LKB1 by phosphatidic acid is essential for development and tumour suppression. Nat Commun. 2022;13(1):1283.
109. Zhang YL, Guo H, Zhang CS, Lin SY, Yin Z, Peng Y, et al. AMP as a low-energy charge signal autonomously initiates assembly of AXIN-AMPK-LKB1 complex for AMPK activation. Cell Metab. 2013;18(4):546-55.
110. Chen J, Ou Y, Li Y, Hu S, Shao LW, Liu Y. Metformin extends C. elegans lifespan through lysosomal pathway. Elife. 2017;6.
111. Tortelote GG, Reis RR, de Almeida Mendes F, Abreu JG. Complexity of the Wnt/betacatenin pathway: Searching for an activation model. Cell Signal. 2017;40:30-43.
112. O'Farrell F, Lobert VH, Sneeggen M, Jain A, Katheder NS, Wenzel EM, et al. Class III phosphatidylinositol-3-OH kinase controls epithelial integrity through endosomal LKB1 regulation. Nat Cell Biol. 2017;19(12):1412-23.
113. Raiborg C, Schink KO, Stenmark H. Class III phosphatidylinositol 3-kinase and its catalytic product PtdIns3P in regulation of endocytic membrane traffic. FEBS J. 2013;280(12):2730-42.
114. Poteryaev D, Datta S, Ackema K, Zerial M, Spang A. Identification of the switch in early-to-late endosome transition. Cell. 2010;141(3):497-508.
115. Rabinowitz JD, White E. Autophagy and metabolism. Science. 2010;330(6009):1344-8.
116. Galluzzi L, Pietrocola F, Levine B, Kroemer G. Metabolic control of autophagy. Cell. 2014;159(6):1263-76.
117. Narbonne P, Roy R. Caenorhabditis elegans dauers need LKB1/AMPK to ration lipid reserves and ensure long-term survival. Nature. 2009;457(7226):210-4.
118. Ylikorkala A, Rossi DJ, Korsisaari N, Luukko K, Alitalo K, Henkemeyer M, et al. Vascular abnormalities and deregulation of VEGF in Lkb1-deficient mice. Science. 2001;293(5533):1323-6.
119. Mizushima N, Levine B, Cuervo AM, Klionsky DJ. Autophagy fights disease through cellular self-digestion. Nature. 2008;451(7182):1069-75.
120. Clancy DJ, Gems D, Harshman LG, Oldham S, Stocker H, Hafen E, et al. Extension of life-span by loss of CHICO, a Drosophila insulin receptor substrate protein. Science. 2001;292(5514):104-6.
121. Wu W, Wang X, Berleth N, Deitersen J, Wallot-Hieke N, Bohler P, et al. The Autophagy-Initiating Kinase ULK1 Controls RIPK1-Mediated Cell Death. Cell Rep. 2020;31(3):107547.
122. Liang J, Shao SH, Xu ZX, Hennessy B, Ding Z, Larrea M, et al. The energy sensing LKB1-AMPK pathway regulates p27(kip1) phosphorylation mediating the decision to enter autophagy or apoptosis. Nat Cell Biol. 2007;9(2):218-24.
123. de Mello NP, Orellana AM, Mazucanti CH, de Morais Lima G, Scavone C, Kawamoto EM. Insulin and Autophagy in Neurodegeneration. Front Neurosci. 2019;13:491.
124. Calamaras TD, Lee C, Lan F, Ido Y, Siwik DA, Colucci WS. Post-translational modification of serine/threonine kinase LKB1 via Adduction of the Reactive Lipid Species 4-Hydroxy-trans-2-nonenal (HNE) at lysine residue 97 directly inhibits kinase activity. J Biol Chem. 2012;287(50):42400-6.
125. Kirkpatrick M. How and why chromosome inversions evolve. PLoS Biol. 2010;8(9).
126. Talbert PB, Henikoff S. Centromeres convert but don't cross. PLoS Biol. 2010;8(3):e1000326.
127. Hazelrigg T, Levis R, Rubin GM. Transformation of white locus DNA in drosophila: dosage compensation, zeste interaction, and position effects. Cell. 1984;36(2):469-81.
128. Pirrotta V, Steller H, Bozzetti MP. Multiple upstream regulatory elements control the expression of the Drosophila white gene. EMBO J. 1985;4(13A):3501-8.
129. Levis R, Hazelrigg T, Rubin GM. Separable cis-acting control elements for expression of the white gene of Drosophila. EMBO J. 1985;4(13A):3489-99.
130. Roger V, Fonty G, Andre C, Gouet P. Effects of glycerol on the growth, adhesion, and cellulolytic activity of rumen cellulolytic bacteria and anaerobic fungi. Curr Microbiol. 1992;25(4):197-201.
131. Pina R, Santos-Diaz AI, Orta-Salazar E, Aguilar-Vazquez AR, Mantellero CA, Acosta-Galeana I, et al. Ten Approaches That Improve Immunostaining: A Review of the Latest Advances for the Optimization of Immunofluorescence. Int J Mol Sci. 2022;23(3).

132. Buchwalow I, Samoilova V, Boecker W, Tiemann M. Non-specific binding of antibodies in immunohistochemistry: fallacies and facts. Sci Rep. 2011;1:28.
133. Kullmann L, Krahn MP. Controlling the master-upstream regulation of the tumor suppressor LKB1. Oncogene. 2018;37(23):3045-57.
134. McDonald JH, Dunn KW. Statistical tests for measures of colocalization in biological microscopy. J Microsc. 2013;252(3):295-302.
135. F OF, Rusten TE, Stenmark H. Phosphoinositide 3-kinases as accelerators and brakes of autophagy. FEBS J. 2013;280(24):6322-37.
136. Baba M, Tomonaga S, Suzuki M, Gen M, Takeda E, Matsuura A, et al. A nuclear membrane-derived structure associated with Atg8 is involved in the sequestration of selective cargo, the Cvt complex, during autophagosome formation in yeast. Autophagy. 2019;15(3):423-37.

Appendix

I. Genetic crosses for generation of recombinants

1. $\frac{lkb1{>}GFP{::}LKB1;Dr}{S-T} \quad X \quad \frac{sp}{CyO} ; \frac{Dr}{TM6c} \longrightarrow \frac{lkb1{>}GFP{::}LKB1}{CyO} ; \frac{Dr}{TM6c}$

2. $\frac{rnGAL4}{TM3} \quad X \quad \frac{sp;ChSNF1a}{S-T} \longrightarrow \frac{rnGAL4}{ChSNF1a}\ ♀$

3. $\frac{rnGAL4}{ChSNF1a}\ ♀ \quad X \quad \frac{sp}{CyO} ; \frac{Dr}{TM6c} \longrightarrow \frac{sp}{CyO} ; \frac{rnGAL4\ |{>}ChSNF1a}{TM6c}$

4. $\frac{rnGAL4}{TM3} \quad X \quad {>}ChWdfy2 \longrightarrow \frac{rnGAL4}{{>}ChWdfy2}\ ♀$

5. $\frac{rnGAL4}{{>}ChWdfy2}\ ♀ \quad X \quad \frac{sp}{CyO} ; \frac{Dr}{TM6c} \longrightarrow \frac{sp}{CyO} ; \frac{rnGAL4\ |{>}ChWdfy2}{TM6c}$

6. $\frac{rnGAL4}{TM3} \quad X \quad {>}CD8ChRFP \longrightarrow \frac{rnGAL4}{{>}CD8ChRFP}\ ♀$

7. $\frac{rnGAL4}{{>}CD8ChRFP}\ ♀ \quad X \quad \frac{sp}{CyO} ; \frac{Dr}{TM6c} \longrightarrow \frac{sp}{CyO} ; \frac{rnGAL4\ |{>}CD8ChRFP}{TM6c}$

8. $\frac{sp}{CyO} ; \frac{rnGAL4\ |{>}ChSNF1a}{TM6c} \quad X \quad \frac{lkb1{>}GFP{::}LKB1}{CyO} ; \frac{Dr}{TM6c} \longrightarrow \frac{lkb1{>}GFP{::}LKB1}{CyO} ; \frac{rnGAL4\ |{>}ChSNF1a}{TM6c}$

9. $\frac{sp}{CyO} ; \frac{rnGAL4\ |{>}ChWdfy2}{TM6c} \quad X \quad \frac{lkb1{>}GFP{::}LKB1}{CyO} ; \frac{Dr}{TM6c} \longrightarrow \frac{lkb1{>}GFP{::}LKB1}{CyO} ; \frac{rnGAL4\ |{>}ChWdfy2}{TM6c}$

10. $\frac{sp}{CyO} ; \frac{rnGAL4\ |{>}CD8ChRFP}{TM6c} \quad X \quad \frac{lkb1{>}GFP{::}LKB1}{CyO} ; \frac{Dr}{TM6c} \longrightarrow \frac{lkb1{>}GFP{::}LKB1}{CyO} ; \frac{rnGAL4\ |{>}CD8ChRFP}{TM6c}$

II. Crossing schemes for generation of recombinants

Scheme 1

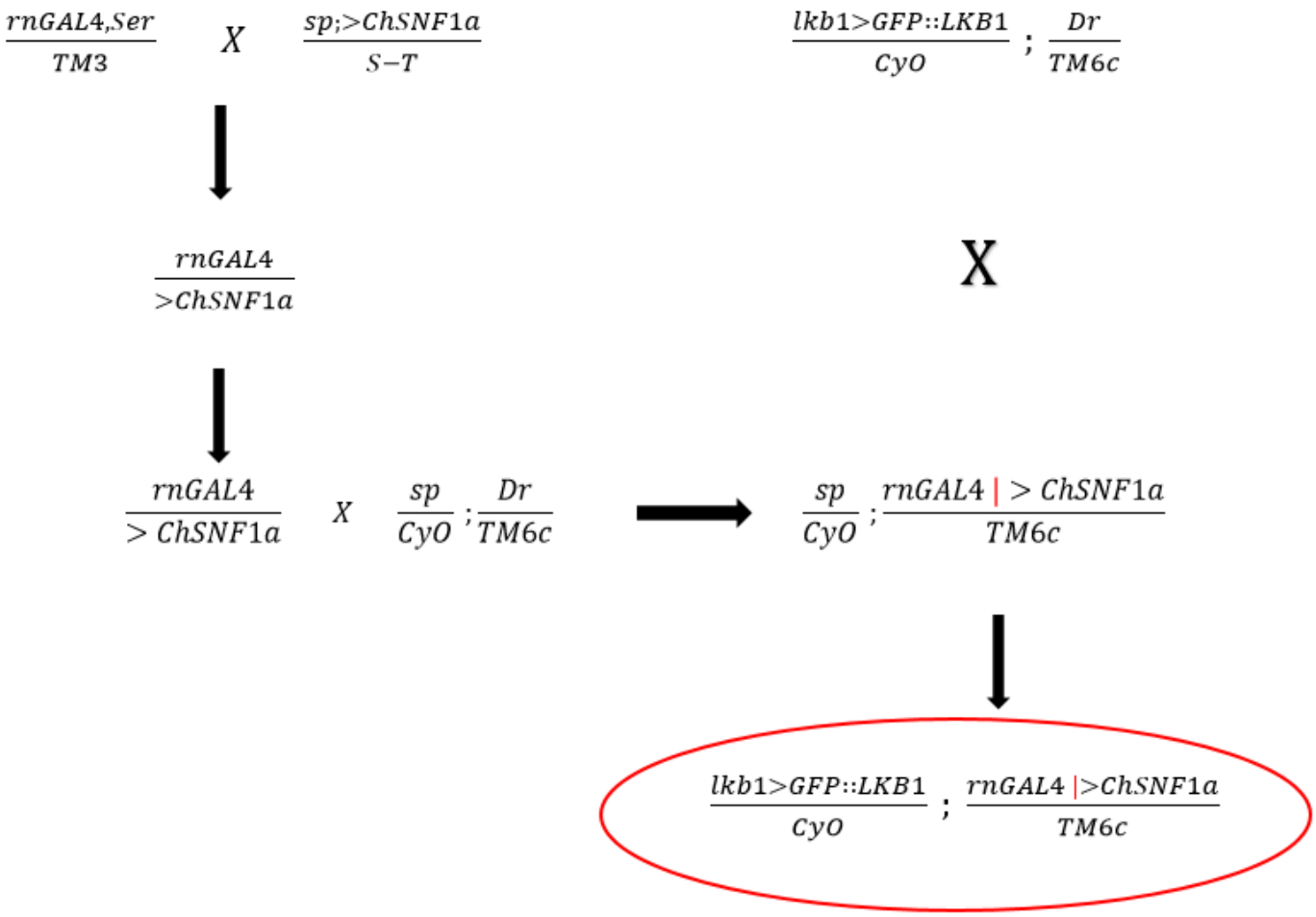

Scheme 2

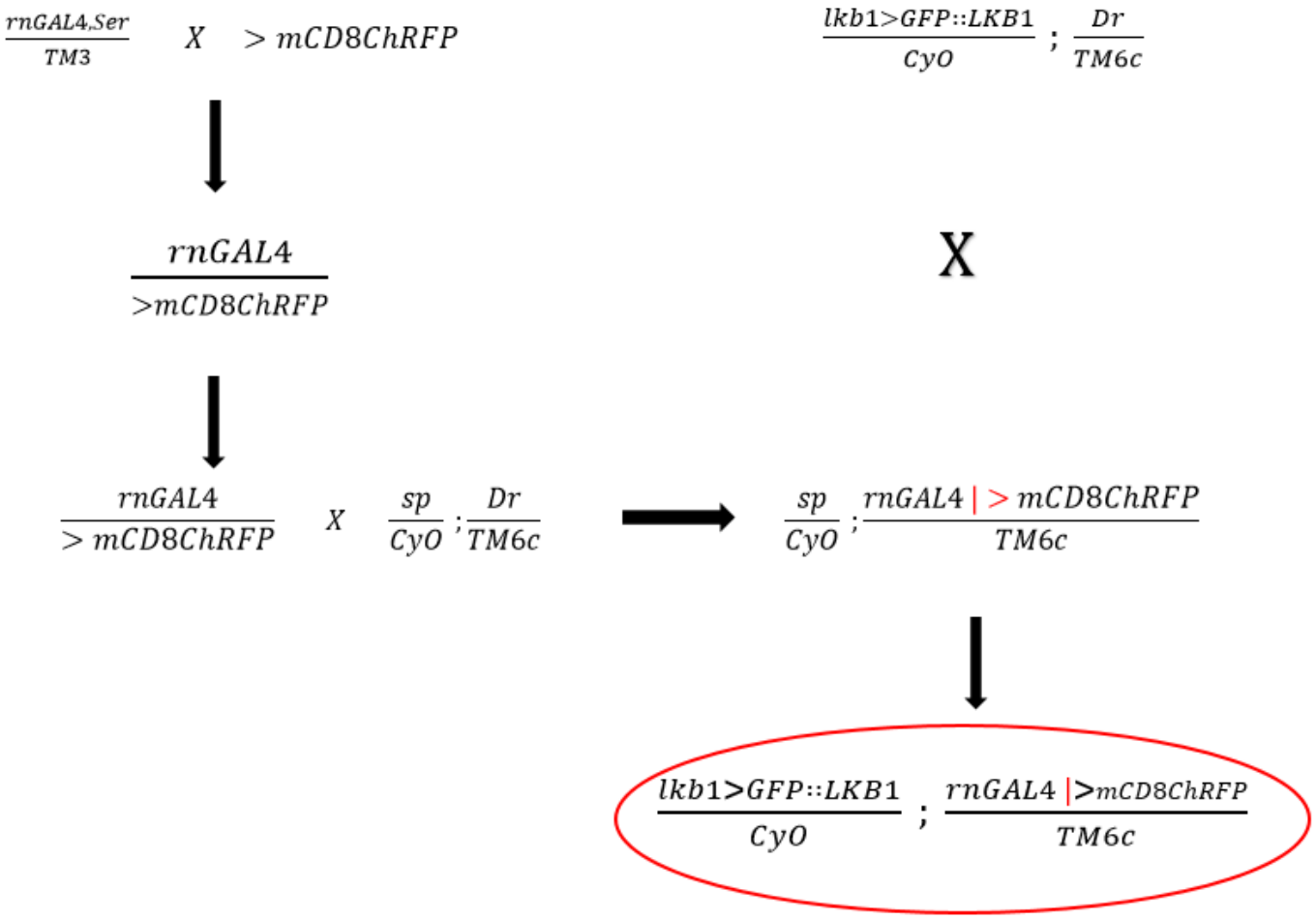
rnGAL4,Ser / TM3 X > mCD8ChRFP
lkb1>GFP::LKB1 / CyO ; Dr / TM6c
rnGAL4 / >mCD8ChRFP
X
rnGAL4 / > mCD8ChRFP X sp / CyO ; Dr / TM6c
sp / CyO ; rnGAL4 | > mCD8ChRFP / TM6c
lkb1>GFP::LKB1 / CyO ; rnGAL4 |>mCD8ChRFP / TM6c

Scheme 3

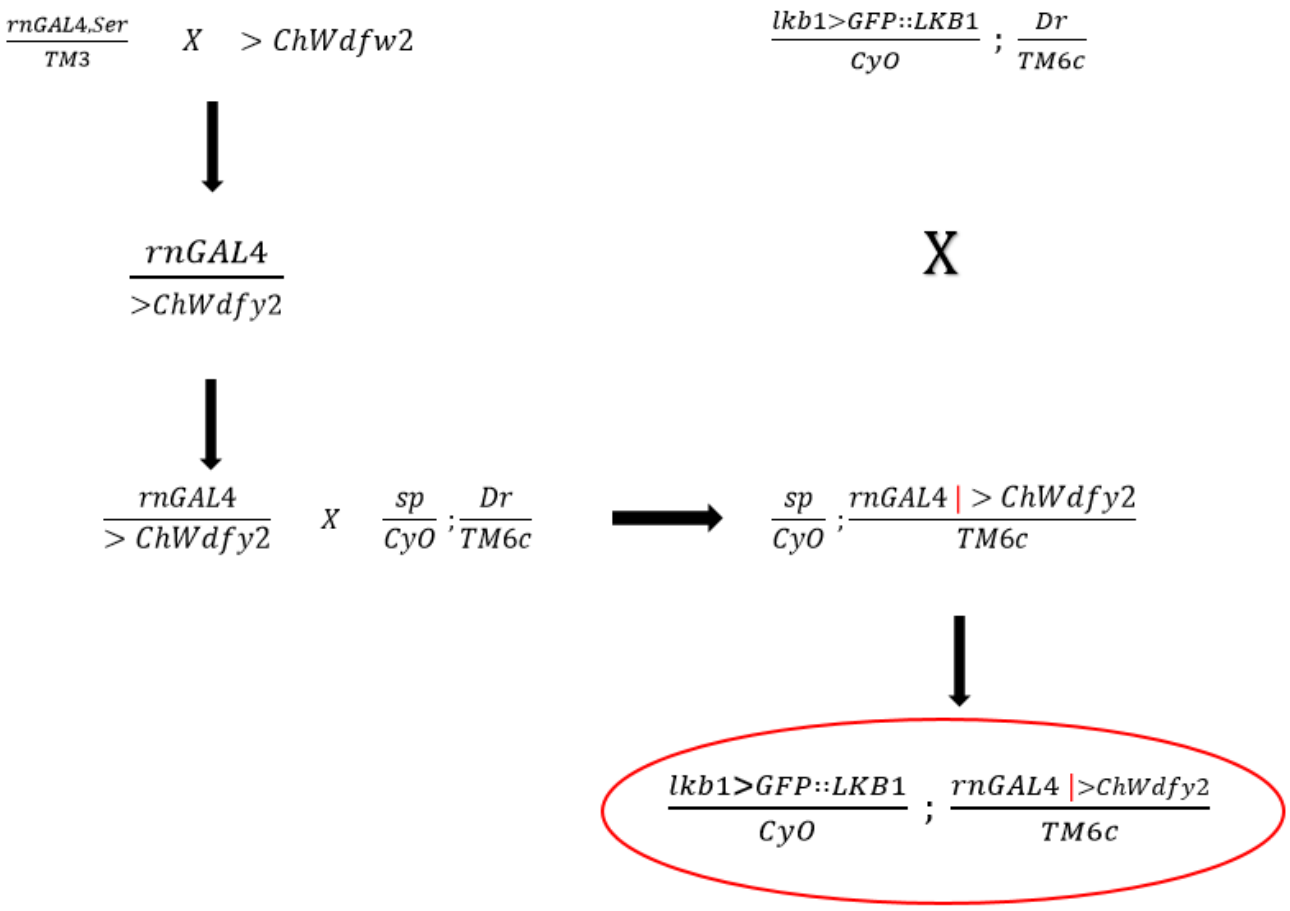
rnGAL4,Ser / TM3 X > ChWdfw2
lkb1>GFP::LKB1 / CyO ; Dr / TM6c
rnGAL4 / >ChWdfy2
X
rnGAL4 / > ChWdfy2 X sp / CyO ; Dr / TM6c
sp / CyO ; rnGAL4 | > ChWdfy2 / TM6c
lkb1>GFP::LKB1 / CyO ; rnGAL4 |>ChWdfy2 / TM6c

III. Phenotypic markers shown in fly stocks

lkb1>GFP::Lkb1/CyO;Dr/Tm6c

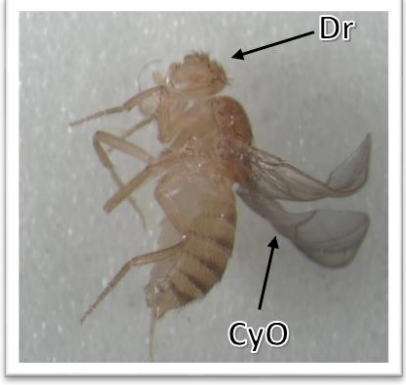

lkb1>GFP::Lkb1ΔLBCA/S-T

lkb1>GFP::Lkb1/CyO;rnG4|
>CD8ChRFP/Tm6c

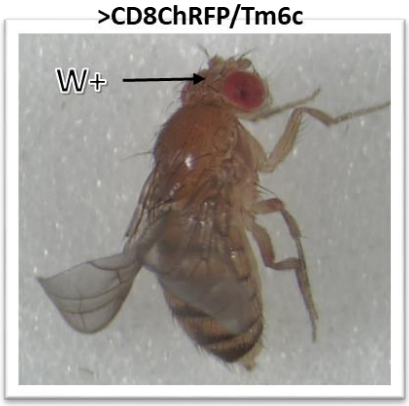

w1118

sp; >ChSNF1a/ S-T

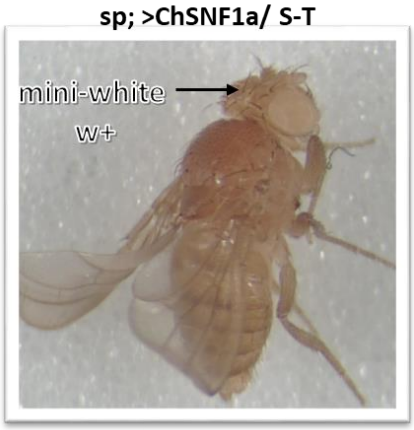

sp/CyO;Dr/Tm6c

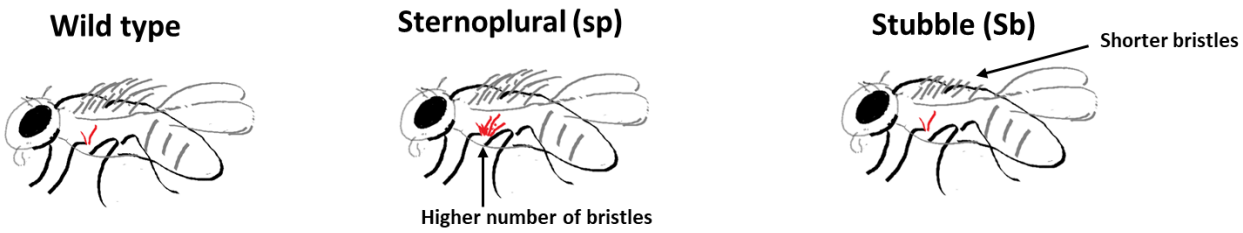
Wild type
Sternoplural (sp)
Higher number of bristles
Stubble (Sb)
Shorter bristles

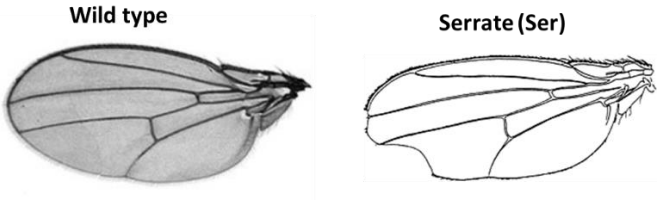
Wild type
Serrate (Ser)

IV. Penetrance of Genotype

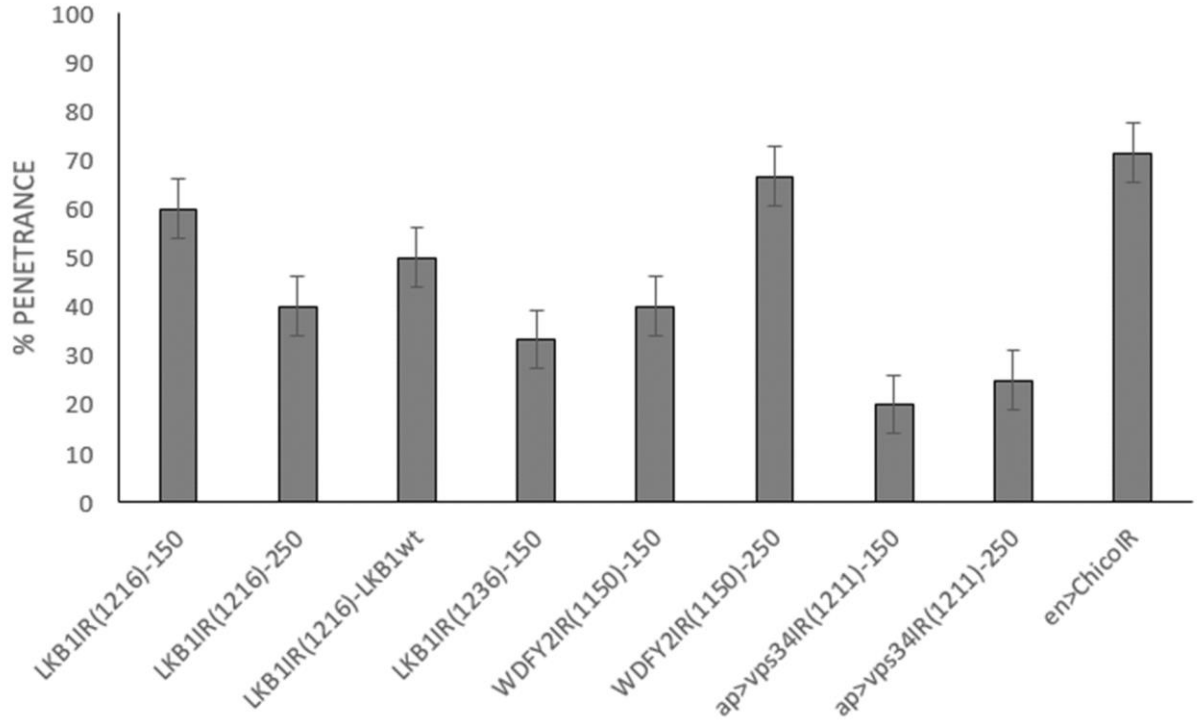

Figure 1: Percentage of penetrance of the knockdown effect. The greatest overall penetrance was seen for LKB1IR (1216). The lowest percentage penetrance was seen for ap>vps34IR (1211). Error bars represent standard error